

Trym Øksenvåg

Online condition monitoring of heat exchangers in a TEG dehydration process

Master's thesis in Mechanical Engineering

Supervisor: Even Solbraa

Co-supervisor: Erling Næss

June 2022

Trym Øksenvåg

Online condition monitoring of heat exchangers in a TEG dehydration process

Master's thesis in Mechanical Engineering
Supervisor: Even Solbraa
Co-supervisor: Erling Næss
June 2022

Norwegian University of Science and Technology
Faculty of Engineering
Department of Energy and Process Engineering



Norwegian University of
Science and Technology

Preface

This master thesis is written in the 10th semester of the five-year integrated master's degree programme Mechanical Engineering, in the specialisation field of energy, process and flow engineering. The work is done in collaboration with Equinor, and the master thesis comprises 30 ETC credits and is conducted in the spring of 2022.

The topic of this thesis is condition monitoring of heat exchangers in a glycol regeneration process. Equinor has provided operation data for a selected glycol process.

I want to express gratitude to my supervisor, Even Solbraa, for sound advice and guidance throughout the semester. I would also like to thank my co-supervisor, Erling Næss, for his assistance and support with this project.

Trym Øksenvåg

Trondheim, 10.06.2022

Abstract

Natural gas produced on the Norwegian Continental Shelf is treated at offshore installations, where water is removed by glycol-based dehydration. The oil and gas industry is constantly working to improve the safety and efficiency of production. Equinor wants to improve the safety of offshore processing plants by making operations on platforms unmanned. Unmanned operations of glycol-based dehydration processes using online condition monitoring is a development area made possible by modern instrumentation and simulation tools. This thesis will focus on condition monitoring of heat exchangers, which is an essential part of the glycol regeneration process.

Fouling is the accumulation of unwanted substances on the heat transfer surfaces of a heat exchanger. Fouling can reduce the performance of the heat exchangers due to reduced heat transfer and increased pressure drop through the exchanger. Fouling occurs over time, and it is challenging to predict how it will develop and how it will affect the heat exchanger's performance. An online condition monitoring model can provide insight into the fouling conditions of the heat exchangers and determine when the exchanger is dirty and in need of maintenance.

The fundamental theory of heat transfer and heat exchangers has been studied and presented to provide insight into this topic. In addition, previous models and research on condition monitoring of heat exchangers have been reviewed. Based on this, four heat exchangers from a TEG regeneration process on an Equinor field have been examined using condition monitoring models. A model that monitors thermal performance based on the overall heat transfer coefficient and a model that monitors hydraulic performance based on the correlation between pressure drop and flow rate are tested and evaluated. The heat exchangers at Equinor's TEG process are monitored over a period of eight months, from September 2021 to May 2022. In addition, a shell-and-plate type heat exchanger is designed and simulated in the process design and simulation tool HTRI Xchanger Suite, where the effects of fouling and the models for condition monitoring are tested and evaluated. In this work, field data from a specific Equinor process is used in combination with simulations from the process and simulation tool NeqSim, and the models are calculated in Python.

The results of this work suggest that the models indicate fouling conditions and performance of the heat exchangers at a sufficient instrumentation level. However, there is uncertainty associated with the models since the instrumentation is insufficient and inaccurate. Eventually, a discussion of the instrumentation level required for online condition monitoring concerning both approaches is included.

Sammendrag

Naturgass produsert på den norske kontinentalsokkelen blir behandlet på offshoreanlegg, hvor blant annet vann fjernes ved glykolbasert dehydrering. Olje- og gassindustrien jobber kontinuerlig med å forbedre sikkerheten og effektiviteten av produksjonen. Equinor ønsker å forbedre sikkerheten på offshore-prosessanlegg ved gjøre operasjonene på plattformer ubemannet. Ubemannende operasjoner av glykolbaserte dehydreringsprosesser ved bruk av online tilstandsovervåkning er et utviklingsområde muliggjort av moderne instrumentasjon og simuleringsverktøy. I denne oppgaven vil fokuset være på tilstandsovervåkning av varmevekslere, som er en essensiell del av dehydreringsprosessen.

Fouling er beleggdannelse ved akkumulering av uønsket stoff på varmeoverflatene i en varmeveksler. Fouling kan redusere ytelseevnen til varmevekslerene i form av redusert varmeoverføring og økt trykktap gjennom veksleren. Beleggdannelsen skjer over tid og det er vanskelig å predikere hvordan forløpet utvikler seg, og hvilken effekt det har på varmevekslerens ytelsesnivå. En modell for online tilstandsovervåkning kan gi innsikt i foulingtilstanden til varmeveksleren, og dermed øke effektiviteten ved å predikere når veksleren er skitten og trenger vedlikehold.

Grunnleggende teori om varmeovergang og varmevekslere har blitt studert og presentert for å gi innsikt i temaet. I tillegg har tidligere modeller og forskning om tilstandsovervåkning blitt studert. På bakgrunn av dette har fire varmevekslerene fra en TEG-regenereringsprosess på et Equinor-felt blitt undersøkt ved bruk av tilstandsovervåkningsmodeller. En modell som overvåker termisk ytelse basert på varmeovergangstall, og en modell som overvåker hydraulisk ytelse basert på korrelasjonen mellom trykktap og strømningshastighet har blitt testet og evaluert. Varmevekslerene ved TEG anlegget til Equinor er overvåket over en periode på åtte måneder, fra september 2021 til mai 2022. I tillegg er en rørsatsvarmeveksler designet og simulert i prosessdesign og simuleringsverktøyet HTRI Xchanger Suite, hvor effekten av fouling og modellene for tilstandsovervåkning er testet og evaluert. I dette arbeidet er feltdata fra et bestemt Equinor-anlegg brukt i kombinasjon med simuleringer fra prosess- og simuleringsverktøyet NeqSim, og modellene er kalkulert i Python.

Resultatene i dette arbeidet antyder at modellene gir en indikasjon på foulingtilstanden og ytelsesgraden til varmevekslerene ved et tilstrekkelig instrumenteringsnivå. Det er i likevel knyttet usikkerhet til modellene siden instrumenteringen på anlegget er mangelfull og unøyaktig. Til slutt er en diskusjon av instrumenteringsnivået som kreves for online tilstandsovervåking for begge tilnærmingene inkludert.

Table of Contents

Abstract	ii
Sammendrag	iii
List of Figures	vii
List of Tables	viii
1 Introduction	1
1.1 Thesis scope	2
1.2 Thesis structure	2
2 Glycol dehydration process	3
2.1 Water in natural gas	3
2.2 Dehydration systems	4
2.3 TEG dehydration process	5
2.3.1 Gas dehydration equipment	5
2.3.2 Glycol regeneration equipment	5
2.4 Equinor process description	8
3 Heat exchangers	10
3.1 Heat transfer fundamentals	10
3.1.1 Conduction	10
3.1.2 Convection	11
3.1.3 Radiation	11
3.1.4 Thermal Resistance	12
3.1.5 The overall heat transfer coefficient	13

3.2	Heat exchangers	13
3.2.1	Heat exchanger types	14
3.3	Heat exchanger fouling	16
3.3.1	Fouling resistance	18
3.3.2	Mitigation of fouling and cleaning	20
4	Heat exchanger calculations	21
4.1	Analytical solutions	21
4.1.1	F-factor method	22
4.1.2	Effectiveness-NTU method	22
4.2	Heat transfer correlations	24
4.2.1	Condensation	25
4.3	Pressure drop	27
4.3.1	Single liquid phase pressure drop	27
4.3.2	Two-phase pressure drop	28
5	Online Condition Monitoring	29
5.1	Thermal performance	29
5.2	Hydraulic performance	30
5.3	Thermal and hydraulic performance	31
6	Equipment setup and field data	33
6.1	HX01 - Cold TEG/TEG exchanger	33
6.2	HX02 - Warm TEG/TEG exchanger	34
6.3	HX03 - TEG Cooler	35
6.4	HX04 - Overhead Condenser	36
6.5	Neqsim - Non-Equilibrium Simulator	38

7	Methods of condition monitoring	39
7.1	Thermal performance method	39
7.2	Hydraulic performance method	40
7.3	HTRI Xchanger Suite	42
8	Results	44
8.1	HTRI simulation	44
8.1.1	Case simulations	45
8.1.2	Condition monitoring of case simulation	48
8.2	Neqsim and field data comparison	49
8.3	Condition monitoring of HX01	50
8.3.1	Thermal performance monitoring	51
8.3.2	Hydraulic performance monitoring	52
8.4	Condition monitoring of HX02	55
8.4.1	Thermal performance monitoring	56
8.4.2	Hydraulic performance monitoring	56
8.5	Condition monitoring of HX03	60
8.5.1	Thermal performance monitoring	60
8.5.2	Hydraulic performance monitoring	61
8.6	Condition monitoring of HX04	63
8.6.1	Thermal performance monitoring	64
8.6.2	Hydraulic performance monitoring	65
9	Discussion	68
9.1	HTRI simulation	68
9.1.1	Case simulations	68
9.1.2	Condition monitoring of case simulations	69

9.2	Neqsim and field data comparison	70
9.3	Condition monitoring of HX01	70
9.3.1	Thermal performance monitoring	71
9.3.2	Hydraulic performance monitoring	71
9.4	Condition monitoring of HX02	72
9.4.1	Thermal performance monitoring	72
9.4.2	Hydraulic performance monitoring	72
9.5	Condition monitoring of HX03	74
9.5.1	Thermal performance monitoring	74
9.5.2	Hydraulic performance monitoring	75
9.6	Condition monitoring of HX04	75
9.6.1	Thermal performance monitoring	76
9.6.2	Hydraulic performance monitoring	76
10	Conclusion	77
10.1	Further work	78
	Bibliography	79
	Appendix	82
A	HTRI heat exchanger design performance	82
B	HTRI heat exchanger design drawings	85
C	Definition of functions	87
D	Neqsim simulation	90
E	Plotted figures scripts	105

List of Figures

2.1	Flow diagram Equinor process	9
3.1	Illustration - convection	11
3.2	Heat transfer plane wall	13
3.3	Heat exchanger flow arrangements	14
3.4	Shell-and-tube heat exchanger	15
3.5	Plate-and-shell heat exchanger.	16
3.6	Fouling resistance plane wall	17
3.7	Characteristic fouling curves	19
4.1	Illustrations of film condensation	26
5.1	TH- λ plot	31
6.1	Flow diagram - HX01	33
6.2	Flow diagram - HX02	34
6.3	Flow diagram - HX03	36
6.4	Flow diagram - HX04	37
7.1	Illustration - UA-model	40
7.2	Pressure drop and flow rate - fouling	41
7.3	Illustration - pressure drop model	41
8.1	HTRI simulation comparison	46
8.2	HTRI simulation comparison	49
8.3	Neqsim copmarison	50
8.4	Thermal performance - HX01	51
8.5	Hydraulic performance - HX01 rich glycol	52
8.6	Pressure drop and flow rate - HX01 lean glycol	53
8.7	Hydraulic performance - HX01 rich glycol	54

8.8	Pressure drop and gas fraction - HX01 rich glycol	55
8.9	Thermal performance - HX02	56
8.10	Hydraulic performance - HX02 rich glycol	57
8.11	Pressure drop and flow rate - HX02 lean glycol	58
8.12	Hydraulic performance - HX02 rich glycol	58
8.13	Pressure drop and flow rate - HX02 rich glycol	59
8.14	Thermal performance - HX03	61
8.15	Hydraulic performance - HX03 rich glycol	62
8.16	Pressure drop and flow rate - HX03 lean glycol	63
8.17	Thermal performance - HX04	65
8.18	Hydraulic performance - HX04 overhead vapours	65
8.19	Pressure drop and flow rate - HX02 rich glycol	67
9.1	Cartridge filter pressure drop	74

List of Tables

2.1	Glycols used in dehydration	4
3.1	Typical fouling factors	19
4.1	Heat exchanger effectiveness relations	23
7.1	HTRI simulation cases	43
8.1	HTRI simulation cases	45
8.2	HX01 - Design comparison	51
8.3	HX02 - Design comparison	56
8.4	HX03 - Design comparison	60
8.5	HX04 - Design comparison	64

Nomenclature

Δp	Pressure difference [<i>bar</i>]
ΔT	Temperature difference [<i>K</i>]
ΔT_m	Mean temperature difference [<i>K</i>]
Δz	Vertical length [<i>m</i>]
δ	Boundary layer thickness [<i>m</i>]
\dot{m}	Mass flow [<i>kg/s</i>]
ϵ	Emissivity
μ	Dynamic viscosity [<i>kg/ms</i>]
∇	Nabla operator
ϕ^2	Two-phase multiplier
ρ	Density [<i>kg/m³</i>]
σ	Stefan Boltzmann constant $5.67 \times 10^{-8} \text{W/m}^2 \text{K}^4$
ε	Thermal effectiveness
A	Surface area [<i>m²</i>]
C	Heat capacity rate [<i>W/K</i>]
C_f	C-factor [<i>m^{3.5}/√(kg)</i>]
c_p	Specific heat capacity [<i>J/kgK</i>]
C_r	Heat capacity ratio
D	Diameter [<i>m</i>]
D_h	Hydraulic diameter [<i>m</i>]
e	Surface roughness [<i>mm</i>]
F	F-factor
f	Friction factor
g	Gravitational acceleration [<i>m/s²</i>]

h	Convective heat transfer coefficient [W/m^2K]
h_{fg}	Latent heat of evaporation [J/kg]
k	Thermal conductivity [W/m^2K]
L	Length [m]
L_{eff}	Effective flow length [m]
$LMTD$	Log mean temperature difference [K]
Nu	Nusselt number
P	Wetted perimeter [m]
Pr	Prandtl number
q	Heat transfer [W]
q''	Heat flux [W/m^2]
R_f	Fouling factor [m^2K/W]
R_t	Thermal resistance [K/W]
R_{tot}	Total thermal resistance [K/W]
Re	Reynolds number
T	Temperature [K]
t	Time [s]
T_s	Surface temperature [K]
T_∞	Free stream temperature [K]
T_{sur}	Temperature surroundings [K]
U	Overall heat transfer coefficient [W/K]
u	Velocity [m/s]
V	Volumetric flow rate [m^3/s]
X^2	Martinelli parameter
y_w	Wall thickness [m]
NTU	Number of transfer units

1 Introduction

Natural gas produced on the Norwegian Continental Shelf usually undergoes a form of treatment at offshore processing plants. The rich gas is prepared for transport by removing heavier hydrocarbons and sour gases and reducing the water content to ensure safe single-phase transport so pipes and equipment are not exposed to damage. The work surroundings on an offshore facility are hazardous, with heavy equipment, machinery operating at high pressures and temperatures and combustible and toxic compounds. In addition, the offshore facilities are placed at remote locations and can be subjected to extreme weather conditions. Due to these dangerous working surroundings, several accidents have transpired over the years. Therefore, the oil and gas industry has a significant focus on safety and is continuously developing safer ways of operating.

Unmanned operation of offshore platforms is a development area that can greatly reduce the risk of personnel-related accidents. For an unmanned facility, the various processes and equipment are controlled by online condition monitoring without personnel present in the field. Krafla is an example of a planned unmanned field under development by Equinor. The operation is controlled from land, and personnel are only offshore for periodic inspection and maintenance. An essential enabler for unmanned offshore operations is reliable condition monitoring of process equipment. The potential for condition monitoring is considerable. In addition to increasing safety, condition monitoring can be used to implement suitable measures and optimise maintenance intervals to ensure high efficiency and reduce downtime.

Heat exchangers are an essential part of oil and gas processing, and in a glycol dehydration process, it is a crucial component. Efficient utilisation of heat exchangers can reduce the energy demand of the process and increase the production rate. Therefore, knowing how the heat exchangers perform is vital to be able to implement suitable measures when efficiency starts to degrade. Fouling in heat exchangers is a well-known problem that affects performance. Fouling is the accumulation of unwanted material on the surfaces inside the exchangers. In general, it reduces heat transfer and increases pressure loss. However, it is difficult to predict when it will occur and how it will affect the exchanger. Which again makes it difficult to predict when cleaning and maintenance should be done. Condition monitoring of heat exchangers can thus be used to see when the efficiency is reduced due to fouling, and necessary maintenance is conducted and reduce unnecessary production shut-down. Despite this, standardised methods of condition monitoring have not been developed.

1.1 Thesis scope

The objective of this thesis will be to evaluate and develop models and tools for condition monitoring of heat exchangers in a glycol regeneration process in cooperation with Equinor. The models should give increased insight into the heat exchangers' performance development and fouling conditions. The models will be established in Python and be based on field data and simulations in Neqsim. In addition, a heat exchanger will be designed in HTRI Xchanger Suite, where various simulated conditions are tested to evaluate how they affect the models. In order to assess and develop methods of condition monitoring, Equinor has provided data from a glycol dehydration process for a field in operation. The level of instrumentation at process plants varies. This work will also evaluate the level of instrumentation needed in combination with process simulations for sufficient condition monitoring. Equinor and NTNU have provided models for simulation of phase equilibria and thermodynamic and physical properties of relevant fluids. This work is limited to only including methods based on thermodynamic and physical relations and will not consider other possible approaches such as digital twin and machine learning.

1.2 Thesis structure

This thesis is structured to provide a basic understanding of the glycol dehydration process simulated in Neqsim and the Equinor process. It then focuses on the fundamental theory of heat transfer and heat exchangers and previous development of condition monitoring methods. This will provide a basis for understanding the models used in this work. This thesis is a continuation of the project assignment. Thus, parts of the theory chapters originate from this work.

The report consists of 11 chapters. Chapter 1 is an introduction to the thesis. In Chapter 2, problems with water in natural gas and the need for gas dehydration are presented. In addition, a description of the various sub-processes and equipment in a TEG dehydration process and a description of the Equinor process. The fundamental theory of heat transfer, heat exchangers, and fouling is presented in chapter 3. Chapter 4 then provides an introduction to different calculation methods for heat exchangers. Chapter 5 presents a review of previous documented methods for condition monitoring. Chapter 6 describes the instrumentation setup around the different heat exchangers for the Equinor process. The methods used in this work are presented in Chapter 7, and the results are presented in Chapter 8, with subsequent discussion in Chapter 9. Finally, chapter 10 provides a conclusion on the work that has been done and provides recommendations for further work.

2 Glycol dehydration process

This chapter presents the fundamentals of gas dehydration and the glycol regeneration process in four sections to understand the principles and equipment, which is further discussed in this thesis. Large parts of this chapter have been persisted from the project work. This chapter is divided into four sections. Section 2.1 presents the general problems with water content in natural gas processing. Section 2.2 gives a brief introduction to different types of dehydration systems. Section 2.3 describes the various sub-processes and equipment in a glycol dehydration process. The last section presents an overview of the dehydration process of the Equinor facility used in this thesis, which will be used in process simulations with NeqSim in this work. The process described in section 2.4 is based on datasheets and P&IDs provided by Equinor.

2.1 Water in natural gas

Water vapour is a typical containment in natural gas (Lyons et al. 2016). A dehydration process of natural gas refers to the removal of water vapour from the gas stream. Water is removed due to problems caused by liquid water, which can occur if the temperature decreases, the pressure increases, or both (Guo and Ghalambor 2005). In natural gas processing, the most common problems related to water is the following:

- Water content decreases the heating value of natural gas. Also, sales gas have specifications on the water content in the natural gas.
- If the natural gas has any content of CO_2 or H_2S , the mixture becomes corrosive with liquid water.
- Liquid water in natural gas can form solid hydrates, which are water molecules in a crystalline structure. Hydrates can plug pipes and damage equipment.
- Liquid water can cause slugging flow conditions, which reduces the efficiency of the flow in pipelines.

The dew point is the temperature at which natural gas is saturated with water vapour at a given pressure. If the temperature goes below the dew point, water will start condensing. The dew point is an indirect indicator of the water content of a natural gas stream (ibid.).

2.2 Dehydration systems

There are four different categories of natural gas dehydration systems used in the industry; cooling, cooling and compression, adsorption, and absorption (Guo and Ghalambor 2005).

Cooling and compression

As described above, the amount of water the natural gas can contain depends on temperature and pressure. Therefore, decreasing the temperature at constant pressure or increasing the pressure at constant temperature saturated natural gas water will start condensing and can be separated from the gas. The gas will remain at the dewpoint at the new conditions with lower water content (ibid.).

Adsorption

Adsorption is a process in which gaseous molecules are removed from a gas stream by adhering to the surface of a solid. In dehydration by adsorption, water from the gas stream is contained on the surface of the solid adsorbent substance. The most common adsorbents used in water removal are Silica Gel and Molecular Sieves. Silica Gel is a jelly-like mixture of sodium silicate and sulphuric acid. Molecular sieves are crystalline materials that can be used to capture or separate gases based on molecular size and shape (Theodore 2008).

Absorption

Absorption is a dehydration process where water vapour is removed from natural gas by bubbling the gas through a liquid absorbent. Water from the natural gas is absorbed in the liquid and removed from the gas stream. The absorbent liquid is usually a glycol desiccant. Glycols that can be used in dehydration is presented in table 2.1. Due to its large dew point depression, operation cost and reliability, TEG is regarded as the most effective glycol (Guo and Ghalambor 2005). A TEG absorption process is used in the Equinor process and will be further presented in detail in chapter 2.

Table 2.1: Glycols used in dehydration

Name	Formula	
Ethylene glycol (EG)	$\text{HO}-(\text{CH}_2)_2-\text{OH}$	$\text{C}_2\text{H}_6\text{O}_2$
Diethylene glycol (DEG)	$\text{HO}-((\text{CH}_2)_2-\text{O})-(\text{CH}_2)_2-\text{OH}$	$\text{C}_4\text{H}_{10}\text{O}_3$
Triethylene glycol (TEG)	$\text{HO}-((\text{CH}_2)_2-\text{O})_2-(\text{CH}_2)_2-\text{OH}$	$\text{C}_6\text{H}_{14}\text{O}_4$
Tetraethylene glycol (T ₄ EG)	$\text{HO}-((\text{CH}_2)_2-\text{O})_3-(\text{CH}_2)_2-\text{OH}$	$\text{C}_8\text{H}_{18}\text{O}_5$

2.3 TEG dehydration process

2.3.1 Gas dehydration equipment

Inlet scrubber/ filter separator

When entering the dehydration process, wet natural gas is first routed through an inlet scrubber or a microfiber filter separator. This unit removes liquid any liquid water, or other liquid or solid impurities (Stewart 2014).

Glycol contactor

Saturated natural gas enters the glycol contactor at the vessel's bottom and flows upwards through liquid glycol. (Operations 1999). The inside of the contactor contains either tray or packed tower (Campbell 1992).

The tray type tower is a vessel containing a series of trays maintaining a certain level of absorbent TEG on each tray. As the gas passes through each succeeding tray, it bubbles through the TEG, which absorbs water from the gas and becomes progressively drier (Stewart 2014). The TEG is provided at the top side of the contactor flowing downwards across each tray and exiting at the bottom. On each tray, a mechanism is implemented for the gas to flow through. This mechanism can either be bubble caps, sieves or valves (Campbell 1992).

Packed type towers consist of either structured or random packing. The principal is the same as tray type; gas and TEG flow counter currently through the packing material. Random packing is discrete, individually shaped small objects randomly packed into the vessel. The objects are designed to provide contact surfaces between the gas and TEG. Structured packing is usually composed of corrugated sheets, wire-mesh weavings or grid type (Coker 2010). Packed towers provide considerably smaller diameter towers than tray type, which is advantageous for offshore processes, where more compact contactors are preferable (Campbell 1992).

2.3.2 Glycol regeneration equipment

Reflux condenser

A reflux condenser is a coil in the top of the reboiler still column. The reflux condenser utilises heat from the vapour leaving the still column to heat the cold lean TEG. The TEG in the vapour condenses to liquid droplets and fall down the still column while water remains as vapour and flows out the top of the still column (Stewart 2014).

Flash drum

The flash drum is a three-phase separator. The glycol can pick up a small amount of glycol when passing through the contactor, which has to be removed during the regeneration process. As the rich TEG is heated before entering the flash drum, the lighter hydrocarbons will be gas and heavier in the liquid phase. The flash drum separates most of the gas and liquid hydrocarbons that have been entrained in the glycol (Stewart 2014).

Filters

Filters are installed after the separation of gas and condensates from the rich TEG (ibid.). First, a filter that removes solid containment down to a size of 5-10 microns. The full-flow type, with two filters in parallel and no by-pass lines, is recommended (Campbell 1992). Hence, switching to a standby filter can be done when the pressure drop in a filter reaches a certain level.

Second, an activated carbon filter is usually installed downstream of the filter. The activated carbon filter removes liquid entrained heavy hydrocarbons (Stewart 2014). It will also adsorb any aromatic hydrocarbon present in the rich glycol (Campbell 1992).

Still column

The still column is a vertical column sitting on top of the reboiler. Heated rich TEG enters and drips down the column, and water vapour from the reboiler flows upward, heating the glycol. The internals of the column is either trays or packed type, which is used to increase surface area and heat distribution through the column. As the glycol gets progressively heated through the still column, water begins to evaporate. The vapour flowing upwards through the still column has a small amount of glycol vapour trapped with it. As described in section (RF), a reflux condenser at the top of the still column will condensate the glycol and prevent losses with the steam (Stewart 2014).

Reboiler

The reboiler is a vessel where water is separated from the glycol by heating. The reboiler utilises either direct-fired, waste heat, steam or electric heater as a heat source (ibid.). In the reboiler, the rich TEG is heated to between 177 and 204°C, which removes enough water resulting in a lean TEG concentration of 99.5% or higher (Guo and Ghalambor 2005). The produced vapour consisting of water, glycol and any remaining hydrocarbons flows back into the still column where distillation occurs.

Stripping column

The utilisation of stripping gas is a common technique for further increasing the concentration of lean TEG (GPSA 2012). It is typically a hot and dry natural gas due to its high affinity with water (Stewart 2014). The stripping gas can be introduced directly into the reboiler or through a stripping column. In a stripping column, the stripping gas and the glycol flow in a countercurrent direction. A stripping column provides a more efficient stripping of the glycol than by introducing it directly into the reboiler (GPSA 2012).

Surge drum

The surge drum is a storage vessel where regenerated lean glycol is accumulated after the reboiler. The surge drum acts as a buffer, capable of accepting liquids from the upstream process or providing glycol to downstream equipment without upsets. The surge drum can be integrated into the reboiler or be a separate vessel (ibid.).

Pumps

Pumps drive the circulation of glycol in the regeneration process. The pumps utilised in a glycol regeneration process are usually electricity or glycol-gas powered pumps. Glycol-gas pumps are powered by natural gas from the rich glycol. Electricity powered pumps are more durable against solid contaminants and hydrocarbon distillate but require a small glycol leakage for lubrication. Electricity pumps are usually applied in larger systems and glycol-gas pumps in smaller isolated systems (Stewart 2014).

Heat exchangers

Heat exchangers have multiple purposes in a glycol regeneration process. In principle, the glycol has to be pre-heated to flash of natural gas, then again heated to remove the water, and thereafter, it has to cool down before entering the contactor. Based on this, heat exchangers are used to recover heat between the lean glycol in need of cooling and the cold rich glycol in need of heating.

Most of the energy demand in a dehydration process is due to the reboiler heat load. A warm lean/rich glycol heat exchanger is used to utilise the excessive heat in the lean glycol to heat up the rich glycol before entering the reboiler. In principle, the efficiency of the heat exchangers has a direct effect on the reboiler heat load (Campbell 1992).

To get efficient separation of light hydrocarbons from the rich glycol in the flash drum, a cold lean/rich glycol heat exchanger is used to pre-heat the rich glycol before entering the flash drum (Stewart 2014). The lean glycol is further cooled by

this exchanger.

At last, the lean glycol entering the contactor has to be near the natural gas temperature to prevent foaming and to prevent the glycol from heating the natural gas above equilibrium temperature (Stewart 2014). A heat exchanger with a cooling medium is used to cool down the lean glycol to near gas temperature.

Heat exchangers will be presented in more detail in chapters 3 and 4.

2.4 Equinor process description

Water saturated natural gas is routed from a dust filter to the bottom section of the glycol contactor. If any free liquids are present, they are separated at the lower section of the contactor and routed to the Gas Export Compressor Suction Scrubbers. Lean glycol is fed into the top of the contactor and is distributed evenly over a structured packing bed. The natural gas is distributed through a chimney tray and flows counter-current through the liquid glycol in the packing bed. The liquid glycol absorbs water from the gas, which reduces the water content in the gas. Dry natural gas leaves from the top of the contactor and is sent to compression and gas export. The rich glycol leaves at the chimney tray and sent to regeneration.

Rich TEG for regeneration is first routed through the reflux condenser for preheating. Here, the rich glycol is sent through a tube bundle, where the glycol is heated by condensing vapour on the tube wall. The rich glycol is then heated in the Cold TEG/TEG Heat Exchanger. After the heat exchanger, the rich glycol enters a Flash Drum where three-phase separation occurs. Light hydrocarbons and CO₂ in the gas phase are flashed out, and hydrocarbon condensates are separated from the TEG by an overflow weir with a constant glycol level in the vessel. Flash gas is mixed with the stripping gas and sent to the stripping column, while the hydrocarbon condensates are routed to the third stage separator.

After gas and condensates are separated in the flash drum, the rich glycol flows through the cartridge and activated carbon filters. The cartridge filters remove solid particles larger than 10 microns, and the activated carbon filter removes any remaining residues of heavy hydrocarbons.

The rich glycol is then heated again in the Warm TEG/TEG heat exchanger before entering the reboiler through the still column. The reboiler produces lean glycol by separating the water from the rich TEG. The lean glycol exits through a stripping column, where stripping gas consisting of gas from the flash drum and fuel gas is

flowing counter-currently with the lean TEG and strips out additional water. The stripping gas and water vapour exit the reboiler through the still column and reflux condenser.

Most of the water vapour in the gas leaving the reflux condenser is condensed through the overhead condenser, where the stream is cooled using a cooling medium. After the overhead condenser, the two-phase stream is routed to the overhead receiver, separating gas and liquids. The liquids are routed to the third stage separator, and the gas is pressurised and sent to the third stage separator gas outlet.

Lean glycol leaving the stripping column is first sent to the warm TEG/TEG heat exchanger, heating the rich glycol entering the reboiler. Then, the stream is routed to the surge drum, where it is maintained a TEG content enough for 15 days of uninterrupted operation. Next, lean glycol flows to the booster pumps from the surge drum, which pumps it through the cold TEG/TEG heat exchanger heating the cold rich glycol. The lean glycol is then cooled in the TEG cooler to 5 degrees above the temperature of the water-saturated feed gas, using a cooling medium. Lastly, the lean glycol flows through the TEG circulation pumps and into the contactor.

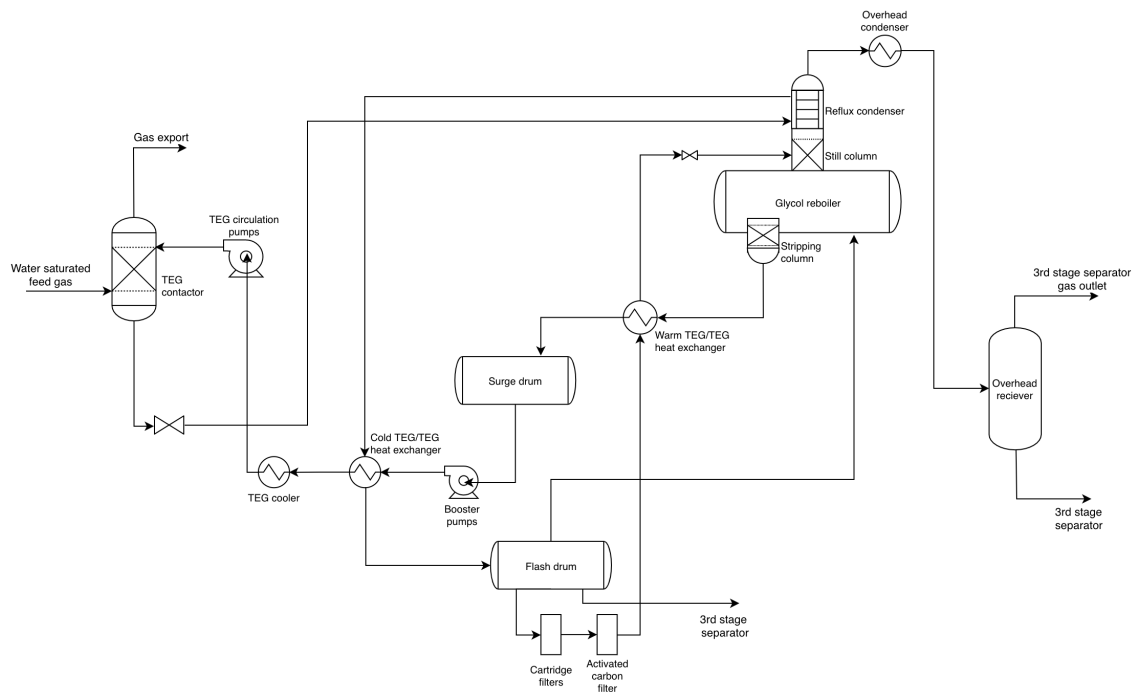


Figure 2.1: Simplified flow diagram of the Equinor TEG dehydration process.

3 Heat exchangers

This chapter presents the fundamental theory of heat exchangers and heat transfer. Some parts of this chapter originate from the project assignment. This chapter is divided into three sections. Section 3.1 presents the fundamental heat transfer theory relevant to a heat exchanger. Further, section 3.2 gives an introduction to heat exchangers. At last, section 3.3 presents fouling in heat exchangers.

3.1 Heat transfer fundamentals

Heat transfer describes the transfer of thermal energy due to temperature differences. If a temperature difference exists in or between a medium, heat will always move from higher to lower temperatures. There are three different mode of heat transfer; conduction, convection and radiation (Incropera et al. 2011).

3.1.1 Conduction

Conduction is described at a molecular level. Conduction is the transfer of thermal energy by the collisions of energetic molecules or other particles. Higher temperatures are associated with higher internal energy for the molecules. This energy is related to rotational and vibrational motions. Thus, when a molecule collides with another molecule, energy from the most energetic molecule will be transferred to the least energetic. Conductive heat transfer can occur in all substances but differs a little. Conduction in gases and liquids are very similar, with molecules in random motion that transfer energy by constantly colliding with other molecules. The difference is for solid substances. In solids, the molecules are not moving but are arranged in a lattice formation. Energy is transferred due to lattice waves induced by atomic vibrations. (ibid.)

A general definition of conduction is given by Fourier's law, or the conduction rate equation, presented in equation (3.1). Where q'' is the heat flux, k is the thermal conductivity, ∇ is the three-dimensional nabla operator, and T is the scalar temperature field (ibid.).

$$\mathbf{q}'' = -k\nabla T \quad (3.1)$$

3.1.2 Convection

The convective heat transfer mode is energy transfer due to the diffusion of energy from high to low temperatures and the fluid's bulk motion. It describes the transfer of heat between a surface and a moving fluid with a temperature difference. The concept of boundary layers is essential to understand convection heat transfer. For flow over any surface, the velocity of the fluid at the surface is zero. The fluid particles close to the surface are slowed down due to the shear stresses acting on adjacent particles in a parallel direction to the velocity. This effect causes a velocity boundary layer where the velocity gradually increases away from the surface. In addition, if the fluid temperature differs from the surface temperature, there will be a thermal boundary layer. The thermal boundary layer is a region of the fluid where the temperature varies from the surface temperature to the free stream temperature. Near the surface, where the velocity is low, heat transfer is dominated by conduction. Further away, the contribution from the bulk fluid motion increases. Figure 3.1 illustrates convective heat transfer by cooling of a heated surface in a boundary layer development. Convective heat can be described by equation (3.2), where h is the heat transfer coefficient, T_s is the surface temperature and T_∞ is the fluid temperature (Incropera et al. 2011).

$$q'' = h(T_s - T_\infty) \quad (3.2)$$

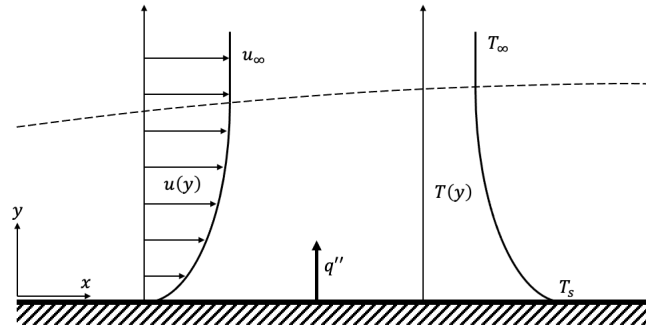


Figure 3.1: Illustration of velocity and temperature profile for convective cooling of a heated surface in boundary layer development.

3.1.3 Radiation

Thermal radiation is electromagnetic radiation emitted from all bodies that have a temperature above absolute zero. Where energy transfer by convection and conduction requires a medium to transport the heat, radiation is transported by electro-

magnetic waves. Thermal radiation is the rate at which a matter releases or emits energy due to the oscillations of the electrons the matter consists of. Thermal radiation can be expressed by equation 3.3, where ϵ is the emissivity, σ is the Stefan Boltzman constant and T_{sur} is the temperature of the surroundings (Incropera et al. 2011).

$$q''_{rad} = \epsilon\sigma (T_s^4 - T_{sur}^4) \quad (3.3)$$

3.1.4 Thermal Resistance

Thermal resistance is a measure of the temperature difference in relation to the rate of heat transfer. Thermal resistance is defined by equation (3.4). Combining equation (3.4) with equation (3.1) or (3.2) gives the conductive and convective terms for thermal resistance, respectively, as shown in equation (3.5). For a given heat transfer rate, high thermal resistance will result in a lower temperature difference (ibid.).

$$R_t = \frac{\Delta T}{q} = \frac{\Delta T}{q'' \cdot A} \quad (3.4)$$

$$R_{t,cond} = \frac{T_{s,h} - T_{s,c}}{q} = \frac{L}{kA} \quad (3.5a)$$

$$R_{t,conv} = \frac{T_s - T_\infty}{q} = \frac{1}{hA} \quad (3.5b)$$

To understand thermal resistance, one can consider heat transfer between two fluids with a plane wall in between, as shown in figure 3.2. By considering thermal resistance as a circuit representation with a series of connecting thermal resistances that the heat is passing through. The total resistance between two points is the summation of all the resistances in between. Hence, for the plane wall in figure 3.2, equation (3.6) represents the total thermal resistance between the hot and cold fluid. Where $R_{t,h}$ and $R_{t,c}$ represent the convective thermal resistance given by equation (3.5b), and R_w is the conductive thermal resistance through the wall given by equation (3.5a) (ibid.).

$$R_{tot} = \sum R_t = R_{t,h} + R_{t,w} + R_{t,c} = \frac{1}{(hA)_h} + \frac{y_w}{(kA)_w} + \frac{1}{(hA)_c} \quad (3.6)$$

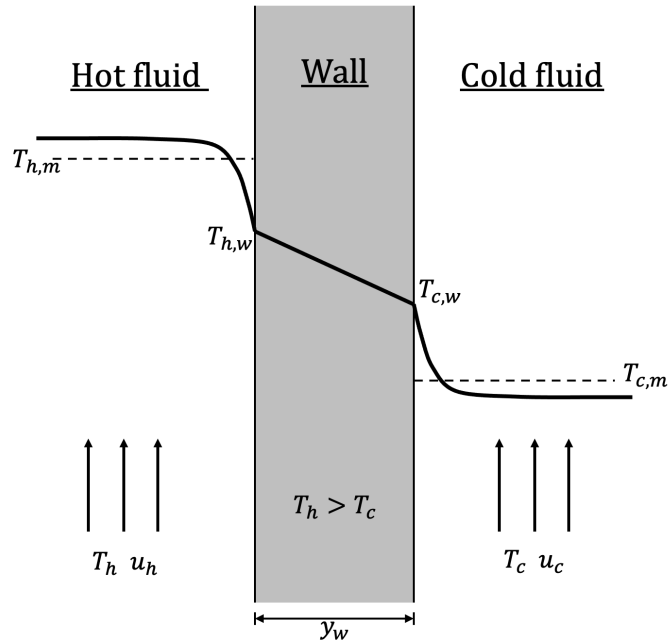


Figure 3.2: Illustration of temperature distribution for heat transfer through a plane wall.

3.1.5 The overall heat transfer coefficient

An essential part of the heat transfer review regarding heat exchangers is the overall heat transfer coefficient. The overall heat transfer coefficient U is defined as the correlation between heat transfer surface area A and the total thermal resistance R_{tot} presented in equation (3.7) (Serth and Lestina 2014).

$$R_{tot} = \frac{1}{UA} \quad (3.7)$$

3.2 Heat exchangers

A heat exchanger is process equipment in which heat is transferred between two fluids at different temperatures, most often separated by a solid wall, as illustrated in figure 3.2. Heat exchangers are an essential part of the process equipment in most industrial plants. The large variety of different process operating situations has resulted in the development of different types of heat exchangers. It is primarily the offshore industry and the development of nuclear power plants that have accelerated the development of heat exchangers. Rigorous safety requirements are set here, and on offshore installations, the weight and size of the heat exchanger will also be decisive (Næss n.d.).

3.2.1 Heat exchanger types

Heat exchangers can be classified in many different ways. The design of a heat exchanger is generally decided by a heat transfer analysis, as well as a consideration of size, weight, installation and fabrication costs (Zohuri 2017). They are used in various industries and products, and fields of application and design techniques generally differ. Heat exchangers are primarily classified according to heat transfer mechanism, transfer process and the number of fluids. Convictional heat exchangers are also classified according to flow arrangement and construction type (Shah and Sekulić 2003). Figure 3.3 show four of the most common types of heat exchangers based on flow path configuration(Zohuri 2017).

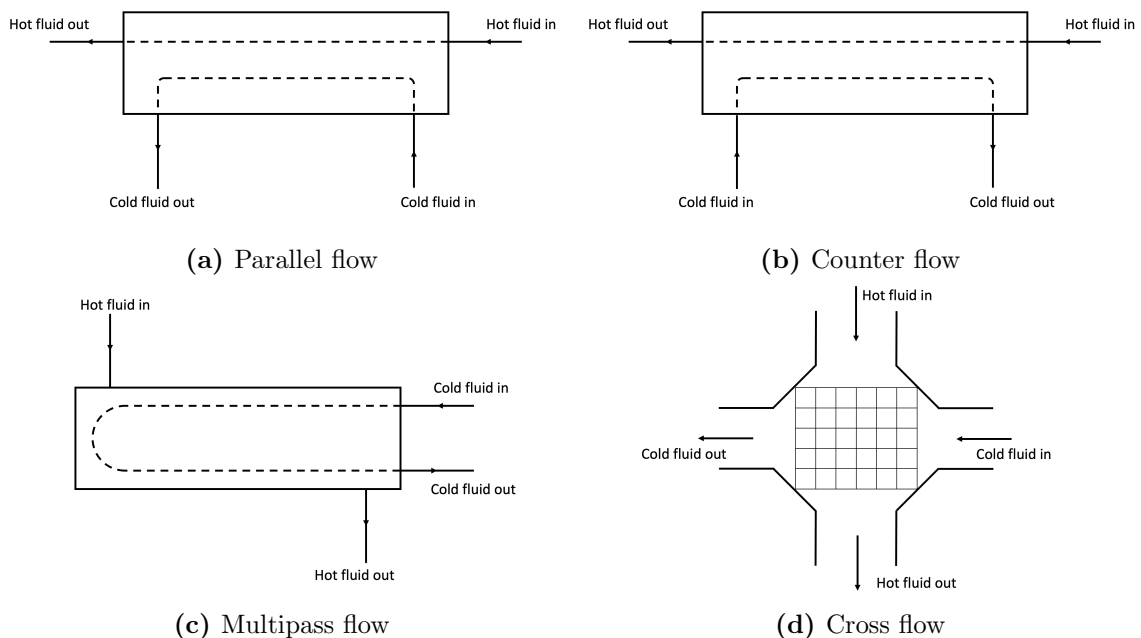


Figure 3.3: Common flow path configurations for heat exchangers.

- (a) Parallel flow arrangement is a configuration where the hot and cold fluids flow in the same direction through the heat exchanger. The fluids enter and leave at the same sides (Incropera et al. 2011).
- (b) In a counterflow configured heat exchanger, the two fluid streams enter at different sides and flow in opposite directions. As a result, the fluids typically enter and leave at opposite sides of the heat exchanger (ibid.).
- (c) In a multipass arrangement, one of the fluid streams are routed back and forth across the flow path of the other fluid(Zohuri 2017). Figure 3.3c illustrates a multipass configuration with two passes.

- (d) For a crossflow configuration, the fluids flow through a heat transfer matrix at right angles to each other (Zohuri 2017).

Double-pipe heat exchangers

The double-pipe heat exchanger is the simplest form of a heat exchanger. It consists of two concentric tubes, where one fluid flows in the inner tube and another in the outer. The fluids can flow both counter-currently or parallel, where counterflow gives the ideal highest performance for any given surface area.(Shah and Sekulić 2003)

Shell-and-Tube Exchangers

Shell and tube heat exchangers make up the majority of heat exchangers in the process industry. They mainly consist of bundles of pipes mounted inside a cylindrical shell. The tubes are oriented parallel to the shell, with one fluid inside the tubes and another outside. Baffles direct the shell side flow alongside and across the tubes. As a result, they increase the velocity and turbulence of the flow, increasing the heat transfer(ibid.). In addition to the thermal benefits, the baffles also physically support the tubes and reduce vibration. On the other hand, the baffles cause a higher pressure drop on the shell side (Næss n.d.). Typically, shell and tube heat exchangers are advantageous at high pressure and temperatures (Shah and Sekulić 2003). A typical design of a two-pass shell-and-tube heat exchanger is illustrated in figure 3.4 (Serth and Lestina 2014).

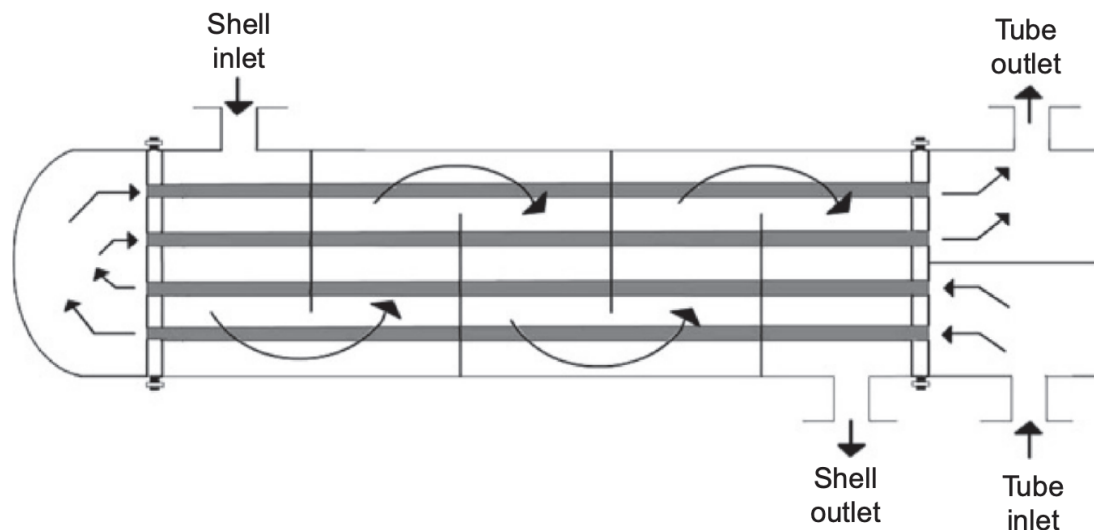


Figure 3.4: Illustration of a shell-and-tube heat exchanger (Serth and Lestina 2014).

Plate heat exchangers

Plate heat exchangers usually consist of thin plates that are either smooth or have a corrugation. The fluids flow between the plates on each side, which gives a large heat

transfer area. These heat exchangers are limited to low pressures and temperatures, and they do not accommodate large pressure or temperature differences between the fluids. (Shah and Sekulić 2003)

Plate-and-shell-exchangers

Plate and shell heat exchanger is a welded plate type heat exchanger. It consists of round corrugating plates mounted in a pressure vessel. An example of a corrugated plate, and how they are packed, are shown in figures 3.5b and 3.5c (Vahterus 2021). Same as for the plate type, fluid flow between the corrugating plates. A typical flow arrangement for plate-and-shell heat exchangers are illustrated in figure 3.5a (Freire and Andrade 2014). This type of heat exchanger is designed to combine the best qualities of plate heat exchangers and shell and tube heat exchangers, with a high heat transfer rate and handling high pressures and temperatures (Bandeira et al. 2020). Plate-and-shell from the manufacturer Vahterus is the type of heat exchanger used in the glycol regeneration process on the Equinor glycol regeneration process.

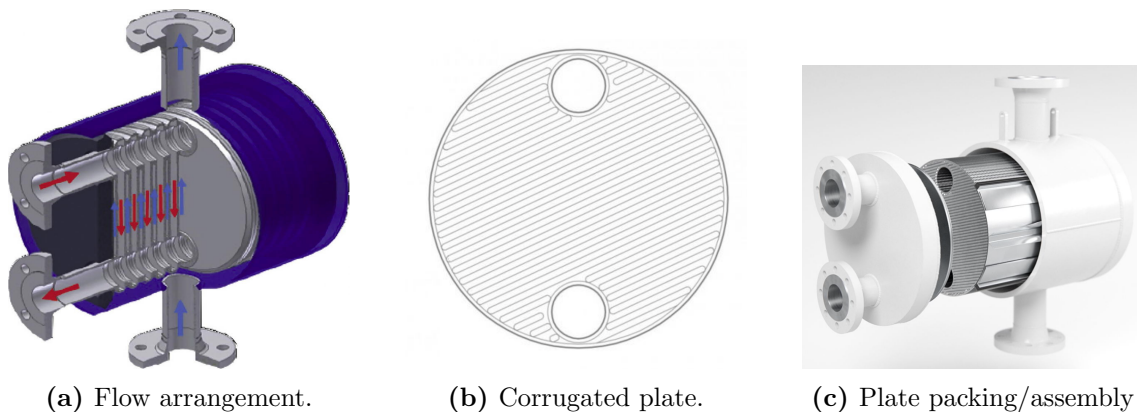


Figure 3.5: Plate-and-shell heat exchanger.

3.3 Heat exchanger fouling

Fouling occurs in almost all heat transfer processes. It is defined as the unwanted deposition of insulating material on a hot surface. Fouling will reduce the efficiency of the heat exchanger due to its insulating effect. In addition, the flow cross-section is reduced, which results in a higher pressure drop. In units with high heat flux, fouling can also lead to local overheating. Fouling can be classified by the following (Shah and Sekulić 2003) (Næss n.d.):

Precipitation or crystallization fouling - If a fluid containing dissolved organic salts becomes supersaturated, crystals will precipitate, adhere to the wall, and

form coatings.

Particulate fouling - Solid particles in both liquid and gas streams deposit on surfaces and form coatings.

Chemical reaction fouling - Chemical reactions in the fluid close to the heat transfer surface can result in a fouling layer.

Corrosion fouling - Process fluid reacts with the heat transfer surface, and corrosion products deposit on the surface.

Biological fouling. - Proceeds from the attachment and growth of organisms to the heat transfer surface.

Freezing (solidification) fouling. - It occurs when the surface temperature is lower than the freezing point of the fluid.

The accumulation of deposits on the heat exchanger surface increases the total overall resistance to the heat transfer. Figure 3.6 illustrates the same case as in figure 3.2, but the heat transfer surfaces are subjected to fouling. The thermal conductivity of the fouling substances is generally deficient compared to metals used in heat exchangers. Hence, considerable temperature differences are required to drive the heat through the coatings (Bott 1995).

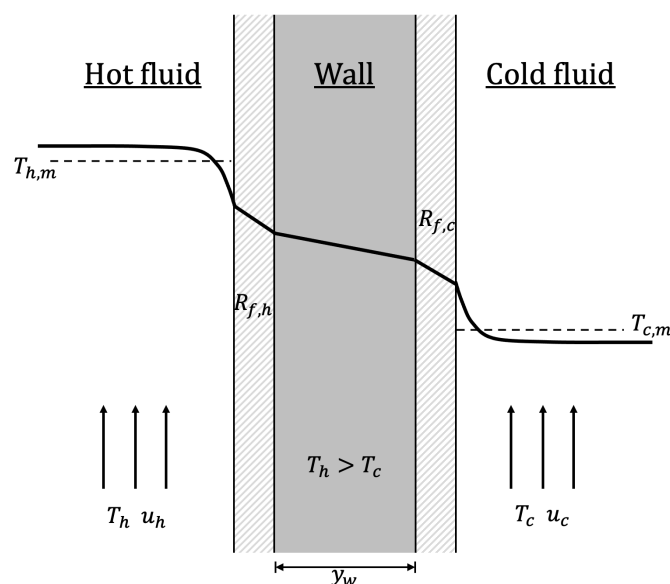


Figure 3.6: Illustration of temperature distribution across a fouled heat exchanger surface.

3.3.1 Fouling resistance

Compared to figure 3.6 the fouled heat exchanger now introduces two new thermal resistances $R_{f,h}$ and $R_{f,c}$ on the hot and cold side of the heat exchanger, respectively. As described in section 3.2.1, the total thermal resistance for the heat transfer, shown by equation (3.8), is the sum of all resistances (Kakaç et al. 2020).

$$R_{tot} = \frac{1}{(hA)_h} + R_{f,h} + \frac{y_w}{(kA)_w} + R_{f,c} + \frac{1}{(hA)_c} \quad (3.8)$$

In many cases, evaluating the overall heat transfer coefficient is of interest. For example, in a fouled heat exchanger, the heat transfer coefficient will be lower than the coefficient for clean conditions of the same exchanger. By utilising the relation between thermal resistance and heat transfer coefficient presented in equation 3.7, the fouling factor can be determined by comparing clean conditions with actual fouling conditions. The correlation between the actual and clean overall heat transfer coefficient and the fouling resistance, is presented in equation 3.9 (Næss n.d.).

$$\frac{1}{U_{actual}} = \frac{1}{U_{clean}} + R_f \quad (3.9)$$

Initiation and development of fouling are affected by several factors. The degree of impact is strongly dependent on the type of coating one is dealing with. In many cases, several types can coincide. Figure 3.7 illustrates four different scenarios for how the time-dependent fouling resistance grows.

The linear fouling behaviour indicates that the difference between the deposition and the removal rate is constant. A decreasing deposition rate typically means that the deposition rate is decreasing but remains higher than the removal rate. Asymptotic fouling behaviour indicates that the deposited layer is fragile. When the layer reaches a certain thickness, the removal rate due to the fluid shear stresses equals the deposition rate. (Bott 1995) As the fouling layer ages, it decreases in strength and coherence. This ageing process causes the sawtooth behaviour, as the layer becomes receptive to the removal processes (Shah and Sekulić 2003). The different curves have an initiation period t_d . The initiation period can be very challenging to predict, so it is ignored in most mathematical models for fouling (Bott 1995).

Calculating the overall heat transfer coefficient of a heat transfer process subjected to fouling is complicated. Factors such as fluid properties and conditions, heat

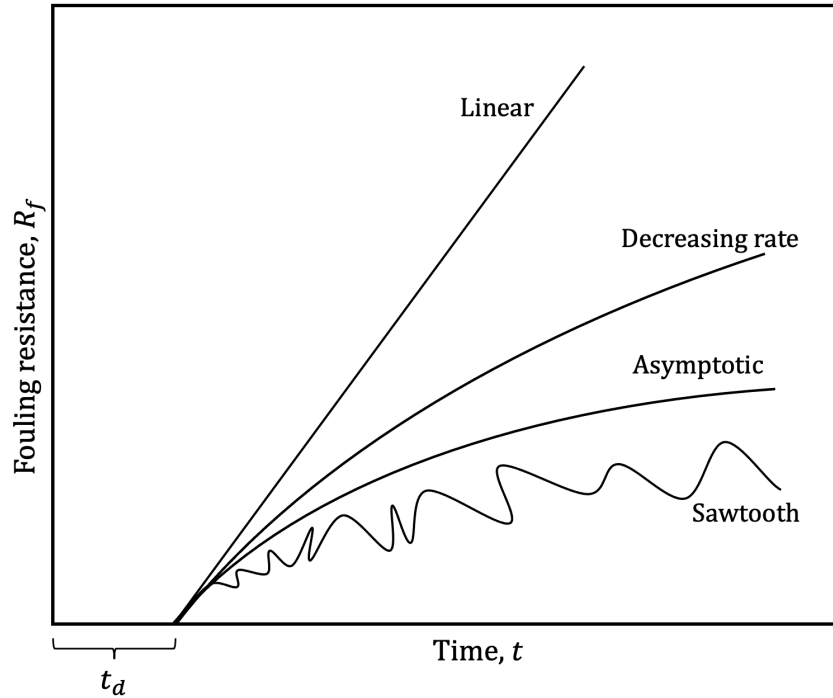


Figure 3.7: Illustration of the time dependence of the fouling resistance.

exchanger geometry and configuration, temperature and time impact the fouling development and the effective resistance of the deposited layer. Therefore, the fouling resistance is typically chosen from data from experience to estimate the overall heat transfer coefficient when designing common heat exchangers. Table 3.1 presents the heat transfer coefficients and fouling resistances for selected fluid conditions for a shell-and-tube heat exchanger (Næss n.d.).

Table 3.1: Typical heat transfer coefficients and fouling resistances for shell-and-tube heat exchangers for different fluids (Næss n.d.).

Fluid condition		h [W/m^2K]	R_f'' [m^2K/W]
Water	Liquid	5 000 - 7 500	$1 \times 10^{-4} - 2.5 \times 10^{-4}$
Light organics	Liquid	1 500 - 2 000	$1 \times 10^{-4} - 2 \times 10^{-4}$
Medium organics	Liquid	750 - 1 500	$1.5 \times 10^{-4} - 4 \times 10^{-4}$
Heavy organics	Liquid		
	Heating	250 - 750	$2 \times 10^{-4} - 1 \times 10^{-3}$
	Cooling	150 - 400	$2 \times 10^{-4} - 1 \times 10^{-3}$
Gas	Pressure 1 - 2 bar	80 - 125	$0 - 1 \times 10^{-4}$
Gas	Pressure 10 bar	250 - 400	$0 - 1 \times 10^{-4}$
Gas	Pressure 100 bar	500 - 800	$0 - 1 \times 10^{-4}$

3.3.2 Mitigation of fouling and cleaning

The deposited layer must be removed from the heat transfer surface when fouling reduces the heat exchanger's performance below an acceptable level. There are several available technologies concerning mitigating fouling and cleaning heat transfer surfaces. Generally, these technologies are separated into online and offline cleaning (Kulacki et al. 2018).

Online methods aim to preclude the formation of fouling deposits during operation. The most common examples of online technologies are filters, biocides, electrical and magnetic treatment, continuous cleaning projectiles, inhibitors, and pulsed acoustic and ultrasonic energy. Filters are used to prevent particulate build-up and sediment. Biocides, or chemical agents, are used to hinder biological growth in water. Electrical and magnet treatment is a principle where an electromagnetic field is applied to a water flow to reduce bio- and crystallisation fouling. Continuous cleaning projectiles are systems where projectiles consisting of sponge balls and brushes are injected into the equipment. Inhibitors are chemicals used to mitigate crystallisation and corrosion fouling. At last, Pulsed acoustic and ultrasonic energy are used to diminish bio- and chemical reaction fouling (ibid.).

Offline cleaning methods differ from online methods in that they require a complete shut down of the heat exchanger. These cleaning methods are effective in the removal of fouling layers but do not mitigate the gradual degradation due to fouling. Offline methods are generally distinguished into mechanical and chemical cleaning methods (Müller-Steinhagen et al. 2011). Mechanical cleaning methods involve the use of high-pressure water jets, brushes or scrapers, air pressure systems, and the launching of projectiles inside tubes (ibid.)(Kulacki et al. 2018). Chemical cleaning involves circulating different chemical cleaning agents over the heat transfer surface. Acidic and alkaline solutions penetrate the fouling layer, where the deposits get loosened and removed. Alkaline solutions can remove organic fouling, and acidic solutions can remove biofouling(ibid.). A downside with offline cleaning is that both mechanical and chemical cleaning can also remove parts of the protective oxide layer on the surfaces, which again can result in corrosion problems. However, regular removal of fouling deposits avoids the development of chemical environments and flow conditions that promote corrosion. Mechanical and chemical cleaning methods can be used in a combination, which is recommended for heat exchangers subjected to severe fouling(Müller-Steinhagen et al. 2011).

4 Heat exchanger calculations

This chapter presents the different heat exchanger calculations utilised in this work. It also describes the different heat transfer correlations relevant for a heat exchanger, which is essential to understanding the condition monitoring methods in chapters 5 and 7. This chapter is divided into three sections. Parts of this chapter is also a continuation of the project work. Section 4.1 presents analytical methods for calculating the heat transfer in a heat exchanger. Further, section 4.2 describes the different heat transfer correlations determined by flow regime. Finally, section 4.3 presents pressure drop correlations for single-phase and two-phase flow.

4.1 Analytical soultuions

In order to evaluate or predict the performance of a heat exchanger, it is important to understand the correlation between heat transfer q , the overall heat transfer rate U , heat transfer surface A and inlet/outlet temperatures T . In section 3.1.5, the correlation between thermal resistance and the overall heat transfer coefficient is presented. By considering the two fluids and a plane wall in figure 3.2, the heat transfer between the fluids is defined in equation (4.1). Where ΔT_m is the mean temperature difference between the two fluids.

$$q = UA\Delta T_m \quad (4.1)$$

The energy balance of the simple heat transfer between two fluids, shown in figure 3.2, is presented by equation (4.2). This energy equation is valid under the assumption of constant overall heat transfer coefficient, mass flow, and heat capacity, as well as negligible heat transfer with the surroundings. Where T_i and T_o is the mean temperatures in and out of the exchanger, \dot{m} is the mass flow, c_p is the specific heat capacity and the subscripts h and c denotes to the hot and cold fluid (Incropera et al. 2011).

$$q = \dot{m}_h c_{p,h} (T_{h,i} - T_{h,o}) = \dot{m}_c c_{p,c} (T_{c,o} - T_{c,i}) \quad (4.2)$$

The specific heat is dependent on the temperature and will vary to some degree due to temperature variations. In addition, the overall heat transfer coefficient will change with changes in fluid properties or flow conditions. Despite this, it is feasible to use average values for c_p and U in applications where variations are not significant

(Incropera et al. 2011).

As presented in section 3.2.1 the simplest configuration of a heat exchanger is a counterflow double pipe heat exchanger. For this type of heat exchanger the appropriate mean temperature difference ΔT_m in equation (4.1) is the log mean temperature difference $LMTD$ defined in equation (4.3) (ibid.).

$$\Delta T_m = \frac{(T_{h,i} - T_{c,o}) - (T_{h,o} - T_{c,i})}{\ln \left(\frac{T_{h,i} - T_{c,o}}{T_{h,o} - T_{c,i}} \right)} \equiv LMTD \quad (4.3)$$

4.1.1 F-factor method

For flow arrangements other than a pure counterflow heat exchanger, ΔT_m can not be determined by only considering the log mean temperature difference. Hence, the F-factor method is introduced. The F-factor method applies the energy equation (4.1) with a correction factor F for $LMTD$, presented in equation (4.4) (Næss n.d.).

$$\Delta T_m = LMTD \cdot F \quad (4.4)$$

The F-factor expresses the ratio between the area of a counterflow heat exchanger with the required area for the given case. The use of the F-factor varies with different references, but the principle is the same. It can be determined based on geometry, flow pattern and thermal efficiency. For a counterflow heat exchanger, the correction factor is $F = 1$. For other arrangements it will always be $F \leq 1$. For a good design, $F \geq 0.75$, and if $F < 0.7$, then another heat exchanger configuration should be considered (ibid.).

4.1.2 Effectiveness-NTU method

The effectiveness of a heat exchanger can be determined by considering the ratio of actual heat transfer rate to the maximum possible heat transfer rate. The maximum possible heat transfer q_{max} is determined by evaluating an idealised counterflow heat exchanger with infinite surface area and no wall heat conduction. q_{max} is used as a benchmark to estimate the effectiveness of a heat exchanger, ranging from 0 to 1. The thermal effectiveness ε is given by equation (4.5), where $C = \dot{m}c_p$ is the heat capacity rate and C_{min} is the minimum value of C_h and C_c (Shah and Sekulić 2003).

$$\varepsilon = \frac{q}{q_{max}} = \frac{C_h (T_{h,i} - T_{h,o})}{C_{min} (T_{h,i} - T_{c,i})} = \frac{C_c (T_{c,o} - T_{c,i})}{C_{min} (T_{h,i} - T_{c,i})} \quad (4.5)$$

The number of transfer units, or NTU , is a dimensionless parameter defined as the ratio of the overall thermal conductance to the minimum heat capacity rate, presented in equation (4.6) (Shah and Sekulić 2003).

$$NTU = \frac{UA}{C_{min}} \quad (4.6)$$

For any heat exchanger, the thermal effectiveness can be expressed as a function of NTU and the heat capacity ratio $C_r = C_{min}/C_{max}$, as shown in equation (4.7) (Incropera et al. 2011).

$$\varepsilon = f(NTU, C_r) \quad (4.7)$$

The result of equation (4.7) varies for different types of heat exchangers. The correlation of equation (4.7) depends on the flow arrangement in the heat exchanger. Hence, a variety of expressions to this equation have been established. Some selected examples for relevant heat exchanger effectiveness relations are presented in table 4.1 (ibid.).

Table 4.1: Heat exchanger effectiveness relations for selected heat exchanger (Incropera et al. 2011)

Flow arrangement	Relation
Parallel flow	$\varepsilon = \frac{1 - \exp[-NTU(1+C_r)]}{1+C_r}$
Counterflow	$\varepsilon = \frac{1 - \exp[-NTU(1-C_r)]}{1-C_r \exp[-NTU(1-C_r)]} \quad (C_r < 1)$
	$\varepsilon = \frac{NTU}{1+NTU} \quad (C_r = 1)$
Shell-and-tube	
One shell pass(2,4,... tube passes)	$\varepsilon_1 = 2 \left[1 + C_r + (1 + C_r^2)^{1/2} \times \frac{1 + \exp[-(NTU)_1(1+C_r^2)^{1/2}]}{1 - \exp[-(NTU)_1(1+C_r^2)^{1/2}]} \right]^{-1}$
n shell pass($2n, 4n, \dots$ tube passes)	$\varepsilon = \left[\left(\frac{1 - \varepsilon_1 C_r}{1 - \varepsilon_1} \right)^n - 1 \right] \left[\left(\frac{1 - \varepsilon_1 C_r}{1 - \varepsilon_1} \right)^n - C_r \right]^{-1}$
All exchangers ($C_r = 0$)	$\varepsilon = 1 - \exp(-NTU)$

4.2 Heat transfer correlations

There are several correlations to determine the heat transfer coefficient h , and with no knowledge of the plate-and-shell design, general correlations for internal flow will be presented. However, the heat transfer coefficient is usually not straightforward to determine. Hence, the Nusselt number is defined as the correlation between convective heat transfer and conduction heat transfer for fluid under the same conditions. The definition of the Nusselt number Nu is presented in equation (4.8), where h and k is the fluid convective heat transfer coefficient and conductivity, respectively, and D_h is the hydraulic diameter (Incropera et al. 2011).

$$Nu = \frac{hD_h}{k} \quad (4.8)$$

For laminar flow, the heat transfer coefficient only depends on conductance and the geometry of the duct. For example, for a case with fully developed laminar flow in a circular tube with a constant heat rate, the Nusselt number is constant, as shown in equation (4.9) (Næss n.d.).

$$Nu = \frac{hD}{k} = 4.364 \quad (4.9)$$

For fully developed turbulent flow, empirical correlations for the Nusselt number is applied. The Nusselt number can be determined by the geometry of the duct, the Reynolds number Re , and the Prandtl number Pr . The empirical correlation for the Nusselt number is typically on the form presented in equation 4.10, where C_0 , C_1 and C_2 are constants (Incropera et al. 2011) (D. Taler and J. Taler 2017). An example of this is the Dittus-Boelter correlation presented in equation (4.11), which can be used to determine the Nusselt number for turbulent flow in a smooth circular tube (Incropera et al. 2011).

$$Nu = f(\text{geometry}, Re, Pr) = C_0 Re^{C_1} Pr^{C_2} \quad (4.10)$$

$$Nu = \begin{cases} 0.0243 Re^{0.8} Pr^{0.4} & \text{for heating} \\ 0.0265 Re^{0.8} Pr^{0.3} & \text{for cooling} \end{cases} \quad (4.11)$$

The Prandtl number Pr is defined as the ratio of kinematic viscosity to thermal

diffusivity, and the Reynolds number Re is defined as the ratio of inertial to viscous force and is presented in equation (4.12). Where ρ is the density and μ is the dynamic viscosity of the fluid. D_h is the hydraulic diameter. For non-tubular flow and channels, the hydraulic diameter correlates to the wetted perimeter P , where $D_h = \frac{4A}{P}$. The Reynolds number characterises the flow regime, a high and low Reynolds number indicates a turbulent and laminar flow, respectively. For example, in a tubular flow, the transition from laminar to turbulent flow begins at a Reynolds number around 2300 (Incropera et al. 2011).

$$Re = \frac{\rho u_m D_h}{\mu} \quad (4.12)$$

It has been shown that the Nusselt number for laminar flow is constant and independent of the velocity. However, for turbulent flow, the Nusselt number depends on the velocity. An increase in velocity increases the Reynolds number and the Nusselt number. Thus, increased turbulence of a flow increases the heat transfer coefficient.

4.2.1 Condensation

Understanding the heat transfer mechanisms of condensation is essential when considering a heat exchanger where condensation transpires. Condensation occurs when the temperature of a fluid in the gas phase gets lower than the fluid's dew point. In a process plant, this usually happens when hot steam comes in contact with a cold surface, the latent energy of the gas is released, heat gets transferred to the surface, and liquid condensate gets produced. There are two types of surface condensation, droplet and film condensation (ibid.).

Figure 4.1a shows the boundary layer effects for film condensation on a vertical wall for laminar flow and constant properties for the fluid film, and the gas is pure steam. The boundary layer thickness $\delta(x)$ increases with the vertical length x as more vapour condenses (ibid.).

Condensation in tube flow is illustrated in figure 4.1. For low velocities, illustrated in figure 4.1b, the vapour condenses in the tube's upper part, flows down, and settles in a pool at the bottom part of the tube. Shear forces between the gas and the liquid propel the liquid onwards in the tube. For low velocities, the Reynolds number is calculated using equation (4.13), where the subscript i refers to the tube and v to the vapour flow. The Nusselt correlation for low velocity tubular condensation is presented in equation (4.14), where $h'_{fg} = h_{fg} + 0.375c_{p,l}(T_{sat} - T_s)$ (Incropera et al.

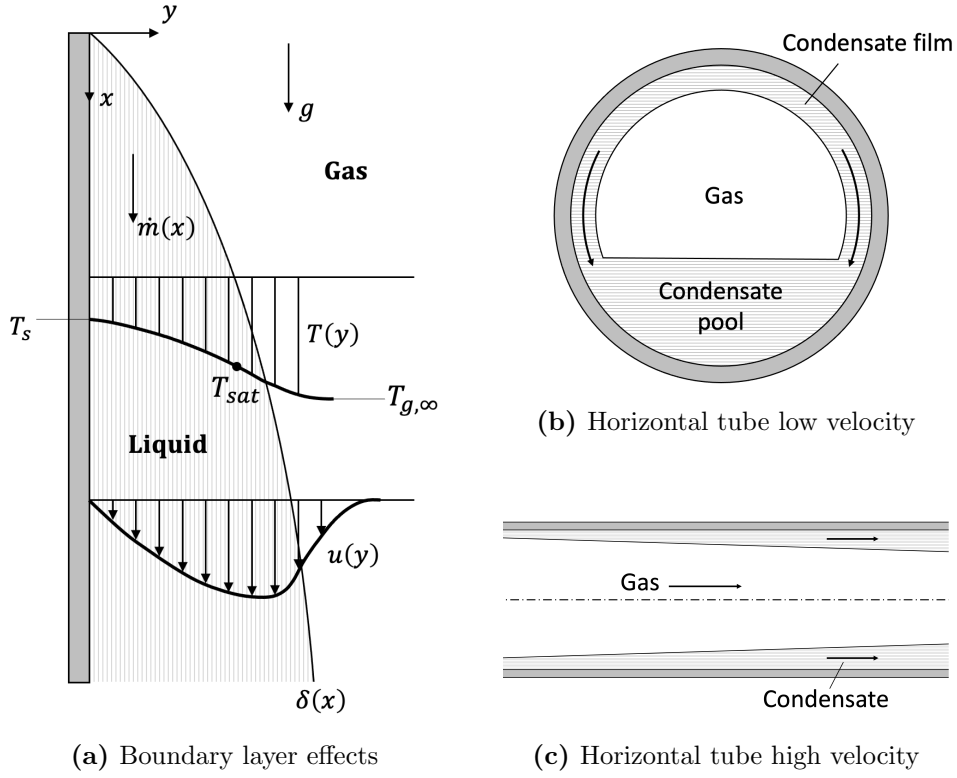


Figure 4.1: Illustration of different cases of film condensation. (a) Boundary layer effects for condensation on a vertical surface. (b) Cross-section of a condensing flow inside a horizontal tube at low velocity. (c) Longitudinal section of a condensing high-velocity flow inside a horizontal tube.

2011).

$$Re_{v,i} = \left(\frac{\rho_v u_{m,v} D}{\mu_v} \right)_i < 35000 \quad (4.13)$$

$$N\bar{u}_D = \frac{\bar{h}_D D}{k_l} = 0.729 \left[\frac{\rho_l g (\rho_l - \rho_v) h'_{fg} D^3}{\mu_l k_l (T_{sat} - T_s)} \right]^{1/4} \quad (4.14)$$

For tubular flow condensation at high velocities, illustrated in figure 4.1c, the flow becomes annular and turbulent. The gas flows in the centre with decreasing radius as more gas condenses into liquid. The heat transfer coefficient is calculated using suitable empirical correlations for the Nusselt and Reynolds number (ibid.).

4.3 Pressure drop

Fluids flowing through heat exchangers are subjected to a pressure drop. Pressure losses relevant for heat exchangers for one and two-phase flow will be presented.

4.3.1 Single liquid phase pressure drop

The pressure drop in a liquid phase plate-and-shell heat exchanger is the summation of pressure losses due to frictional forces, hydraulic head changes and losses at inlet and outlet. The pressure loss component is expressed in equation (4.15). ΔP_{tot} is the total pressure drop through the exchanger, ΔP_f is the frictional pressure drop, ΔP_g is the gravity head loss, and ΔP_m is the pressure loss at the inlet and outlet (Wang et al. 2020).

$$\Delta P_{tot} = \Delta P_f + \Delta P_g + \Delta P_m \quad (4.15)$$

The frictional pressure drop can be expressed by equation (4.16), where f is the friction factor, D_h is the hydraulic diameter, u is the velocity, and L_{eff} is the effective flow length (ibid.).

$$\Delta P_f = f \frac{\rho u^2}{2} \frac{L_{eff}}{D_h} \quad (4.16)$$

The friction factor can be obtained from equation (4.16) for fully developed laminar flow (Incropera et al. 2011).

$$f = \frac{64}{Re} \quad (4.17)$$

For fully developed turbulent flow, the friction factor can be obtained from the Colebrook equation (4.18), where e is the surface roughness (ibid.).

$$\frac{1}{\sqrt{f}} = -2.0 \log_{10} \left[\frac{e/D_h}{3.7} + \frac{2.51}{Re\sqrt{f}} \right] \quad (4.18)$$

The gravitational pressure drop can be estimated by equation (4.19), where Δz is the change in vertical length and g is the gravitational acceleration. The pressure loss at the inlet and outlet can be estimated by equation (4.20) (Wang et al. 2020).

$$\Delta P_g = \rho g \Delta z \quad (4.19)$$

$$\Delta P_m = 1.5 \frac{\rho u^2}{2} \quad (4.20)$$

From the equations presented, it is evident that the pressure drop is highly dependent on the velocity of the fluid. Frictional pressure drops, and the losses at the inlet and outlet increase exponentially with the flow rate. In addition, the friction factor is dependent on the flow rate. It is also worth mentioning that the friction factor varies when fouling occurs due to changes in the surface roughness. Fouling will also reduce the cross-sectional area in the heat exchanger, which will increase the flow velocity, and therefore the pressure drop.

4.3.2 Two-phase pressure drop

In a glycol regeneration process, heat exchangers can be subjected to fluids in a two-phase flow. The Lockhart-Martinelli method can be used to estimate the two-phase frictional pressure drop. It is a method using the two-phase multiplier ϕ_L^2 defined by the ratio of the two-phase to the single-phase liquid pressure gradient, presented in equation (4.21).

$$\phi_L^2 = \frac{(dP_f/dz)_{TP}}{(dP_f/dz)_l} \quad (4.21)$$

The Martinelli parameter, X^2 , is the ratio between the single liquid phase pressure gradient to the single gas phase pressure gradient. It is defined by equation (4.22), where $(dP_f/dz)_L$ is the liquid pressure gradient, and $(dP_f/dz)_G$ is the gas pressure gradient. Based on this, the two-phase multiplier can be expressed as equation (4.21) for smooth pipes, where C is dependent on the flow characteristics for the different phases (Wang et al. 2020).

$$X^2 = \frac{(dP_f/dz)_L}{(dP_f/dz)_G} \quad (4.22)$$

$$\phi_L^2 = 1 + \frac{C}{X} + \frac{1}{X^2} \quad (4.23)$$

5 Online Condition Monitoring

Offshore oil and gas platforms are usually attended by a permanent human crew running the daily production. The working environment is defined by complex process equipment that operates at high pressures and temperatures with highly combustible hydrocarbons. In addition to the hazardous environment, the platforms are remote with limited access. Implementing digitalised process control systems, automation, and robotic solutions reduces the number of people needed to run the operation. Online condition monitoring is one of the enablers for unmanned operations (Tan et al. 2020).

Online condition monitoring is the utilisation of measurements from equipment and software to continuously monitor the state of systems, machines, or processes. Online condition monitoring enables the prediction of equipment deterioration or failures. Hence, scheduled maintenance or preventive actions can be performed at the optimal moment to minimise downtime (ibid.). This chapter presents a selection of brief summaries of developed methods for condition monitoring heat exchangers. The chapter is divided into three sections, where section 5.1 presents thermal performance approaches. Section 5.2 presents research on a hydraulic performance approach. And lastly, section 5.3 presents research on a method utilising both the thermal and hydraulic performance.

5.1 Thermal performance

A common approach in the industry is to monitor the thermal performance of the heat exchanger. This is typically done by calculating or measuring the overall heat transfer coefficient for clean conditions without fouling and comparing it to the actual heat transfer coefficient to determine performance degradation. Following are examples of industry applications and research on condition monitoring using thermal performance.

Astorga-Zaragoza et al. 2008 present a method for monitoring the performance degradation in a counter-flow double-pipe heat exchanger. An adaptive observer is developed to estimate the overall heat transfer coefficient U based on temperature measurements. Observers are software sensors used as an alternative where there is a lack of online sensors. The observers estimate unknown parameters or state variables. An adaptive observer estimates the parameters simultaneously for the ongoing process. This method monitors U as a function of operational variables and uses the information to determine when the heat exchanger needs maintenance

(Astorga-Zaragoza et al. 2008).

The drawback of this model is that the observers are derived from a simplified lumped model and do not take care of spatial information. Hence, the model does not relate the overall heat transfer coefficient to the axial position in the heat exchanger. The benefit of this method is the small amount of input information the observers need to estimate the overall heat transfer coefficient U . It does not need any assumptions regarding system dynamics or any assumptions to initialise the computation (ibid.).

Jerónimo et al. 1997 presented a simplified method for performance monitoring by assessing the thermal efficiencies and the number of transfer units. This method considers the deviation between operational conditions and design conditions for heat exchangers. In other words, a heat exchanger's design conditions do not necessarily correspond to the actual operating conditions. Hence, to evaluate fouling and performance degradation, actual condition should be compared to a calculated clean condition based on flow rates, fluid conditions, physical properties etc. Due to these calculations being complex and time demanding, a simplified method is introduced. This procedure determines the degree of fouling by assessing the calculated thermal effectiveness ε_{actual} and the estimated effectiveness at clean and fouled conditions, ε_{clean} and ε_{dirty} , respectively. ε_{actual} is calculated based on measured temperatures at the inlet and outlet. ε_{clean} and ε_{dirty} are estimated based on a prediction of the number of transfer units for the given operation (ibid.).

5.2 Hydraulic performance

Mohanty and Singru 2011 present a method of monitoring a shell-and-tube heat exchanger for fouling using hydraulic performance. They introduce the C-factor, a parameter that correlates the pressure drop and mass flow in the heat exchanger. The C-factor correlation is defined by equation 5.1, where V is the volumetric flow rate and Δp is the pressure drop in the heat exchanger. The concept is developed from an analysis of a flow through a fixed-size orifice, and C_f is a constant, where $V = C_f \sqrt{\Delta p}$. The fouling layer will give a smaller flow area and change the surface friction factor. The deposited layer will cause the pressure drop to increase compared to the flow rate. Hence, the C-factor is constant for no fouling and will increase when fouling occurs (ibid.).

$$C_f = \frac{V}{\sqrt{\Delta p}} \quad (5.1)$$

An advantage of this method is the use of only two input parameters, flow rate and pressure difference, and simple calculations. Hence, this method does not require a high level of instrumentation or heavy mathematical calculations. Furthermore, the results indicate that the C-factor method detects fouling and performance degradation efficiently (Mohanty and Singru 2011).

5.3 Thermal and hydraulic performance

(Diaz-Bejarano et al. 2020) propose an analysis method and visualisation of operational data for condition monitoring heat exchangers using dynamic thermo-hydraulic monitoring, or the TH- λ plot. This method uses three different indicators: thermal, hydraulic and temporal, to monitor a heat exchanger. The thermal and hydraulic indicators are the ratio of actual to clean heat duty (Q/Q_{clean}) and pressure drop ($\Delta P/\Delta P_{clean}$), respectively. The temporal indicator is various intervals that show the time evolution. These thermal and hydraulic indicators are plotted as TH-lines at different time intervals. The TH-lines can be compared to either limit lines or conductivity lines. Limit lines are predetermined operational constraints for thermal and hydraulic performance. And conductivity lines (λ -lines) are reference lines of expected performance development for different constant deposit conductivities. These lines are calculated with a suitable thermo-hydraulic model with a uniform deposit. At last, a predicted thermal hydraulic line (PTH-line) can be included in the visualisation as a reference to predict the future fouling development of the heat exchanger. The PTH-line is calculated using fouling models adjusted to previous plant data (ibid.).

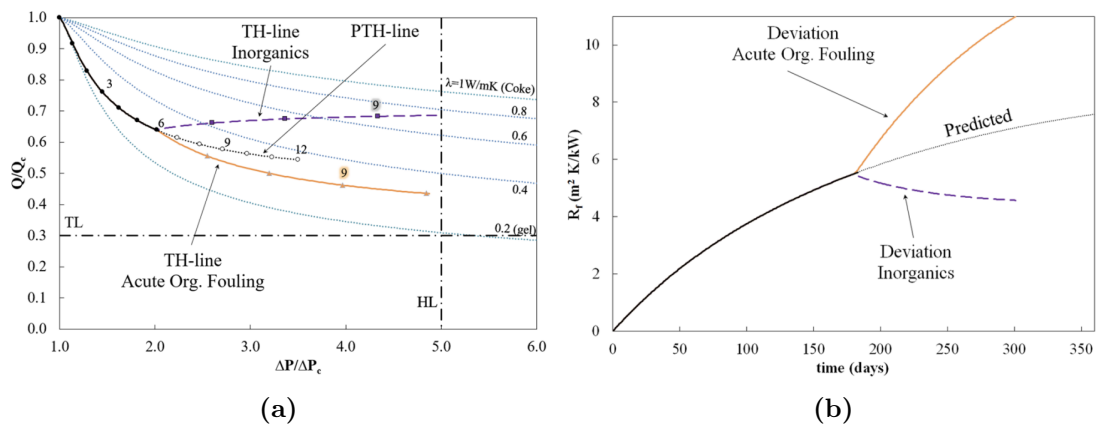


Figure 5.1: Performance of a heat exchanger subjected to changes in fouling behaviour. (a) Fouling resistance development over time (b) TH- λ plot.(Diaz-Bejarano et al. 2020)

Figure 5.1 shows the use of the TH-lambda model for two cases where the fouling deviate from the predicted performance due to acute fouling. This example shows

how the TH-lambda model can be used to monitor the changes in fouling behaviour as well as the thermal and hydraulic performance. The black line displays the plot of the TH-line for the six first months with a predicted fouling development for the next six months in the PTH-line. The thermal limit line (TL-line) is plotted horizontally and preset to 30%. The hydraulic limit line (HL-line) is plotted vertically and preset to 5 times the pressure drop for clean conditions. The lambda-lines are plotted for the development of organic fouling from fresh gel deposits, with $\lambda = 0.2W/mK$, to completely coked deposits, with $\lambda = 1.0W/mK$. The two cases show a deviation in fouling behaviour after six months due to acute organic and inorganic fouling because of changes in fluid conditions (Diaz-Bejarano et al. 2020).

6 Equipment setup and field data

This chapter describes the setup of the process around the heat exchangers on the Equinor glycol regeneration process. Equinor has provided P&IDs, process data sheets and field data for appropriate equipment and instrumentation used in this work. The data provided is from 29 September 2021 until 20 May 2022. This chapter goes through the processes in detail and highlights which instruments have been used in this work.

6.1 HX01 - Cold TEG/TEG exchanger

The cold TEG/TEG exchanger, hereinafter referred to as HX01, is a plate-and-shell type heat exchanger. The application of the HX01 is heat recovery from hot lean glycol to rich glycol.

Figure 6.1 illustrates the equipment set up around HX01 and the different streams in and out of the exchanger. Cold rich glycol enters from the reflux condenser at approximately 50°C and is heated to 70°C before it is routed to the flash drum. This temperature will allow efficient separation of potential liquid hydrocarbons in the flash drum. Hot lean glycol enters HX01 from the booster pumps, and cools down from approximately 97 to 76°C.

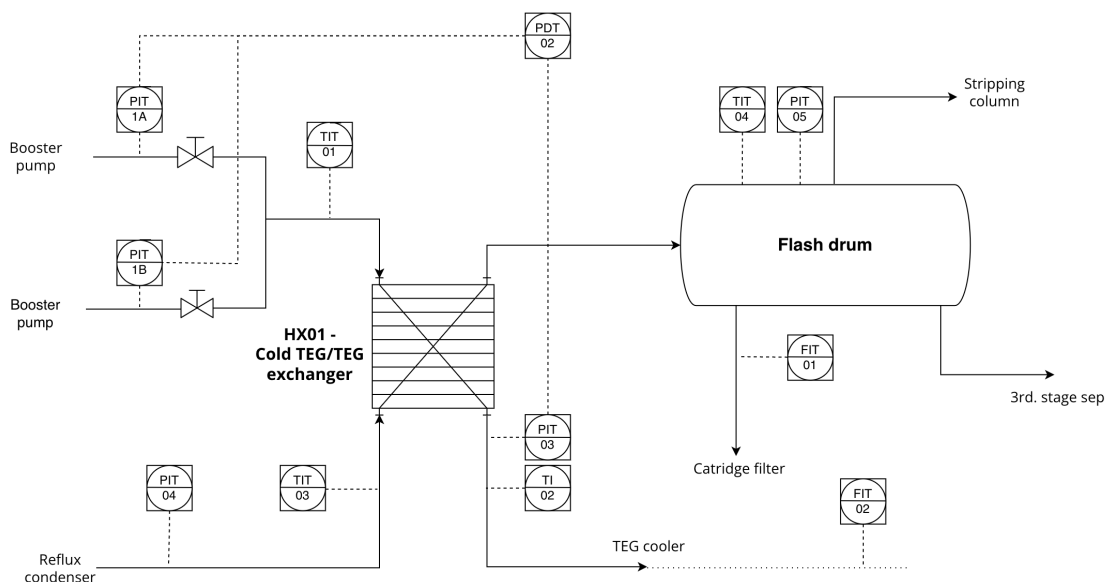


Figure 6.1: Flow diagram of the process equipment and instrumentation around the cold TEG/TEG exchanger.

For this work, the data is collected from the instrumentation shown in figure 6.1. There are temperature transmitters installed at the hot lean TEG inlet and outlet side of HX01, and the inlet of the cold rich TEG side. Pressure transmitters are installed at the inlet and outlet at the hot lean glycol side of the exchanger. These pressure transmitters are sending to a pressure difference transmitter measuring the pressure drop in the exchanger. For the cold rich glycol side there is a pressure transmitter installed on the inlet side. There is no instrumentation between the cold rich glycol side outlet and the flash drum. Hence, temperature and pressure transmitter inside the flash drum is used. The only flow rate transmitters available in the glycol regeneration process are placed downstream of the flash drum outlet for the rich glycol flow, and for the lean glycol flow it is placed downstream the recirculation pumps.

6.2 HX02 - Warm TEG/TEG exchanger

The warm TEG/TEG exchanger, referred to as HX02, is also a plate-and-shell type heat exchanger. The application of the HX02 is heating the rich TEG to approximately 150°C before it enters the still column.

Figure 6.2 illustrates the flow sheet of the equipment set up around the HX02 and the different streams in and out of the heat exchanger. Hot lean glycol, at around 180°C, from the stripping column is routed to HX02 heating rich glycol coming from the activated carbon filter. The rich glycol is heated from approximately 67°C to 146°C before it is routed to the still column. Lean glycol leaves the exchanger at about 96°C and is sent to the surge drum.

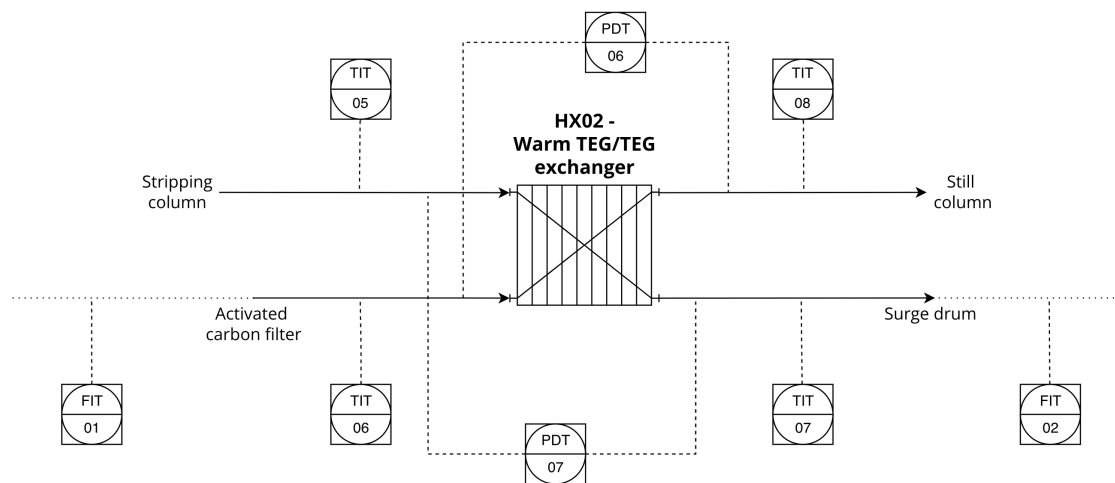


Figure 6.2: Flow sheet of the process equipment and instrumentation around HX02.

For this heat exchanger, there are installed pressure difference transmitters measuring the pressure loss in the exchanger for both streams. In addition, there are temperature transmitters at all inlet and outlet streams of the heat exchanger. Figure 6.2 shows the schematic placement of the different instrumentation. For HX02, the rich glycol flow rate can easily be measured using the flow rate transmitter installed upstream for the filters. Determining the lean glycol flow rate is more problematic, as the flow rate transmitter is installed at the surge drum outlet. As described in chapter 2, the surge drum is used to regulate the amount of glycol in the system. Hence, the flow rate of lean glycol through the exchanger can not be determined by this transmitter since the flow rate in and out of the surge drum might not be the same.

6.3 HX03 - TEG Cooler

Lean TEG leaving from HX01 is further cooled down in the TEG cooler referred to as HX03. This cooler is a compact shell and plate type heat exchanger that aims to cool the lean TEG below a target temperature before entering the contactor.

Figure 6.3 shows a flow sheet of HX03 and illustrates the equipment set up around the exchanger. Lean TEG flows on the hot plate side and a cooling medium consisting of 70 wt% water and 30 wt% MEG on the cold shell side. Lean TEG flows from the HX01 and enters HX03 at approximately 76°C and leaves at around 47°C. The cooling medium's inlet temperature is approximately 15°C, and the outlet temperature is approximately 17.5°C. The flow rate of the cooling medium is regulated by a temperature control valve installed downstream of the outlet. Lean TEG leaving HX03 is routed to the circulation pumps before entering the contactor. The circulation pumps is installed on two different routes, and it is alternated which one is operational. The flow in these pipes is controlled by valves downstream of the pumps.

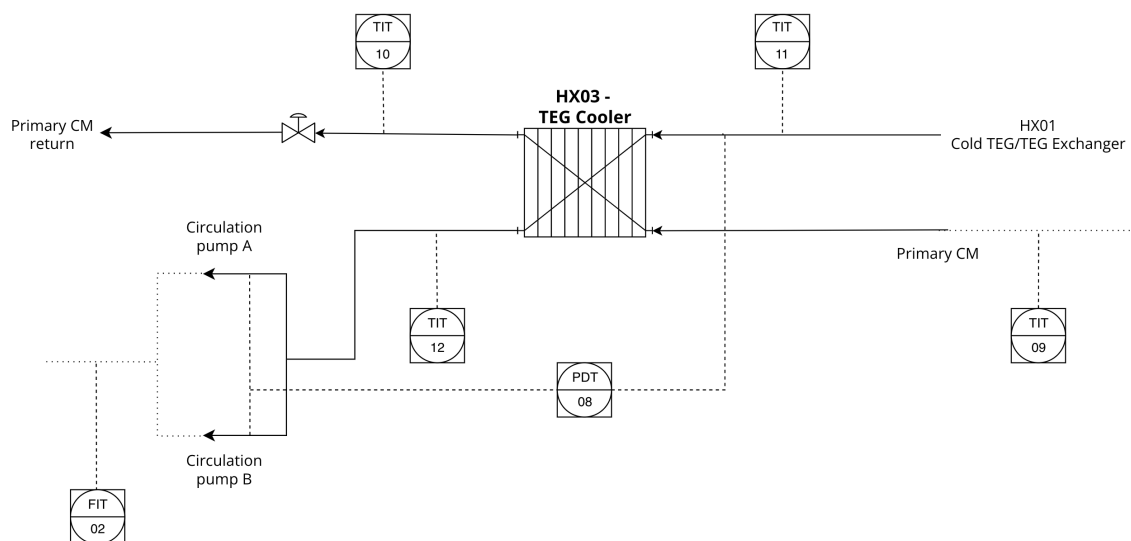


Figure 6.3: Flow sheet of the process equipment and instrumentation around the TEG cooler.

For HX03, there are temperature transmitters at the inlet and outlet for the hot TEG side of the heat exchanger. A temperature transmitter is installed only at the outlet for the cold cooling medium side. However, it is a temperature transmitter further upstream for the exchanger. This transmitter is general for the whole cooling medium system. There are no pressure or flow rate transmitters installed on the cooling medium flow side. On the hot lean TEG side, a temperature transmitter is installed at the inlet and outlet of the heat exchanger, as well as a pressure difference transmitter that measures the pressure drop between the heat exchanger inlet and before the circulation pump inlet for both pipe branches. Figure 6.3 shows the schematic placement of the different instrumentation mentioned.

6.4 HX04 - Overhead Condenser

The overhead condenser, referred to as HX04, is a shell and plate type heat exchanger. HX04 cools down overhead vapours leaving the reflux condenser on top of the reboiler, and water will condense. The cooled gas-liquid solution is then routed to the overhead receiver, where condensed water is separated from the overhead vapours.

Figure 6.4 illustrates the flow diagram and equipment setup around HX04. A gas mixture consisting mainly of water vapour and lighter hydrocarbons flows on the hot shell side of the heat exchanger, and a cooling medium flows on the cold plate side. The cooling medium is the same as in HX03, 70 wt% water and 30 wt% MEG. The inlet temperature of the cooling medium is approximately 15°C, and the outlet

temperature is around 25°C. The cooling medium flows at approximately 3900 kg/s. This flowrate is regulated by a control valve downstream of the cooling medium outlet of the heat exchanger. The overhead vapours enter HX04 at around 84°C and leave at approximately 50°C. The overhead vapour is a single gas phase at the inlet of HX04 and around 75-85 wt% gas at the outlet.

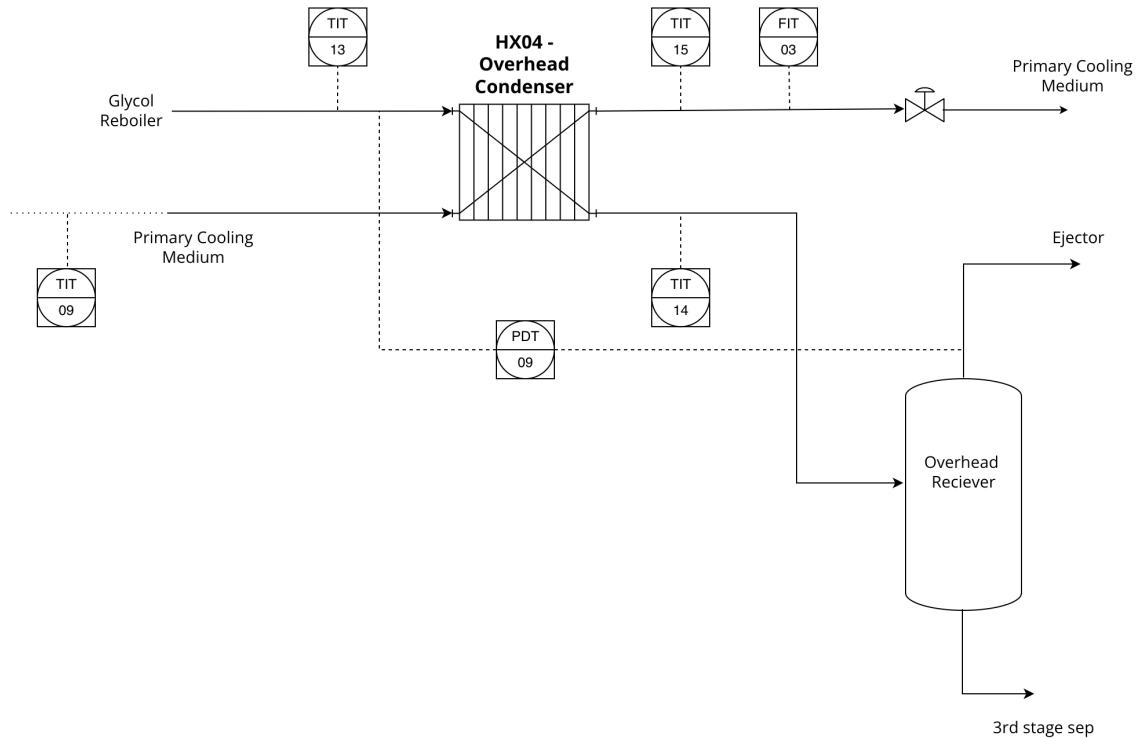


Figure 6.4: Flow sheet of the process equipment and instrumentation around the overhead condenser.

There are installed temperature transmitters for this heat exchanger at the inlet and outlet of the hot overhead vapours side. However, there is only a temperature transmitter at the outlet for the cold cooling medium side. As described for HX03, there is a temperature transmitter further upstream of the heat exchanger, which can be used to determine the inlet temperature of the cooling medium. There is no instrumentation for pressure measurement on the cold cooling medium side of the exchanger. For the hot overhead vapour side, it is a pressure transmitter at the inlet but not at the outlet. However, there is a pressure drop cell between the inlet transmitter and a pressure transmitter at the gas outlet of the overhead receiver. For flow rate measurements, a flow rate transmitter is installed at the cooling medium outlet. Furthermore, no flow rate instrumentation is installed for the overhead vapour stream. Figure 6.4 shows the schematic placement of the different instrumentation mentioned for HX04.

6.5 Neqsim - Non-Equilibrium Simulator

Neqsim is tool for estimation of fluid properties and process simutlation of oil and gas production. It is a library written in Java, although there are available toolboxes for the alternative programming languages Matlab, Python, and with restricted access .NET. Neqsim was developed by Even Solbraa at the Department of Energy and Process Technology NTNU (*Neqsim* 2021).

7 Methods of condition monitoring

This chapter presents the different methods utilised and evaluated for condition monitoring of the heat exchangers in this thesis. The models are based on the heat exchanger theory presented in chapters 3 and 4 and the previous research presented in chapter 5. The models will be calculated in Python using field data and simulations from Neqsim. The results from these models will be presented in chapter 8 and discussed in chapter 9. This chapter is divided into three sections, where section 7.1 introduces the thermal performance method. Further, section 7.2 presents the hydraulic performance method. At last, section 7.3 introduces the simulations conducted in HTRI Xchanger Suite.

7.1 Thermal performance method

As presented in chapter 5, there are some developed methods for performance monitoring of heat exchangers. But since they are primarily developed for shell-and-tube heat exchangers, the uncertainty of the correlation is too great to apply on a shell-and-plate heat exchanger. Therefore, a more simplified approach has been conducted for these shell-and-plate heat exchangers in order to determine the performance development over time.

The instrumentation level around the heat exchangers allows for a calculation of the overall heat transfer coefficient without knowing the design or geometries of the heat exchanger. Furthermore, by monitoring the development of the UA values, fouling can be indicated by a decrease in these values. As presented in chapter 3, fouling decreases the overall heat transfer coefficient and reduces the heat transfer surface. It would be optimal to know the clean conditions for the heat exchangers, but since the operation on the Equinor process is relatively new and there is no information about the heat exchangers being washed, the design value for UA will be used as a basis for comparison. Hence, by comparing the actual UA to the UA value for design conditions, the performance should decrease when fouling starts to influence the heat transfer. In addition, this gives an indication of how the heat exchanger is performing compared to the designed performance Figure 7.1 illustrates how the UA to UA_{design} ratio can develop over time for both clean and fouling conditions.

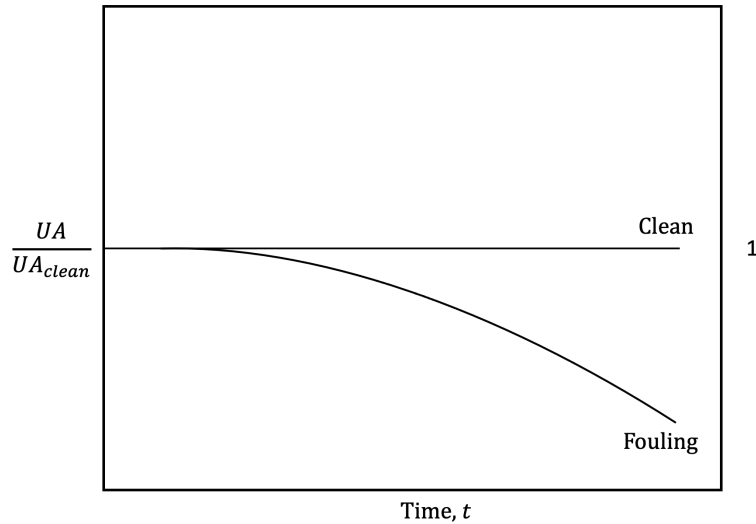


Figure 7.1: Illustration of the performance degradation due to fouling.

The thermal performance is calculated with UA_{design} values from the performance data sheet for the different heat exchangers. The operating UA value is calculated for each time stamp using the effectiveness NTU method presented in chapter 4. The model uses mass flow, specific heat capacity and inlet and outlet fluid temperatures for input parameters.

7.2 Hydraulic performance method

Due to the complexity of fouling and all the parameters that can influence heat exchanger conditions, it is not sufficient to only monitor the thermal performance development of the heat exchangers. Therefore, based on the presented C-factor method in 5, a hydraulic performance model will be applied to facilitate a better understanding of the total performance of the heat exchangers. As presented in section 4.3, the pressure drop is highly dependent on the velocity of the flow. Fouling in a heat exchanger will reduce the cross-sectional area of the flow, which will increase the velocity at a constant flow rate, increasing the pressure drop. In addition to the reduced flow area, the fouling material can increase the surface roughness, which will add to the pressure drop. Figure 7.2 presents an example of the pressure drop and flow rate behaviour of a shell and tube type heat exchanger at different degrees of fouling (Mohanty and Singru 2011).

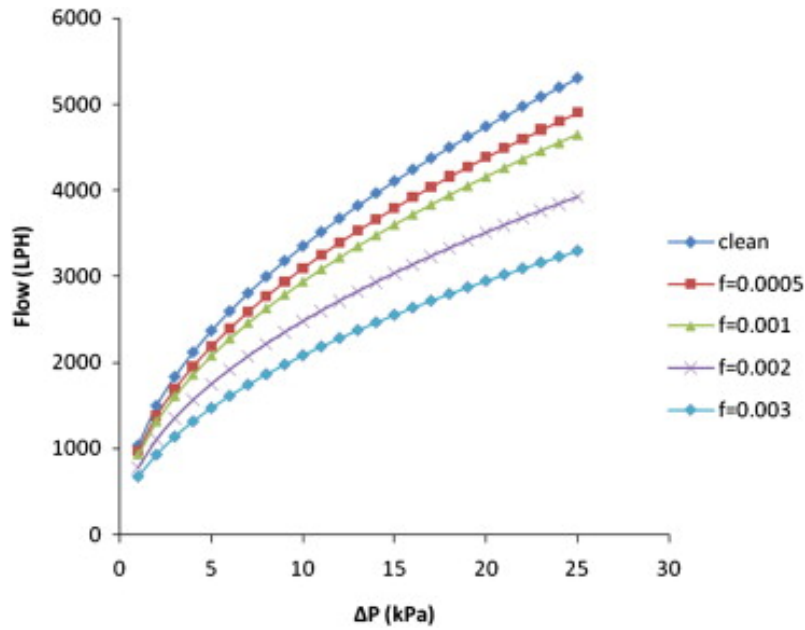


Figure 7.2: Variation of flow rate and pressure drop for different fouling factors (Mohanthy and Singru 2011)

A model based on the pressure drop divided by the mass flow squared is expected to directly correlate the variation in pressure drop and the flow rate. Figure 7.3 illustrates how a single-phase fluid is expected to behave with and without fouling. The rich glycol and overhead vapours in HX01, HX02 and HX04 are subjected to two-phase flow, and it will be valuable to investigate how this affects the pressure loss in the heat exchangers.

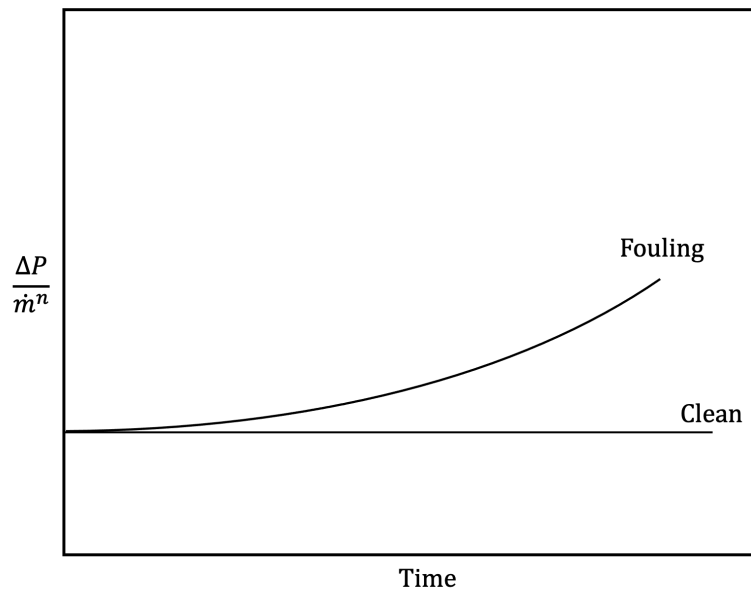


Figure 7.3: Illustration of pressure loss ratio development in a fouled heat exchanger.

7.3 HTRI Xchanger Suite

HTRI Xchanger Suite is a thermal process design and simulation software. This software can be utilised to design, rate, and simulate heat transfer equipment such as shell-and-tube and plate-and-frame heat exchangers.

Typical instrumentation around a heat exchanger is pressure, temperature, and flow rate transmitter. By only using this level of instrumentation, the heat exchanger performance and fouling development should be able to be monitored. However, numerous things can occur and alter with both the heat exchanger and the fluids, which again can impact the different measurable parameters. A simulation is conducted in HTRI Xchanger Suite to investigate how varying the conditions of the heat exchanger and the fluids affect the measurable values. A shell-and-tube heat exchanger is designed in HTRI Xchanger Suite for the design conditions of HX03, the TEG cooler. This heat exchanger design is then simulated for different operating cases presented in table 7.1.

Table 7.1: Overview of different case simulations conducted in HTRI Xchanger suite.

Case	Condition change	Details
1	Fouling on hot TEG side of the heat exchanger.	Fouling factor $R_f = 0.00035$
2	Fouling on cold CM side of the heat exchanger.	Fouling factor $R_f = 0.0002$
3	Fouling on both sides of the heat exchanger.	$R_f = 0.00035$ on hot TEG side and $R_f = 0.0002$ on cold CM side
4	Hot side composition change: Water in TEG.	95wt% TEG and 5wt% water
5	Hot side composition change: Liquid hydrocarbon in TEG.	95wt% TEG and 5wt% hexane
6	Hot side composition change: Condensing hydrocarbon in TEG	95wt% TEG and 5wt% propane
7	Geometry change: Reduced tube-to-baffle clearance by 50%.	0.4 mm reduction
8	Geometry change: Reduced baffle-to-shell clearance by 25%	2.38 mm reduction
9	Increased inlet temperature on hot side fluid by 10%.	Temperature increased from 77.5 to 85.25 degC
10	Decreased inlet temperature on hot side fluid by 10%.	Temperature decreased from 77.5 to 69.75 degC
11	Increased inlet temperature on cold side fluid by 10%.	Temperature increased from 15.0 to 16.5 degC
12	Decreased inlet temperature on cold side fluid by 10%.	Temperature decreased from 15.0 to 13.5 degC
13	Increased inlet pressure on hot side fluid by 10%.	Pressure increased from 2.4 bar to 3.6 bar
14	Increased flow rate on hot side fluid by 10%.	Flow rate increased from 1.474 to 1.621 kg/s
15	Decreased flow rate on hot side fluid by 10%.	Flow rate decreased from 1.474 to 1.327 kg/s
16	Increased flow rate on cold side fluid by 10%	Flow rate increased from 1.650 to 1.815 kg/s
17	Decreased flow rate on cold side fluid by 10%	Flow rate decreased from 1.650 to 1.485
18	Geometry change: Reducing the number of tubes.	Reducing from 42 tubes to 37.

8 Results

This chapter presents the results from the models and simulation described in chapter 7. The results will be further discussed in chapter 9. The results are divided into five sections. First, in section 8.1 are the results from the HTRI Xchanger Suite simulation. Further, a comparison between Neqsim simulation and the field data is presented in section 8.2. Then, the results from each heat exchanger are presented. Each heat exchanger is first presented with an overall comparison between the operating conditions and design conditions before the results from the thermal and hydraulic performance models are presented.

The results from HX01 is presented in section 8.3, HX02 in section 8.4, HX03 in section 8.5 and HX04 in section 8.6. The Python scrips for the essential functions used to calculate the results are presented in appendix C. The script used to conduct simulations in Neqsim is presented in appendix D. Finally, the scripts used to plot the figures in this chapter are presented in appendix E.

8.1 HTRI simulation

Key parameters from the heat exchanger design result in HTRI are presented in table 8.1. The complete design result is presented in appendix B. Drawings of 2D models of the heat exchanger design geometry are presented in appendix B. HX03 is used as a basis for the HTRI design. The same inlet and flow conditions were used, but for a simple shell-and-tube heat exchanger instead of a shell-and plate type heat exchanger. The presented heat exchanger is a TEMA AES type heat exchanger, with lean TEG flowing on the hot shell side and a cooling medium of 30 wt% MEG 60 wt% water flowing counter-currently on the cold tube side. The heat exchanger is designed with the operational conditions for HX03 on the hot TEG side and design conditions on the cold cooling medium side. In addition, the allowable pressure drop is increased from 0.05 to 0.5 bar compared to HX03. Clearances are chosen based on TEMA standards.

Table 8.1: Overview of different case simulations conducted in HTRI Xchanger suite.

Heat Exchanger Performance			
Fluid allocation		Shell Side	Tube Side
Fluid		TEG	Cooling medium
Flow rate	kg/s	1.47	1.65
Temperature in	°C	77.5	15
Temperature out	°C	47.5	31.0
Pressure in	bar	2.4	6.5
Pressure drop, allow/calc	bar	0.5/0.13	0.5/0.21
Average film coefficient	W/m ² K	748.5	2887.7
Heat transfer	kW		102.7
Heat transfer coefficient	W/m ² K		555.8
Heat exchanger geometry			
TEMA type			AES
Flow direction			Countercurrent
Shell inner diameter	mm		205
Number of tubes			42
Tube outer diameter/thickness	mm		16/1
Baffle-to-shell clearance	mm		3.175
Tube-to-baffle clearance	mm		0.79375

8.1.1 Case simulations

In this work, 18 different cases presented in 7.1 were simulated to determine the effects on monitored variables for a heat exchanger. These different cases were chosen based on typical operation variations and fouling development. The results of these simulations are presented in figure 8.1. This figure shows how the temperature difference, pressure difference, overall heat transfer coefficient and heat duty vary for the different cases compared to the design. Furthermore, each case will be presented in detail.

Case 1: The heat exchanger is simulated with a fouling layer on the hot tube side. The layer is set to a 3mm thickness and a fouling resistance of 0.00035. Due to a reduced flow area in the tubes and an increased roughness on the deposit surface, the pressure drop is increased by 16.2%. Due to the low thermal conductivity in the fouling layer, the overall heat transfer coefficient

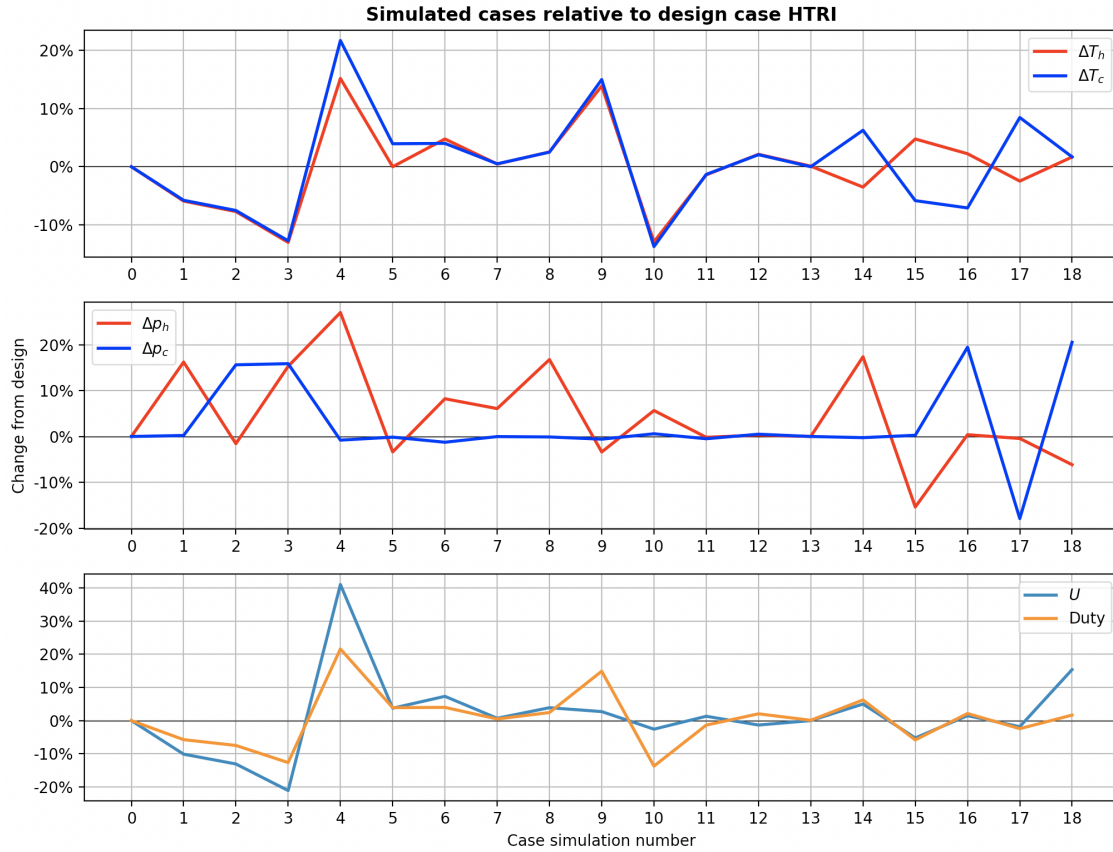


Figure 8.1: Comparison of case simulations to design for a shell-and-tube heat exchanger in HTRI Xchanger Suite.

and the heat transfer decrease by 10.1% and 5.7%, respectively. Hence, a lower temperature difference on both the hot shell side and the cold tube side.

Case 2: Simulation with fouling on the cold side of the heat exchanger. The fouling layer applies a fouling resistance of 0.0002, with a 2mm layer thickness. Similarly to case 1, the reduced flow area and change in surface roughness increases the pressure. In addition, thermal resistance increases, which causes a reduction in heat transfer. Hence, the pressure drop on the tube side increases by 15.3%, and the overall heat transfer coefficient decreases by 13.1%.

Case 3: This case simulates fouling on both sides of the heat exchanger. This is a combination of cases 1 and 2, with the same fouling factors. Fouling on both sides of the exchanger results in a 15.3% increased pressure drop on the hot shell side and 15.9% on the cold tube side. The heat transfer decreases by 12.7% and the overall heat transfer coefficient by 21.1%.

Case 4: The hot fluid composition is changed from 100 wt% TEG to 5 wt% water and 95 wt% TEG. The change in hot fluid composition results in a 27% increased pressure drop, 21.6% increased heat transfer, and 41% increased heat

transfer coefficient on the hot shell side.

Case 5: For this case, the hot fluid composition is changed to 5wt% hexane and 95wt% TEG. The hexane is in a single liquid phase for these heat exchanger conditions. Unlike in case 4, the pressure drop decreases slightly, but the heat transfer increases by changing the composition. The pressure drop decreases only by 0.2%, and the heat transfer increases by 3.7% and U by 3.8%.

Case 6: This is a case where a condensing hydrocarbon is added to the hot side. The hot fluid composition is changed to 5 wt% propane and 95 wt% water. The gas phase fraction at the heat exchanger inlet is 4.78%, and 4.71 at the outlet. Similarly to case 4, both the pressure drop and heat transfer increase. The pressure drop increases by 7.3%, heat transfer by 4% and heat transfer coefficient by 7.3%.

Case 7: For this case, the tube-baffle-clearance was reduced by 50%. This reduction imitates the effect of deposits in the space between the tubes and baffles. The effect of this change was a 6.1% increase in pressure drop only.

Case 8: Reduction of baffle-to-shell clearance by 25% to emulate the effect of deposits clogging the space between the baffle and the shell. This reduction in clearance increases the pressure drop on the shell side by 16.8% and slightly increases the heat transfer and U with 2.4% and 3.9%, respectively.

Case 9: Simulation of 10% increased inlet temperature on the shell side. This results in a 3.4% lower pressure drop on the shell side, 2.7% increased heat transfer coefficient and a 14.9% increased heat transfer.

Case 10: For this case, the inlet temperature on the shell side is reduced by 10%. This results in a 5.7% higher pressure drop on the shell side and a 13.7% lower heat transfer, and a 2.6% lower U value than the design.

Case 11: The inlet temperature of the cooling medium is increased by 10%. This has minimal effect on the resulting conditions. The pressure drop on the tube side decreases by 0.5%, the heat transfer decreases by 1.3% and the overall heat transfer rate increases by 1.3%

Case 12: The outlet temperature of the cooling medium side is decreased by 10%, and this also has a small effect on the conditions. 0.5% increase in tube side pressure drop, 2% increased heat transfer, and 1.3% decreased U value.

- Case 13:** For this case, the inlet pressure was increased by 10% on the shell side. The results of this simulation show that the change in heat exchanger conditions is insignificant. Moreover, both fluids were simulated with both higher and lower inlet pressure, and all results show a negligible change in conditions.
- Case 14:** This is a case where the flow rate of TEG is increased by 10%. The increased flow rate results in a 17.4% increased pressure drop on the shell side, 4.5% increased overall heat transfer coefficient, and 6.23% increased heat transfer.
- Case 15:** For this case, the flow rate of TEG is decreased by 10%. The reduced flow rate results in a 15.4% lower pressure drop, 5.2% lower heat transfer coefficient, and 5.8% lower heat transfer.
- Case 16:** The heat exchanger is simulated with a 10% increased flow rate on the tube side. As a result, the pressure drop on the tube side is increased by 19.5%, and the heat transfer and U value are increased by 2.14 and 1.5%, respectively.
- Case 17:** This case is simulated with a 10 reduced flow rate on the tube side of the heat exchanger. The reduced flow rate of cooling medium result in a 17.9% lower pressure drop on the tube side, 1.83% lower U value and 2.4% lower heat transfer.
- Case 18:** The last case simulation is a geometry change, where 12% of the tubes are removed. The removal of tubes is to mimic the effect of clogged tubes due to fouling. By removing five tubes, the pressure drop on the tube side increases by 20.5%, the pressure drop on the shell side decreases by 6.1%, the U value increases by 15% and the heat transfer increases by 1.7%.

8.1.2 Condition monitoring of case simulation

The condition monitoring methods presented in chapter 7 are applied to the HTRI case simulation results to evaluate the efficiency of the methods. Figure 8.2 presents the results for the hydraulic and thermal performance of the different case simulations relative to the design. The hydraulic performance on the hot shell TEG side increases by 16.2% and 15.3% for cases 1 and 3, where fouling is applied. There is a substantial increase of 24% for case 4, where water is present in the TEG. Cases 5 and 6 are the other cases with fluid composition, and these have a 3.2% and 8.2% increased hydraulic performance, respectively. Cases 7 and 8, where baffle clearances are changed, give a 6.1% and 16.8% increase in hydraulic performance. Case

9 and 10, where shell side inlet temperature was changed, yielded a 3.4% decrease and 5.7% increase in the pressure drop to mass flow ratio. Cases 11 to 17 are within $\pm 1.5\%$ change in hydraulic performance. Case 17, where the number of tubes is removed, resulted in a 6.1% ratio. For the hydraulic performance on the cold tube side, only cases 2, 3, and case 18 show a substantial increase in performance, 15.6%, 15.9%, and 20.5%, respectively. Cases 4-17 are within $\pm 1.5\%$ change in performance. The thermal performance is, in principle, a comparison between the actual overall heat transfer coefficient compared to the design, which is presented in section 8.1.1.

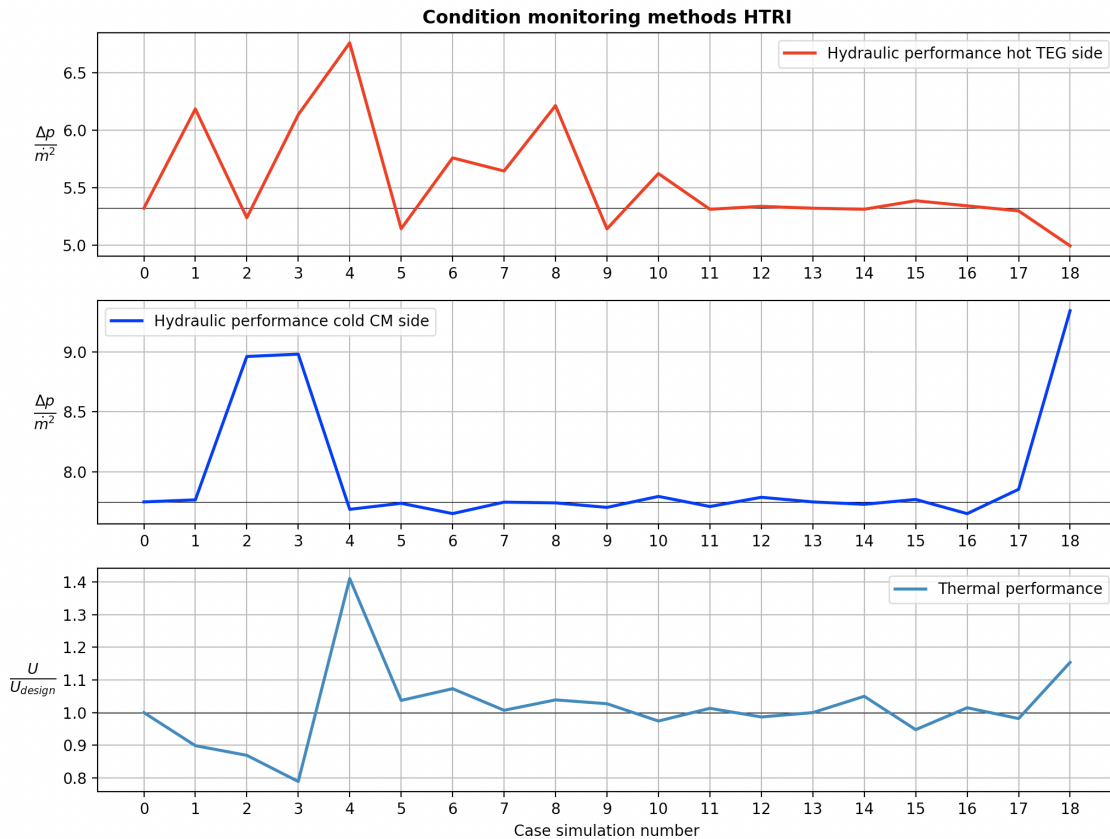


Figure 8.2: Comparison of case simulations to design for a shell-and-tube heat exchanger in HTRI Xchanger Suite.

8.2 Neqsim and field data comparison

In a glycol regeneration process, it is evident that the flow rate of rich glycol must be higher than the flow rate of lean glycol due to the added content of water and any hydrocarbons in the rich glycol. However, the field data provided indicate the opposite. In addition, are there only two flow rate transmitters in the glycol where "FIT-01" is placed after a flash drum as indicated in figure 6.1, and "FIT-02" is placed before the TEG contactor. These placements result in an inaccurate

measurement of the rich glycol flow rate for HX01 since the flash drum will separate gases from the stream before the flow rate transmitter. For HX02, the lean flow rate will be inaccurate due to a surge drum between the heat exchanger and flow rate transmitter "FIT-02". Due to these implications, the results presented in the following sections are calculated by utilising simulated flow rates. The simulations are conducted in Neqsim. A comparison between the measured and simulated flow rates is presented in 8.3 to evaluate the accuracy of the simulations. The simulated flow and the measured flow rates show the same development pattern over the monitored period, where the differences are generally constant. The simulated lean glycol flow rate is 1.4% lower than the measured on average. However, the simulated rich glycol flow rate is 7.9% higher than the measured flow rate. It is also worth noting that the measured lean glycol is distorted while the simulated results are more readable.

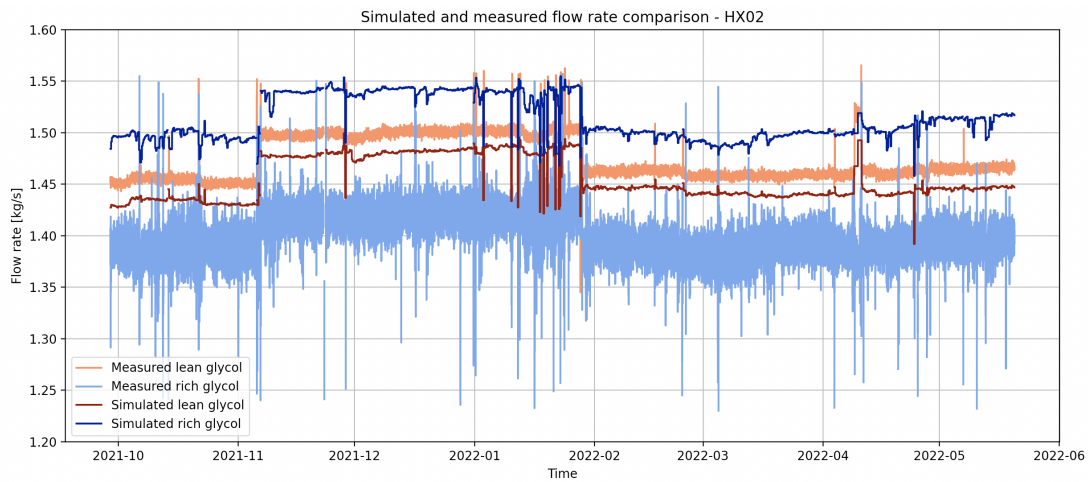


Figure 8.3: Comparison between simulated and measured flow rates for HX02.

8.3 Condition monitoring of HX01

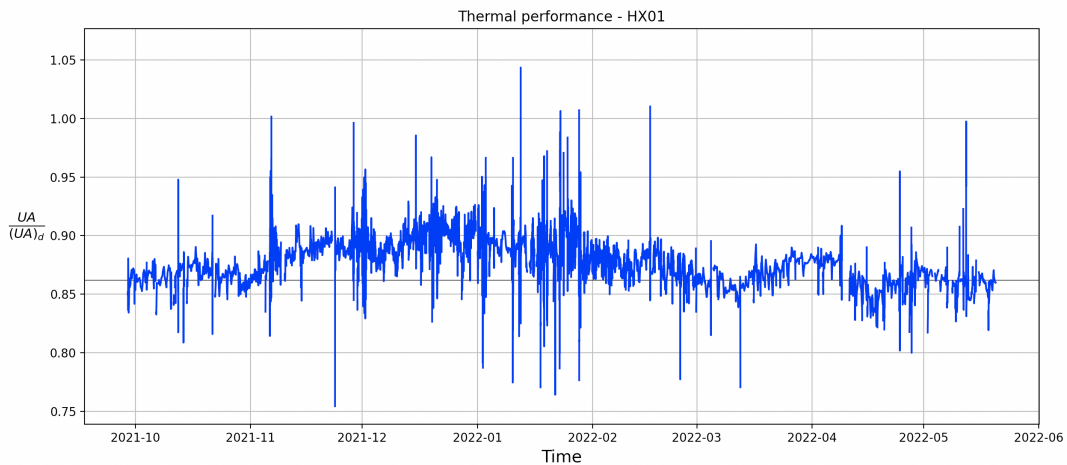
This section provides the results for HX01. Table 8.2 presents an overview of design conditions and performance compared to the actual measured parameters with averaging values. On average, this exchanger operates with a 25% lower flow rate and 15% lower temperature difference on the hot side and 25% lower flow rate and 22% lower temperature difference on the cold side compared to the design. The change in inlet temperatures and reduced flow rates results in a significantly lower total heat transfer rate. However, the overall heat transfer coefficient is only 13% lower on average.

Table 8.2: Comparison between design performance and measure performance for HX01

Performance		Design		Measured	
		Hot Plate Side	Cold Shell Side	Hot Plate Side	Cold Shell Side
		Lean TEG	Rich TEG	Lean TEG	Rich TEG
Flow rate	<i>kg/s</i>	1.95	2.04	1.46	1.53
Inlet temperature	$^{\circ}\text{C}$	115	44.5	99	50
Outlet temperature	$^{\circ}\text{C}$	90	70	78	70
Pressure drop	<i>bar</i>	0.05	0.05	0.26	0.21
Gas fraction in	<i>wt%</i>	–	1.06	–	5.83
Gas fraction out	<i>wt%</i>	–	1.10	–	5.85
Duty	<i>kW</i>	135		74	
UA	<i>W/°C</i>	3006		2644	

8.3.1 Thermal performance monitoring

Figure 8.4 presents the thermal performance of HX01 from the end of September 2021 to the middle of May 2022. The overall heat transfer coefficient and area (UA) are calculated based on inlet and outlet temperature measurements on both the hot and cold sides and simulated data for flow rates and specific heat capacity using Neqsim. The thermal performance is relatively steady between 0.85 and 0.93 for the present period. A level line showing the average performance value for the first period, at 0.86, is plotted as a benchmark. The thermal performance slightly increases between 2021-11 and 2022-02, varying around 0.90 before declining to and varying around the benchmark value.

**Figure 8.4:** The time developed thermal performance of HX01.

8.3.2 Hydraulic performance monitoring

Figure 8.5 shows the hydraulic performance for the monitored period for HX01 on the hot lean glycol side of the heat exchanger. The hydraulic performance is calculated based on measured pressure drop and simulated flow rate. A benchmark line is plotted from the average of the first period at 0.128. The resulting hydraulic performance fluctuates slightly below the benchmark line. Generally, the performance is steady for the period at around 0.125, with fluctuations reaching approximately 12% higher and lower.

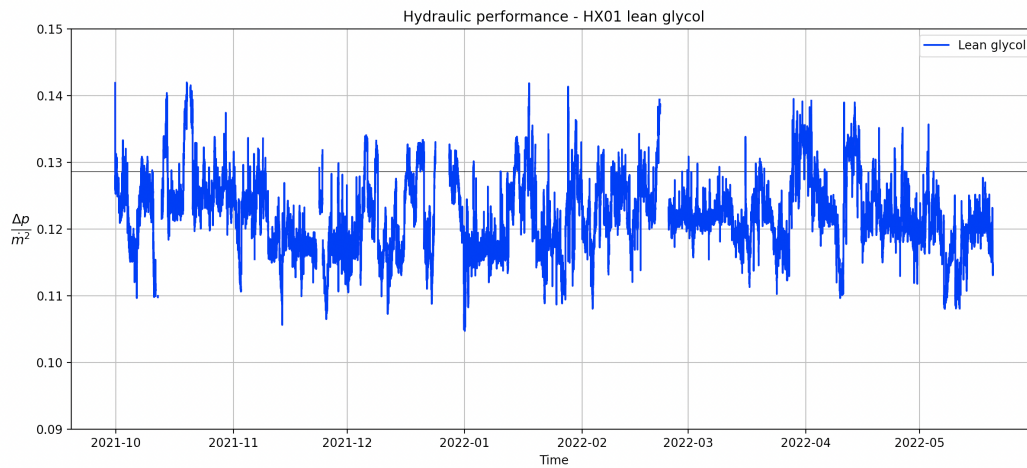


Figure 8.5: The time developed hydraulic performance of HX01 on the hot lean glycol side.

To control the correlation between the flow rate and the pressure drop presented in figure 8.5, the mass flow and the pressure drop are assessed separately. Figure 8.6 shows the plotted measured pressure drop and the simulated flow rate for the lean glycol in HX01. The pressure drop ranges between 0.23 and 0.29 bar for the whole period. The flow rate is at around 1.42 kg/s until the start of November, before it has an approximate 3% increase to 1.48 kg/s. From November, the flow rate slightly increases to around 1.49 kg/s over the next 2.5 months before dropping down 1.45 - 1.44 kg/s at the end of January 2022. From the end of January, the flow rate is generally stable at around 1.44-1.45 kg/s.

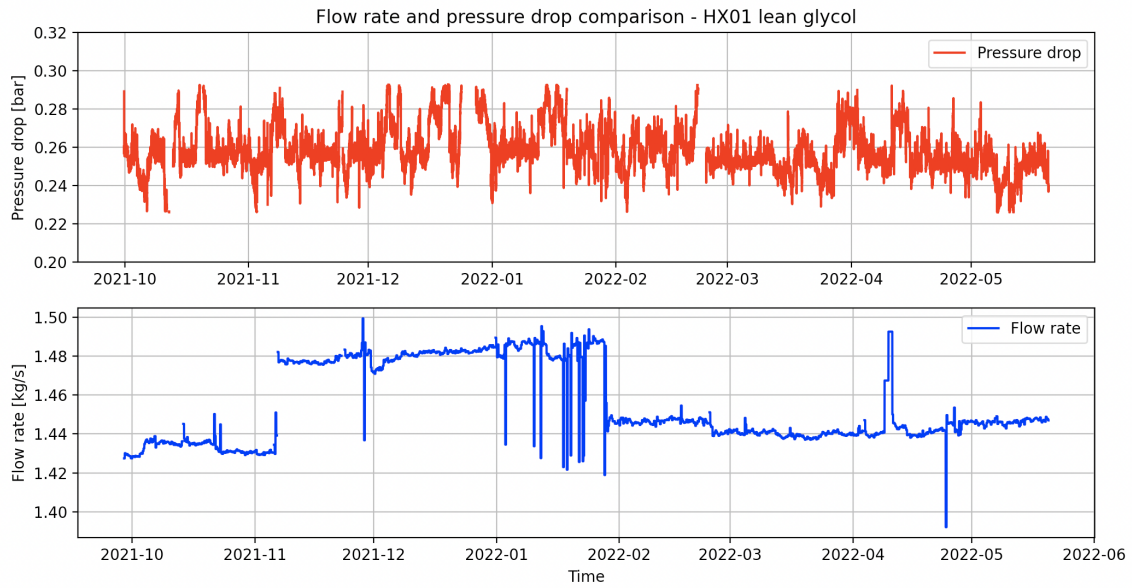


Figure 8.6: A plot of the pressure difference and the flow rate of hot lean glycol in HX01.

Figure 8.7 presents the hydraulic performance on the cold rich TEG side of HX01. The hydraulic performance is calculated using the pressure transmitters "PIT-04" and "PIT-05", shown in figure 6.1, and simulated flow rates. In the same way as for figures 8.4 and 8.7, a benchmark line for the average value of the first period is plotted at 0.087. The pressure drop to the mass flow squared ratio has more significant deviations from the benchmark line. In general, there are no increasing or decreasing trends, but the deviations are significant. At the beginning of November, the ratio rises up to 37% higher than the starting point before declining again. After that, the ratio varies high above and below the benchmark, with occasional rapid momentary changes. During January and the beginning of March, the ratio goes up to 57% below the measuring line. It is also worth mentioning that there are more considerable distortions in the measurements.

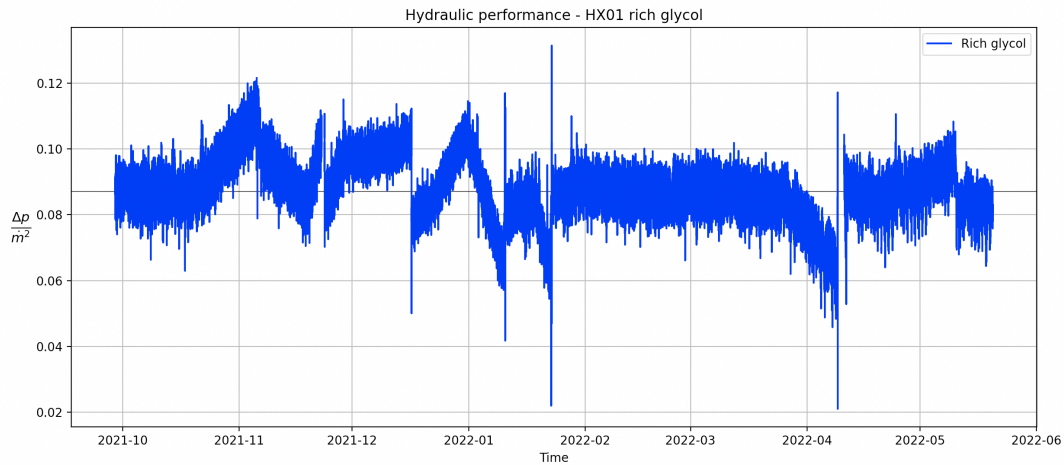


Figure 8.7: The time developed hydraulic performance of HX01 on the cold rich glycol side.

Similarly to the lean side, to evaluate the correlation between the pressure drop and the flow rate, they are assessed separately. In addition, the rich glycol will be in a two-phase flow, and it is necessary to evaluate the variation in the amount of gas and how it affects the pressure. Hence, figure 8.8 presents a comparison of the pressure drop, flow rate and gas-phase fraction. The gas-phase fraction data is retrieved from simulations. The pressure drop varies between 0.11 and 0.28 bar but is generally around 0.20. The gas mass fraction is relatively stable between 5.8 and 6.0 wt% from 2021-10 to 2022-02, with some spikes on 6.2 -6.4 wt%. From 2022-02 the gas fraction increases gradually to 6.2 wt% at mid-2022-03 before declining to 5.2 wt% over the following months, with a drop in early 2022-04. The flow rate, however, fluctuates around 1.52 kg/s before an immediate increase to 1.56 kg/s early in 2021-11. The flow rate is stable at 1.56 kg/s with some drops down to 1.50 kg/s until late 2022-01, where it drops to 1.525 and declines to 1.51 for the next month. From 2022-03 the flow rate gradually increases to 1.54 kg/s.

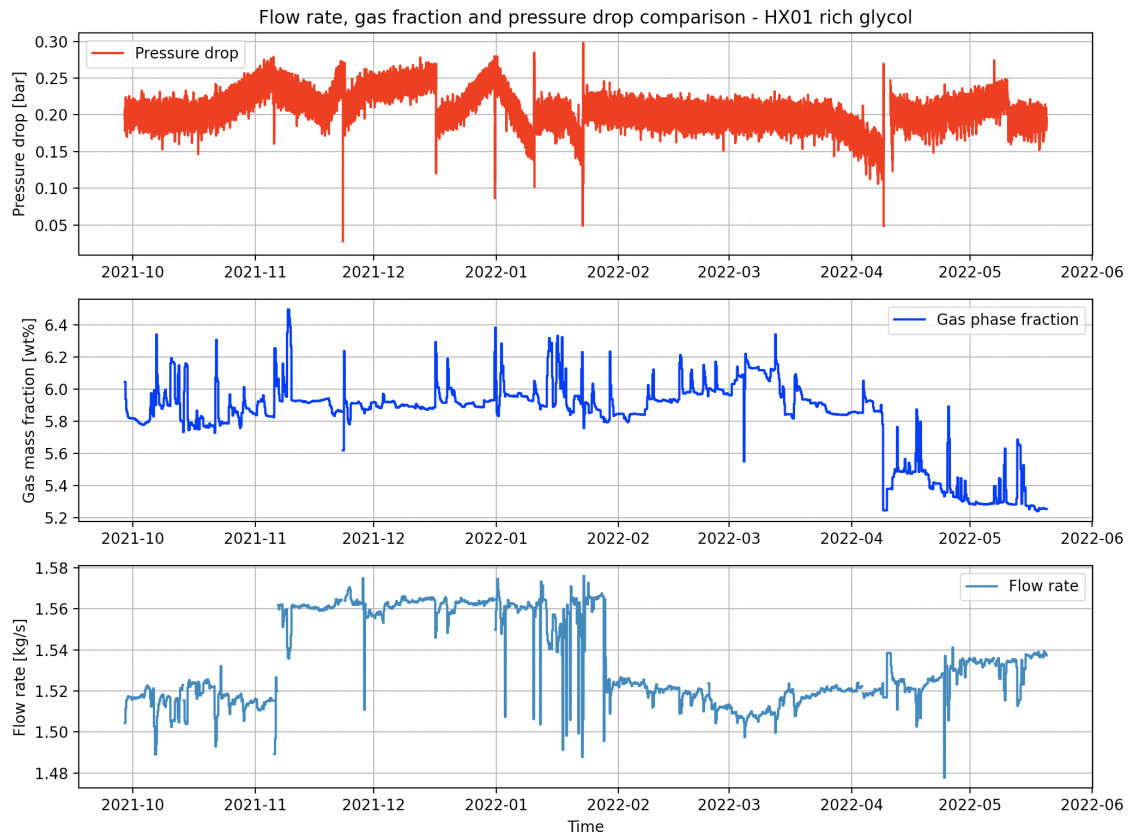


Figure 8.8: A plot of the pressure difference and gas mass fraction of rich glycol in HX01.

8.4 Condition monitoring of HX02

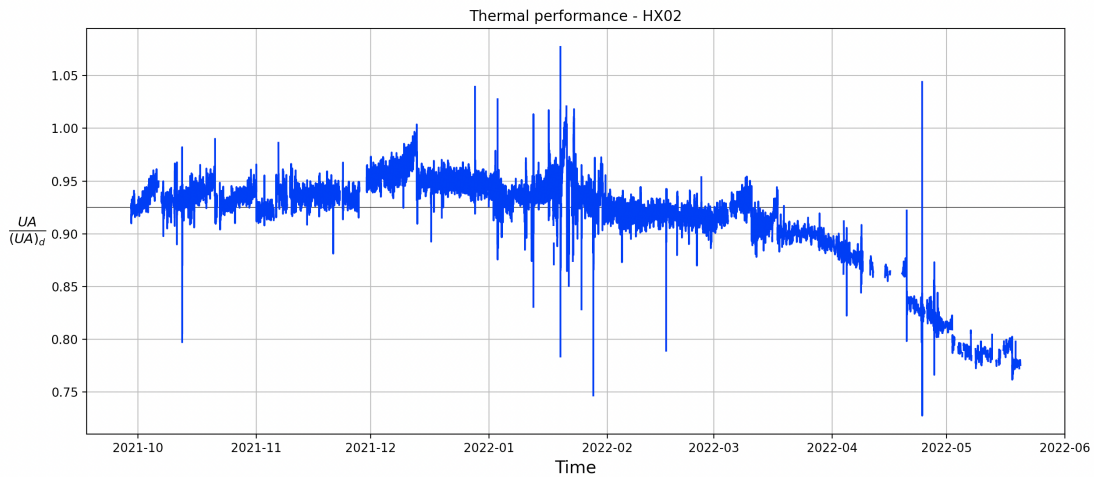
This section provides the results for HX02. Table 8.3 presents an overview of design conditions and performance compared to the actual measured parameters with averaging values. This exchanger operates with a 25% lower flow rate on both sides and 6% lower inlet temperature on the hot side and 25% lower flow rate, and 1.5% lower inlet temperature on the cold side compared to the design. The change in inlet temperatures and reduced flow rates results in a significantly lower total heat transfer rate. The overall heat transfer coefficient is 7% lower on average. The heat exchanger also operates with a 20% lower pressure drop on the hot lean TEG side and a 300% higher on the cold rich TEG side. For design conditions, there is also no gas present. However, there is a 0.01 wt% present on average on the rich TEG side for the measured operating condition.

Table 8.3: Comparison between design performance and measure performance for HX02

Performance		Design		Measured	
		Hot Plate Side	Cold Shell Side	Hot Plate Side	Cold Shell Side
		Lean TEG	Rich TEG	Lean TEG	Rich TEG
Flow rate	<i>kg/s</i>	1.95	2.02	1.46	1.51
Inlet temperature	$^{\circ}\text{C}$	193	70	181	69
Outlet temperature	$^{\circ}\text{C}$	115	150	98	147
Pressure drop	<i>bar</i>	0.05	0.05	0.04	0.15
Gas fraction in	<i>wt%</i>	–	–	–	0.010
Gas fraction out	<i>wt%</i>	–	–	–	0.012
Duty	<i>kW</i>	457		303	
UA	<i>W/C</i>	10385		9700	

8.4.1 Thermal performance monitoring

Figure 8.9 presents the calculated thermal performance of HX02. The UA-values are calculated based on simulated flow rates, simulated heat capacities, and measured temperatures. A benchmark line for comparison is plotted at 0.92. The thermal performance is relatively stable, between approximately 0.92 and 0.96, until 2021-12. From the start to the early middle of December, the performance increases to around 0.98 before dropping to around 0.95. From here, the performance gradually declines to the end of the measuring period ending at approximately 0.78.

**Figure 8.9:** The time developed thermal performance of HX02.

8.4.2 Hydraulic performance monitoring

For HX02, the hydraulic performance on the hot lean glycol side is presented in figure 8.10. The pressure drop to mass flow ratio is calculated using historical data from

the pressure drop transmitter "PDT-07" shown in figure 6.2, and mass flow from the results of Neqsim simulations. The hydraulic performance starts out at around 0.0220 before dropping down to approximately 0.0205 at the beginning of November. The ratio fluctuates around 0.0205 before rising to approximately 0.0215 at the end of January. From February and forth, the hydraulic performance is between 0.0210 and 0.0220. However, there is a slight incline to the middle of 2022-03 and a slight decline from here towards the end.

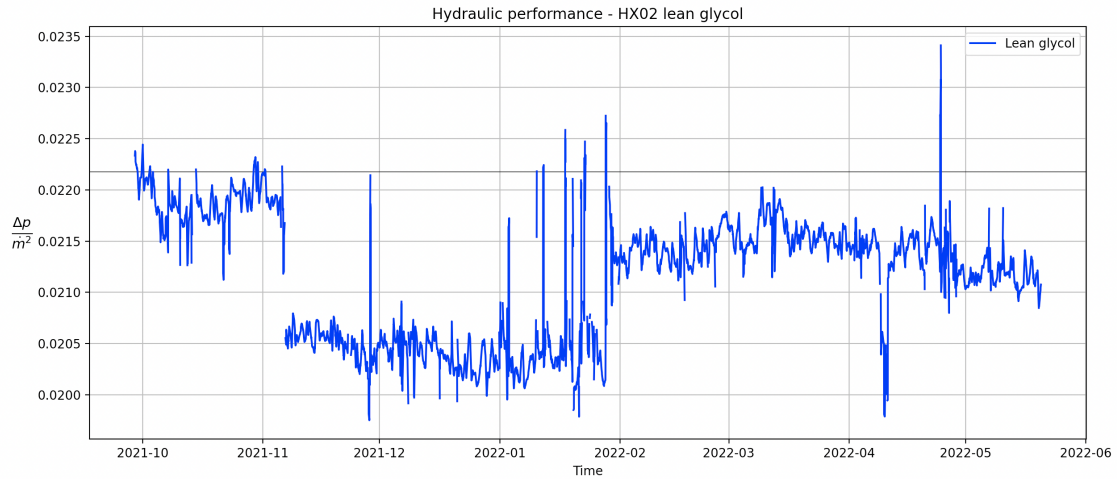


Figure 8.10: The time developed hydraulic performance of HX02 on the hot lean glycol side.

Similarly, as for HX01, are the pressure drop and mass flow for HX02 considered separately to evaluate the correlation between the measured pressure drop and the simulated mass flow. Figure 8.11 shows the plotted pressure drop and mass flow rate for the lean glycol in HX02. The pressure drop is stable between 0.044 and 0.046 bar for the whole period. A slight decrease in the pressure drop, towards 0.044 bar, can be noted towards the end of the monitored period. The flow rate is stable at different levels for different periods. First around 1.43 kg/s until the beginning of November, before it jumps to 1.48 kg/s. The flow rate remains above 1.48 until the end of January before dropping to approximately 1.45 kg/s. From February onwards, the flow rate is around 1.44-1.45 kg /s.

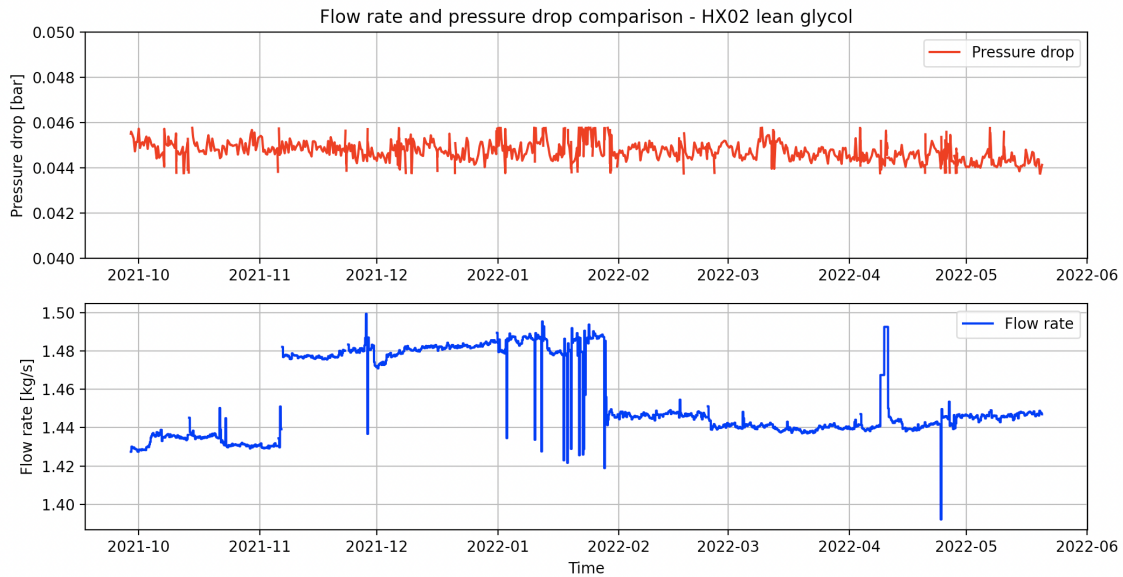


Figure 8.11: A plot of the pressure difference and hot lean glycol flow rate in HX02.

Figure 8.12 shows the hydraulic performance on the cold rich glycol side of the heat exchanger. In these calculations, the pressure drop is acquired from the measured data from the pressure drop transmitter "PDT-06", shown in figure 6.2. The mass flow is gathered from simulations conducted with Neqsim. The pressure drop to mass flow squared ratio presents a cycling pattern of a gradual increase before a rapid drop. This pattern is smaller for the first month, where the increasing top is at around 0.75, and the bottom of the drop is around 0.65. From 2021-11 the ratio variations are more significant, ranging from 0.055 to 0.075. From around 2022-04 the interval between the build-up and drop gets smaller, and the value range gets more compressed, with the last periodic cycle in mars being between 0.57 and 0.66.

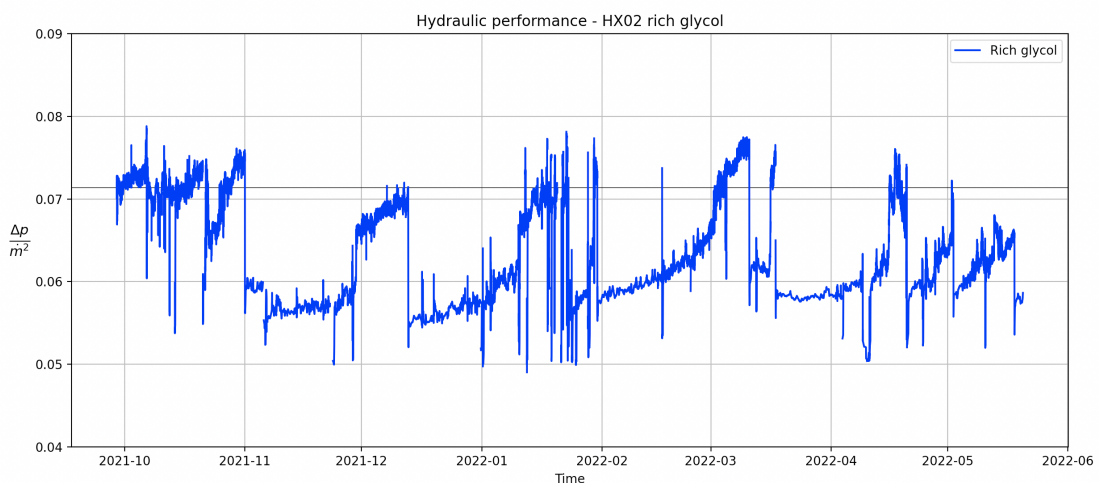


Figure 8.12: The time developed hydraulic performance of HX02 on the cold rich glycol side.

The pressure drop and mass flow for the rich glycol in HX02 are assessed separately. Similarly to the cold rich TEG side of HX01, there is a gas phase present in the cold rich TEG side of HX02. Hence, in addition to the flow rate, the development of the gas phase fraction is also considered. Figure 8.13 presents a comparison between the flow rate, gas-phase fraction and pressure drop. The pressure drop ranges between 0.12 and 0.17 bar, with a repeating cyclic pattern of gradually increasing to 0.17 bar before dropping to 0.13 bar. The gas mass fraction shows the same pattern, where the gas fraction varies between 0.055 and 0.035 wt%. The flow rate, however, does not follow the same pattern. It is around 1.49-1.50 kg/s for the first month, before a sudden increase to 1.54 kg/s in early 2021-11. Late in 2022-01, it drops to 1.50 kg/s with a continued decrease to 1.48 early in 2022-03. Hereafter, the flow rate increases gradually to the middle of Mars, ending at 1.52 kg/s.

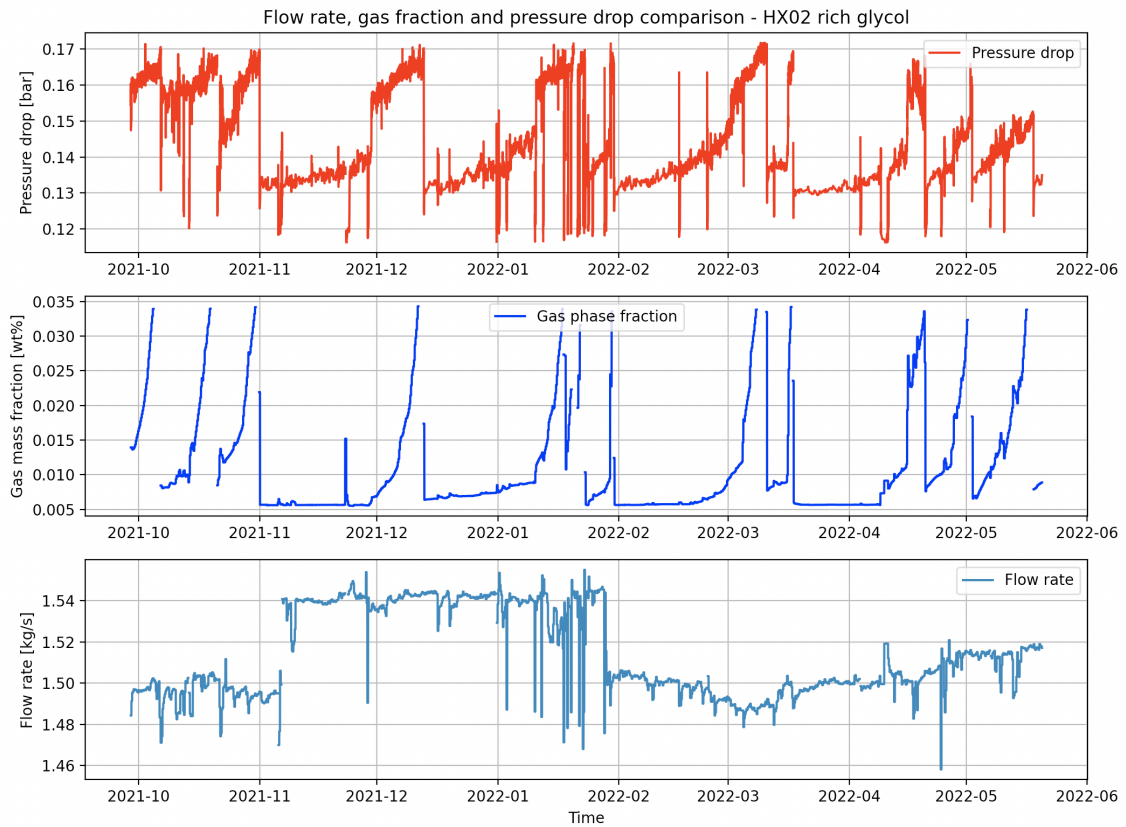


Figure 8.13: A plot of the pressure difference, flow rate and gas mass fraction of rich glycol in HX02.

8.5 Condition monitoring of HX03

In this section, the results for HX03 will be presented. Table 8.4 presents an overview of design conditions and performance compared to the actual measured parameters with averaging values. This heat exchanger does not have any pressure or flow rate meters on the cooling medium side of the exchanger. However, a flow rate measurement has been conducted on the outlet stream at 100% valve opening, with the reported result of 8.72 kg/s. This flow rate has been used as a basis for further calculations. This heat exchanger operates with a 25% lower flow rate and 14% lower inlet temperature on the hot side, and a 348% higher flow rate and equal inlet temperature on the cold side compared to the design. HX03 operates at a 60% lower heat transfer rate than design, and the overall heat transfer coefficient is 74% lower on average. The heat exchanger also operates with a 20% lower pressure drop on the hot lean TEG side. There are no gas phases present for this heat exchanger on either side.

Table 8.4: Comparison between design performance and measure performance for HX03

Performance		Design		Measured	
		Hot Plate Side	Cold Shell Side	Hot Plate Side	Cold Shell Side
		Lean TEG	Cooling Medium	Lean TEG	Cooling Medium
Flow rate	<i>kg/s</i>	1.95	1.65	1.47	8.72
Inlet temperature	$^{\circ}\text{C}$	90	15	77.5	15
Outlet temperature	$^{\circ}\text{C}$	40	55	47.5	17.4
Pressure drop	<i>bar</i>	0.05	0.05	0.04	–
Gas fraction	<i>wt%</i>	–	–	–	–
Duty	<i>kW</i>		248		96
UA	<i>W/C</i>		8384		2404

8.5.1 Thermal performance monitoring

The thermal performance of HX04 is calculated using measured inlet and outlet temperatures on both fluids for the heat exchanger. Simulated flow rate and heat capacity on the hot glycol side. However, the conditions for the cooling medium conditions can not be obtained from simulations because this heat exchanger is modelled as a cooler in Neqsim with an applied cooling duty. Hence, the one-time flow measurement and heat capacities from thermodynamic tables are utilised for the cooling medium stream. The resulting thermal performance is presented in figure 8.14. The thermal performance starts at around 0.258, where a benchmark line is plotted for comparison. From the beginning, the measurements fluctuate, resulting in a performance ranging from 0.23 to 0.3 in the first month. At the beginning

of 2011-11 the thermal performance reaches 0.28 before dropping and stabilising at 0.235. From 2021-12 to 2022-01 the performance increases to 0.255 before dropping down to approximately 0.23. The performance is relatively stable between 0.22 and 0.24 from 2022-01 to 2022-03, where it starts to increase towards 0.26-0.27 at the end gradually. Overall the thermal performance varies between 0.22 and 0.30 for the whole period.

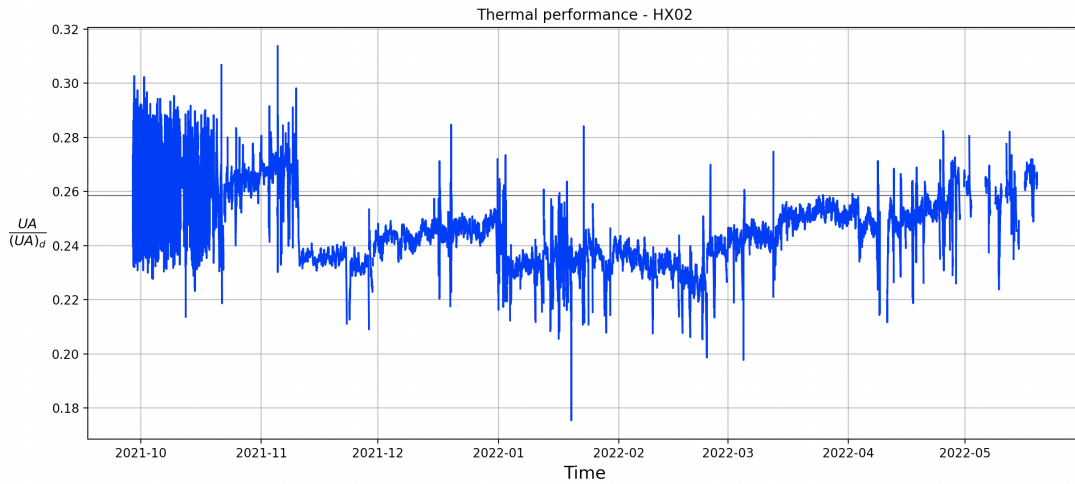


Figure 8.14: The time developed thermal performance of HX03.

8.5.2 Hydraulic performance monitoring

For HX03, there are no pressure or flow rate meters on the cooling medium side of the exchanger. The shortage of instrumentation limits the possibilities for monitoring the hydraulic conditions to the glycol side only. Figure 8.15 presents the hydraulic performance on the hot glycol side of HX03. The hydraulic performance is calculated using simulated flow rate and pressure drop transmitter "PDT-08" shown in figure 6.3. The pressure drop to mass flow squared ratio presents a pattern where it alters between two levels. These two levels are at approximately 0.077 and 0.020. The hydraulic performance is stable at each level, with a rapid change between them.

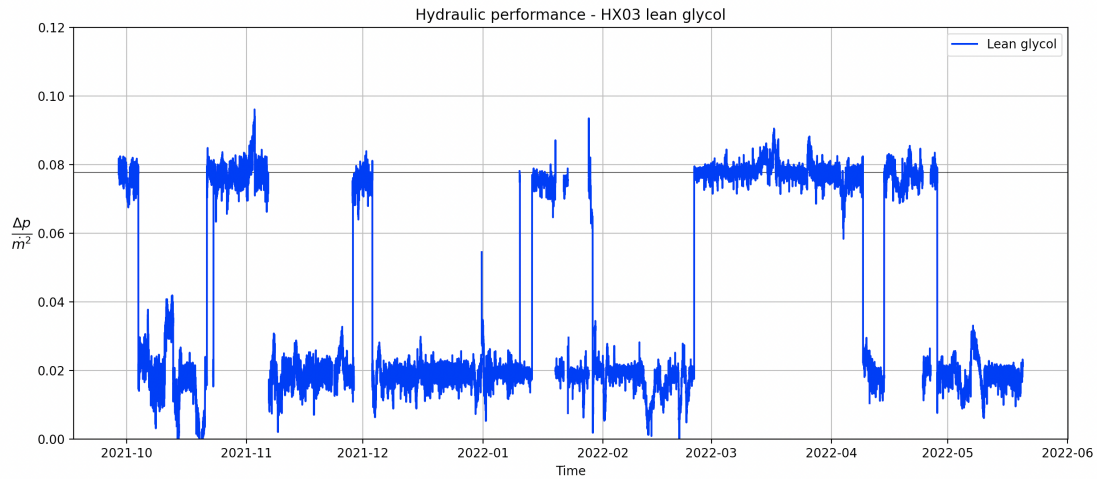


Figure 8.15: The time developed hydraulic performance of HX03 on the hot lean glycol side.

The pressure drop and flow rate on the hot lean glycol side are presented separately in figure 8.16 to evaluate their correlation. As presented in chapter 6.3, the pressure drop transmitter measures the pressure difference for two different outlet meters installed at separate lines before the circulation pumps. These two meters measure a different pressure drop for the two streams, which can be seen in figure 8.16. The pressure drop alternates in accordance with which pump is active. The pressure drop for one line is around 0.16 bar and the other at around 0.04 bar. The flow rate is stable at approximately 1.455 kg/s until it jumps to 1.50 kg/s at the beginning of 2021-11. It is stable at 1.50 kg/s until the end of 2022-01, when it drops to 1.465. From 2022-02 to the end of the measuring period, the flow rate is stable at around 1.6-1.65 kg/s.

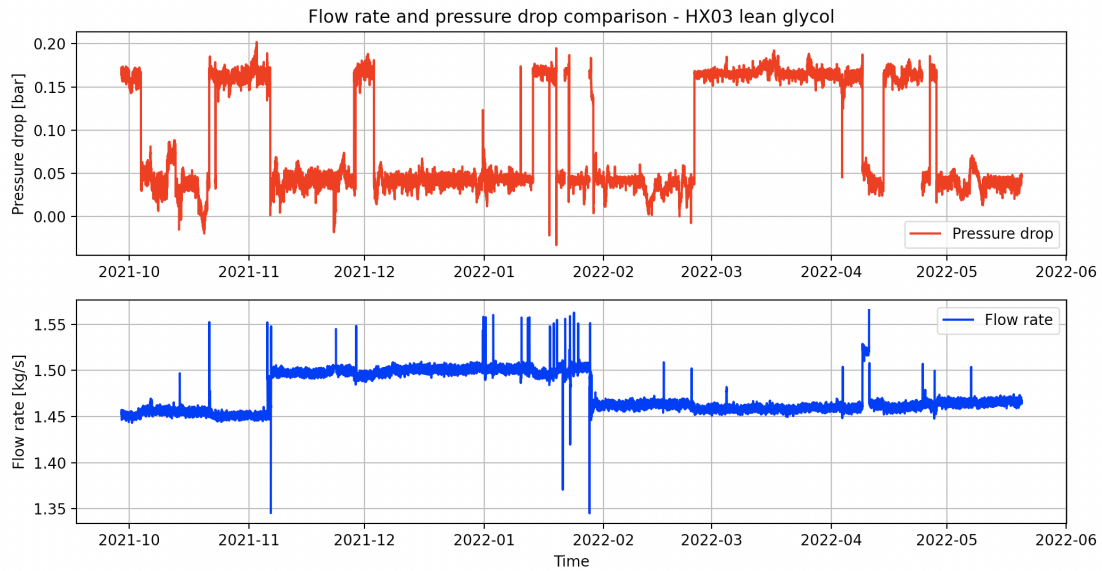


Figure 8.16: A plot of the pressure difference and hot lean glycol flow rate in HX03.

8.6 Condition monitoring of HX04

In this section, the results for HX04 will be presented. Table 3.5 presents an overview of design conditions and performance compared to the actual measured parameters with averaging values. This flow rate has been used as a basis for further calculations. This heat exchanger operates with an average of 36% lower flow rate and 3% lower inlet temperature on the hot side and a 6% higher flow rate and equal inlet temperature on the cold side compared to the design. HX04 operates with a 72% lower heat transfer compared to design and a 70% lower UA value on average. This heat exchanger does not have any pressure meters installed on the cooling side of the heat exchanger. The pressure drop on the hot condensing side is 20% lower than the design. The inlet overhead vapours coming from the reboiler are in a single gas phase for both design and actual measured. However, the outlet gas mass fraction is 48% lower for the measured compared to the design.

Table 8.5: Comparison between design performance and measure performance for HX04

Performance		Design		Measured	
		Hot Plate Side Overhead vapours	Cold Shell Side Cooling Medium	Hot Plate Side Overhead vapours	Cold Shell Side Cooling Medium
Flow rate	<i>kg/s</i>	0.14	0.98	0.09	1.04
Temperature inn	$^{\circ}\text{C}$	87.0	15.0	84.5	15.0
Temperature out	$^{\circ}\text{C}$	50.0	55.0	42.9	23.0
Pressure drop	<i>bar</i>	0.05	0.5	0.04	–
Gas fraction out	<i>wt%</i>	56.6	–	83.6	–
Duty	<i>kW</i>		147		41
UA	<i>W/C</i>		3247		977

8.6.1 Thermal performance monitoring

The thermal performance of HX04 is calculated using measured inlet and outlet temperatures on both fluids for the heat exchanger. Simulated flow rate and enthalpy change on the hot overhead vapours side. However, the same applies to this exchanger as to the previous one. Neqsim simulates this exchanger as a simple cooler. Thus, the cooling medium's flow rate and heat capacity can not be simulated. This results in the measured mass flow and heat capacity from thermodynamic tables being used for the calculation of the cooling medium. The thermal performance is presented in figure 8.17. The thermal performance fluctuates around 0.36 in the first month. Between 2021-11 and early 2022-01, the thermal performance decreases linearly from approximately 0.36 to 0.23. Between early 2021-11 and early 2022-03, the performance varies between 0.23 and 0.28. From 2022-03 and to the middle of 2022-05, it increases up to 0.45. Overall, the thermal performance first decreases around 13% over two months, stagnates for two months and then increases by 22% over two and a half months compared to the design.

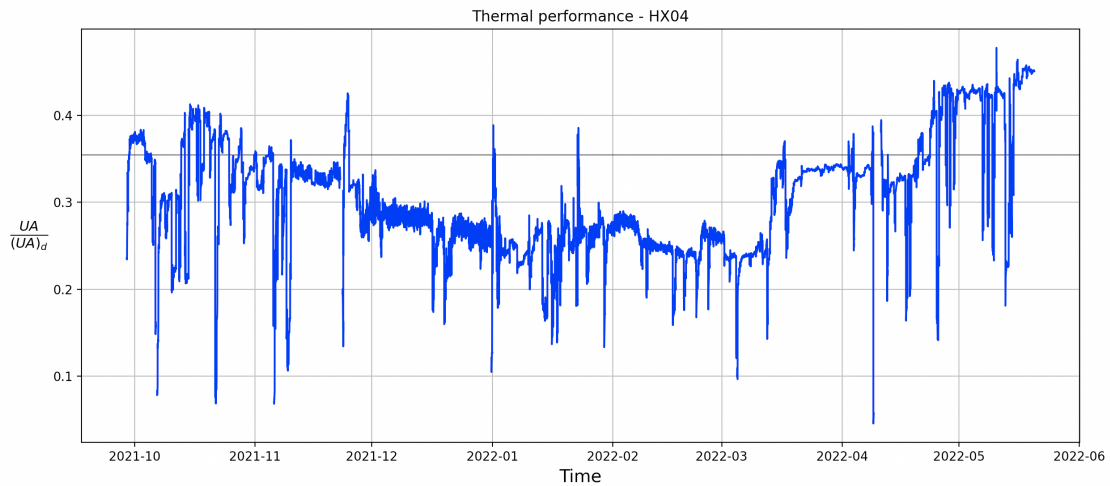


Figure 8.17: The time developed thermal performance of HX04.

8.6.2 Hydraulic performance monitoring

For HX04, there are no pressure meters on the cooling medium side of the exchanger. The lack of instrumentation limits the possibilities for monitoring the hydraulic conditions to the overhead vapours side only. Figure 8.18 presents the hydraulic performance on the hot condensing side of HX04. The hydraulic conditions are calculated using the pressure drop transmitter "PDT-09" and simulated flow rate from Neqsim. The hydraulic performance is overall generally stable, around 5-5.5. Except in the first month, where the hydraulic performance has a rise up 8 in the middle of 2021-10, and in 2021-12, the ratio drops down to around 2 for the whole month.

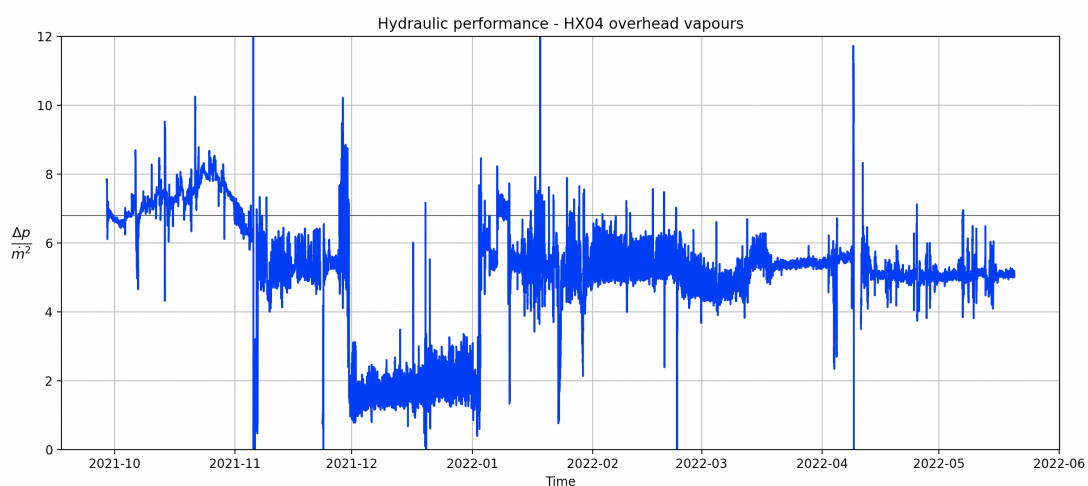


Figure 8.18: The time developed hydraulic performance of HX04 on the hot condensing side.

The pressure drop and mass flow used to calculate the hydraulic performance, as well as the gas phase fraction, are presented separately in figure 8.19. The pressure drop starts at 0.07 bar, increasing to 0.09 bar in the middle of the first month, before decreasing to around 0.05 bar in early 2021-11. The pressure drop fluctuates around 0.05 bar before dropping to approximately 0.015 bar in late 2021-12. Early in 2022-01 the pressure drop increases to around 0.04 bar and fluctuates around that level until 2022-03, where it has a slight dip to 0.03 bar before increasing up to 0.055 bar in the middle of 2022-05. The flow rate starts at 0.10 kg/s, with a slight increase to 0.105 kg/s in the middle of the first month. The flow rate decreases to 0.10 kg/s towards the start of 2021-11, where it drops to around 0.095 kg/s. The flow rate drops to 0.055 kg/s at the end of 2021-11 before jumping up to 0.105 kg/s at the start of 2021-12. From 2021-12 to 2022-01 the flow rate decreases linearly from 0.105 kg/s to 0.081 kg/s, with a sudden spike to 0.11 kg/s at the end. From 2022-01 to the beginning of 2022-03, the flow rate gradually varies from 0.08 up to 0.088 and back down to 0.082. In the last two months, the flow rate has increased from 0.082 kg/s to 0.105 kg/s. The gas mass fraction varies averagely between 0.76 wt% and 0.89wt%. It fluctuates between 80 and 90wt% the first month. The gas fraction is stable from 2021-11 to 2022-01 at around 83wt%. From 2022-01 to 2022-03, the gas phase fraction increases to 89% before decreasing towards 0.76 wt% in the middle of 2022-05.

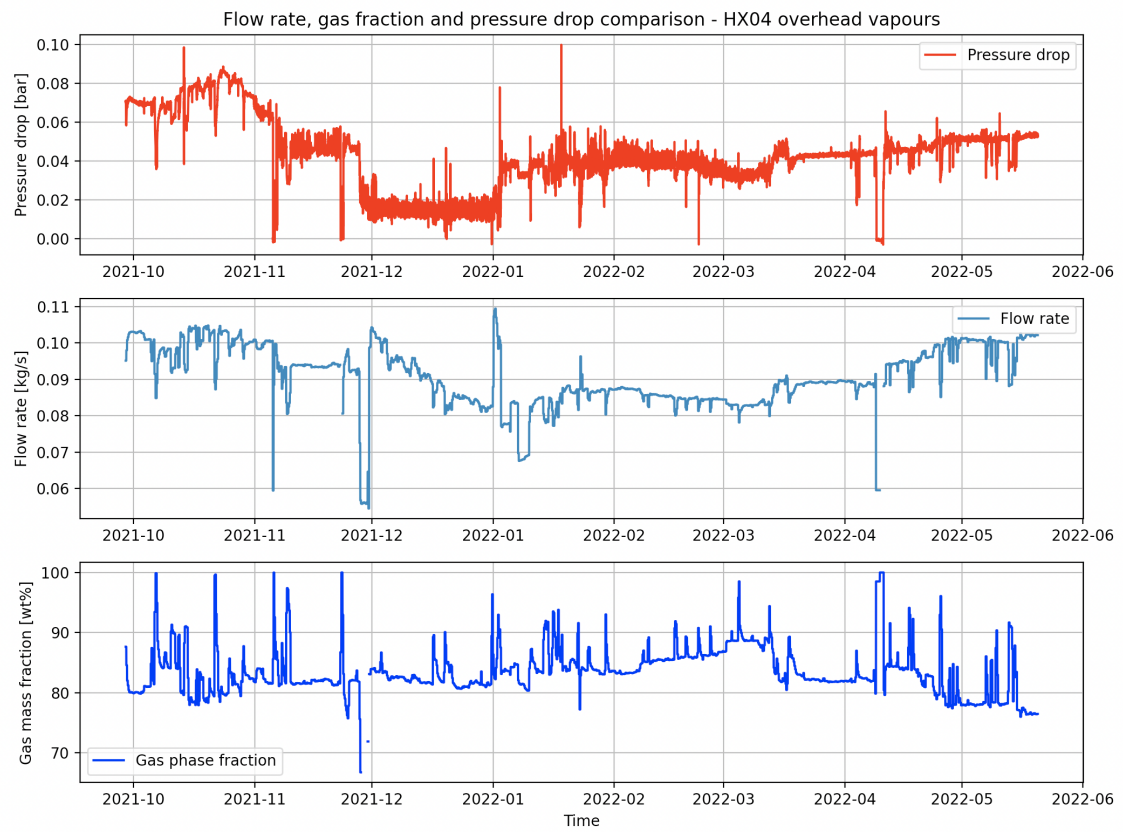


Figure 8.19: A plot of the pressure difference, flow rate and gas mass fraction of overhead vapours in HX04.

9 Discussion

This chapter discusses the results from chapter 8. The chapter is divided into six sections and is structured according to the order of the results. Thus, the HTRI simulation is discussed in section 9.1, the Neqsim comparison in section 9.2, HX01 in section 9.3, HX02 in section 9.4, HX03 in section 9.5 and HX04 in section 9.6.

9.1 HTRI simulation

In a heat transfer process, many parameters affect each other in a state change. Of all the parameters and properties, few are conventionally monitored. When monitoring conditions, assessments of what is happening in the heat exchanger are taken based on the measurable parameters. The results from the HTRI simulations provide an insight into how pressure, temperature and flow rate behave when subjected to different operating conditions.

9.1.1 Case simulations

Case 1, 2 and 3, shown in figure 8.1, are the simulations where a fouling factor and a layer are applied to the heat exchanger. The increased pressure loss due to fouling is approximately the same for each side. However, the heat transfer decreases more for fouling on the tube side compared to the shell side. This is because the convective heat transfer coefficient is higher on the tube side, resulting in a thermal resistance distribution of roughly 74% on the shell side, 23% on the tube side and 3% on the wall. Hence, fouling on the tube side has a more considerable impact on the heat transfer.

For cases 4, 5 and 6, the different changes in the hot fluid composition give various changes in the physical and thermal properties of the fluid. For case 4, the high increase in heat transfer and pressure drop is partly because the heat transfer coefficient of water is higher than TEG but mainly because the fluid's viscosity decreases, which increases the Reynolds number. Ordinarily, the pure glycol flow has a Reynolds number below 800, making the flow laminar for the whole heat exchanger. For 5 wt% water, the viscosity decreases from 5.56/14.2 cP (inlet/outlet) to 1.87/5.94 cP, and the Reynolds number increases to around 2800 for the first part of the heat exchanger. Therefore, the shell side has a turbulent flow regime in the first part of the heat exchanger, transitioning over to a laminar regime at the end. This results in a higher pressure drop due to the turbulent flow and the heat transfer correlations

used by the software to calculate the heat transfer changes from a constant Nusselt number to a turbulent Nusselt correlation. For case 5, the added hexane reduces the viscosity slightly, reducing the pressure drop on the shell side. However, the Reynolds number is around 700 at maximum, maintaining a laminar flow regime. The heat transfer coefficient for hexane is also higher than TEG, increasing the heat transfer slightly. The pressure drop is higher for case 6 with the condensing propane due to the two-phase flow. In addition, the Reynolds number for the liquid in this two-phase flow is up to 6000, resulting in a turbulent flow and increasing the heat transfer.

Case 6, 7, and 18 are cases where the geometry was changed to emulate fouling in specific sections of the heat exchanger. A fouling layer build-up in the clearances will not directly affect the heat transfer as these are not heat transfer surfaces. However, the flow area gets reduced, increasing the flow velocity, resulting in an increased heat transfer and pressure drop. The results from the simulation show that a reduction in tube-to-baffle clearance affects the heat transfer more than a reduction in baffle-to-shell. Both reduction results in a moderate increase in pressure drop on the hot shell side. HTRI don't have the option to clog pipes. Hence, to simulate clogged pipes, five tubes were removed in case 19. The removal of tubes decreases the pressure drop on the shell side due to the increased flow rate. However, on the tube side, the pressure drop increases and the heat transfer increases. The reduced flow area increases the flow velocity, and the flow gets into a turbulent flow regime. The turbulent flow increases the pressure drop, and the software uses different correlations to calculate the heat transfer.

9.1.2 Condition monitoring of case simulations

The results in figure 8.2 show that the condition monitoring models are affected by many different situations. It is clear that in order to detect fouling, both thermal and hydraulic performance must be seen in relation. Cases 1, 2 and 3, where fouling occurs, are the only cases with a significant increase in hydraulic performance and reduction in thermal performance at the same time. For cases 4 and 6, the hydraulic effect also increases. Although this can look like fouling occurs, the thermal performance also increases, which indicates the opposite. Case 7 and 8, where there are deposits on different non-heat transfer surfaces, show an increase in hydraulic performance without a significant change in thermal performance. The same applies to case 10, where the inlet temperature is reduced. The comparison between cases 7 and 8 and case 10 illustrates a flaw in these models. By only considering the thermal

and hydraulic performance for these cases, it's hard to determine what is happening without seeing the decreased inlet temperature in context.

Case 18 shows the effect of pipe clogging. The decreased hydraulic performance is due to the removal of pipes in HTRI discussed above. The increased thermal performance in case 18 can be confusing in determining if fouling is transpiring. However, fouling develops over time. These cases show the result for various immediate states of a heat exchanger. For example, the five pipes in case 18 won't suddenly clog without a build-up of deposit over time, where the effects on the performance will be in the same manner as in case 3. The remaining cases have little impact on the models. It is worth noting that the cases with variation in flow rate correspond sufficiently with the hydraulic performance model.

9.2 Neqsim and field data comparison

The results from the flow velocity comparison between Neqsim and the field measurements presented in figure 8.3, show a good correlation between lean glycol. Still, as described in section 8.2, the measured rich glycol is lower than it should be and characterized by a lot of noise. The Neqsim simulation. Neqsim has been reported to be reliable in mass flow calculations, and when simulating a glycol regeneration process, it uses measurements from multiple instruments in the process as input data. How a simulation is conducted and the various input parameters can be seen in appendix D.

9.3 Condition monitoring of HX01

HX01 operates at high performance compared to design. However, the actual pressure drop is substantially larger than the design on both sides of the heat exchanger. The temperatures on the hot plate side are, on average, 21.2% lower throughout the heat exchanger. The lower temperatures increase the fluid's viscosity, which increases the pressure drop. The inlet temperature is higher for the cold shell side, indicating a less viscous liquid, but the gas fraction is five times higher than the design conditions. As presented in section 4.3, the frictional pressure drop for two-phase flow is substantially higher than for single-phase flow.

9.3.1 Thermal performance monitoring

The thermal performance monitoring of HX01 presented in figure 8.4 shows no indication of a trending decline in performance. The performance increases slightly during the first three months before decreasing and swinging around the benchmark value. The roughly three month period of higher performance can be related to the increased flow rate. Overall there is no indication of fouling development in this heat exchanger.

9.3.2 Hydraulic performance monitoring

The hydraulic performance on the hot lean TEG side of the heat exchanger presented in figure 8.5 shows a relatively stable performance for the whole period. However, the performance fluctuates, regularly deviating up to 12% from the mean value. The pressure drop to mass flow squared ratio does not indicate an inclination trend. Thus no indication of fouling. The pressure drop and mass flow are presented separately in figure 8.16. Generally, it is difficult to see any connection between the pressure drop and the flow rate. Nonetheless, the most significant increase in the flow rate is only around 3%. Considering October, with a flow rate of 1.43 kg/s and an average pressure drop of 0.26 bar, a 3% increase in the pressure loss will give a 6.1% increase in the pressure drop. A 6.1% increase in pressure drop corresponds to a pressure drop of 0.276 bar, which is within the fluctuations of the overall pressure drop.

The hydraulic performance monitoring of the cold rich glycol side of HX01 presented in figure 8.7 show a very inconsistent pattern. The performance varies up to a 30% difference from the mean value and is characterised by inconsistent oscillations and jumps, in addition to a lot of noise. From figure 8.8, it is clear that the noise and unstable pattern comes from the pressure drop data. As described in section 6.1, great uncertainty is associated with one of the transmitters used to calculate pressure drops. The pressure transmitter "PIT-05" is located in the flash drum, where hydrocarbon gas is removed from the process. Due to gas flashing, the pressure drop will probably be greater and inconsistent since the amount of gas will vary. However, there is some coherence between the calculated pressure drop and the flow rate. The pressure drop is stable at around 0.2 bar when the flow rate is stable at around 1.52kg/s. When the flow rate increases in the period between 2021-11 and 2022-02, the pressure drop has a slight increase and fluctuates inconsistently. Also, in the last months, the pressure drop is unstable when the flow rate increases. The gas fraction has been relatively stable except for the last three months. The gas mass

fraction has a good coherence with the flow rate from 2022-02 and onwards. Before 2022-02 it does not correlate particularly to either the flow rate or the pressure drop.

9.4 Condition monitoring of HX02

The overall performance of HX02 is good compared to the design. The average UA value is 93% of the design UA value. The pressure drop on the hot side is 0.01 bar lower. The lesser pressure drop is likely due to the reduced flow rate, although the lower temperatures of the TEG increase the fluid's viscosity, which increases the frictional pressure drop. Considering the hydraulic performance method for this exchanger, the 25% decrease in the mass flow should result in a 50% reduced pressure drop. However, the pressure drop is around 20%, indicating the effect of increased viscosity due to the 10% reduced operating temperature. The pressure drop on the cold shell side is three times higher than the design. The operating temperatures of the rich TEG are almost the same as the design, and the flow rate is 25% lower, but there is a gas phase present. Hence, the high pressure drop is likely due to the increased frictional losses of two-phase flow.

9.4.1 Thermal performance monitoring

The presented thermal performance of HX02 in figure 8.9 shows an apparent degradation in performance. The performance is stable, at around 93% of design performance until 2022-03, when a clear and ongoing decline in performance start. At the end of the monitoring period, the thermal performance is at 77-78%, resulting in a 15% reduction in performance. This clearly indicates that something is impacting the heat transfer, and the heat exchanger may be exposed to fouling.

9.4.2 Hydraulic performance monitoring

Considering the hydraulic performance on the hot lean glycol side presented in figure 8.10 and the plotted pressure drop and flow rate in figure 8.11, it is clear that there is little coherence between the pressure drop and the flow rate. The pressure drop is stable with only a 3% variation from the mean value. The flow rate seems to vary more, but as discussed for the lean flow rate of HX01, the most significant difference in flow rate is only a 3.5% increase in early 2021-11. However, this 3.5% increase should be visible as an approximately 7.1% increase in the pressure drop.

The hydraulic performance of the cold rich glycol in figure 8.12 shows no indication

of an increasing trend. However, the repetitive pattern of build-up and dropping. The hydraulic performance generally has considerable deviations, with up to a 50% difference between the lowest and high values. Considering the rich glycol pressure drop and flow rate in figure 8.13, it is problematic to evaluate the dependency between the pressure drop and flow rate because the flow rate has a 3.4% variation at most. In comparison, the pressure drop varies up to 31%. However, the cold rich glycol pressure drop seems to be dominated by the amount of gas present in the heat exchanger.

The pressure drop behaviour matches the evolution of the gas fraction. Still, there is only an average of 0.002 wt% evaporation in the exchanger, indicating that a significant part of the gas development occurs before HX02. Problems have been reported with precipitation of elemental sulfur, which is collected in the cartridge filters, which has led to a significant pressure drop and must be replaced frequently. By examining simulations and measurements of the equipment between HX01 and HX02, it turns out that the pressure drop in the cartridge filters matches the gas fraction. Figure 9.1 compares the gas fraction in HX02 and the pressure losses in cartridge filters A and B. The filters are operated in turn. Hence, combining the pressure drop for each filter matches the gas fraction development exact. This indicates some lighter hydrocarbons in the rich teg, leaving the flash drum at the bubble point and evaporating when the pressure decreases. Which again results in an increased pressure drop in HX02 due to increased two-phase frictional losses.

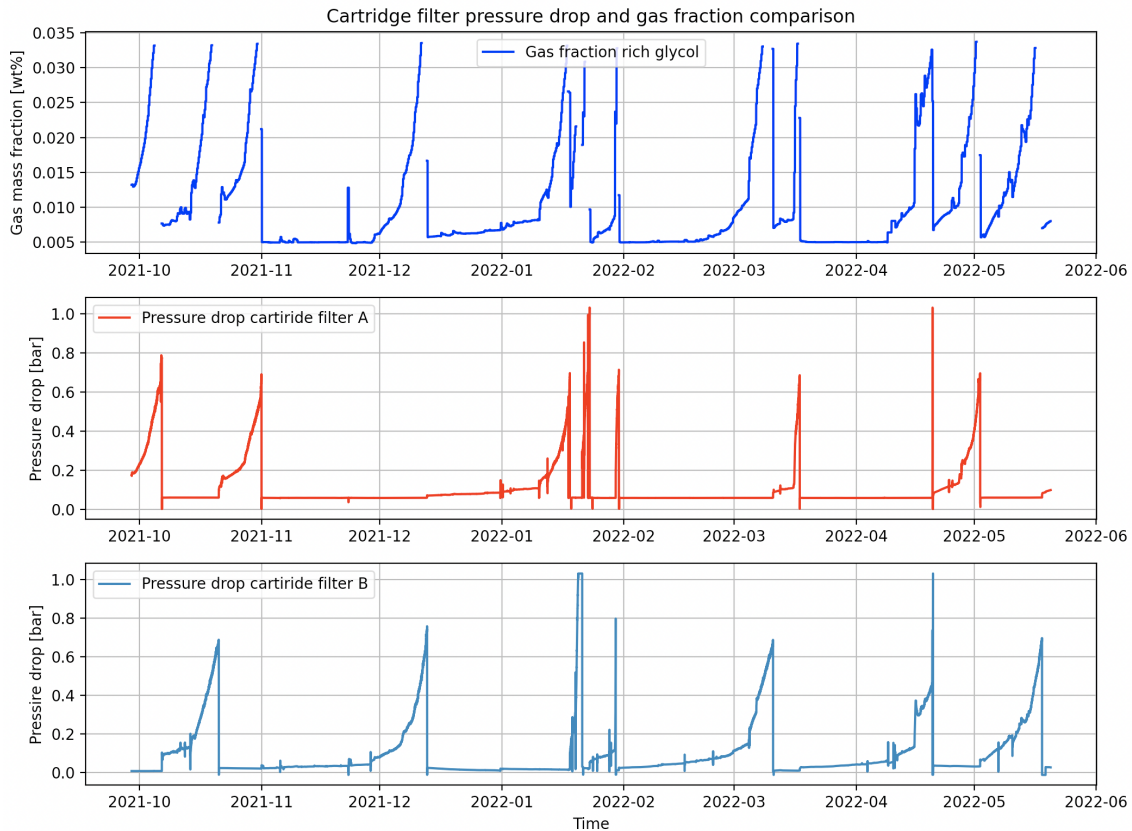


Figure 9.1: A comparison between the time developed pressure drop in cartridge filter A and B, and the gas mass fraction in HX02.

9.5 Condition monitoring of HX03

Unlike HX01 and HX02 operating close to design condition, HX03 operate at poor performance. The general problem with monitoring HX03 is the lack of instrumentation on the cooling medium side of the heat exchanger. As described in section 8.5, the flow rate has only been measured once, and the inlet temperature transmitter is placed far from the heat exchanger. In addition, there are no pressure transmitters at all measuring the cooling medium. However, by evaluating the data from the instrumentation present, it is clear the heat exchanger operates at deficient performance. The lower pressure drop on the hot lean TEG side can be explained similarly to the lean TEG side of HX03 with a lower flow rate and lower inlet temperature.

9.5.1 Thermal performance monitoring

The thermal performance for HX03, presented in figure 8.14, is low for the whole period. Unless the heat exchanger was subjected to fouling immediately during

start-up, something else is causing the poor performance. There are significant uncertainties concerning the accuracy of the thermal performance calculation due to the lack of instrumentation. However, the instrumented glycol side and outlet temperature of the cooling medium give a clear indication of stable, poor performance.

9.5.2 Hydraulic performance monitoring

By assessing the hydraulic performance plot in figure 8.15, there is no notable change in the performance for the period. The pressure drop presented in figure 8.16, shows two different pressure levels. These different levels come as a result of inaccuracies from the pressure gauges. As described in section 6.3, there are two different pipelines the fluid can flow through according to which pump is operating. There are two different pressure gauges on these lines that measure up to a 320% difference in pressure loss. The transmitters are located at the same height and relatively the same distance from the heat exchanger, indicating that the pressure drop should be approximately the same. In addition, it is reported that these pressure gauges have a high range, up to 285 bar, which indicates that they have poor accuracy on low measurements, in this case, around 0.05-0.15 bar. The changes in flow rate are not visible for this case due to the slight variation in flow rate, a maximum of 3.5%, and the significant variations in the pressure drop.

9.6 Condition monitoring of HX04

The overhead condenser, HX04, operates at relatively low performance compared to the design. However, considering that the temperature difference is higher and the outlet gas fraction is higher for the measured overhead vapours than the design indicates that the fluid composition is different. A larger temperature difference should result in a more considerable amount of condensed liquid. A change in the fluid composition could alter the heat transfer coefficient of the fluid and the viscosity, changing the flow regime and heat transfer. The instrumentation around HX04, like HX03, is insufficient. On the gas side, there is no flow rate transmitter, and the pressure drop transmitter measures the difference between the inlet of the heat exchanger and the gas outlet of the overhead receiver. As with the HX03, there is no direct temperature transmitter at the inlet and no pressure gauges on the cooling medium side. In addition, it has been reported that the mass flow transmitter is inaccurate, which can also be noticed in the data, where the flow rate peak and stagnate at around 1.05 kg/s.

9.6.1 Thermal performance monitoring

Due to the absence of reliable flow rate transmitters and two-phase flow, simulated enthalpy change and temperature data were used to calculate the thermal performance presented in figure 8.17. The effectiveness-NTU method of calculating UA struggles with two phase flow, and LMTD is derived under the assumption of constant specific heat capacity and overall heat transfer coefficient. In this particular case, LMTD is used as a simplification to calculate the overall heat transfer coefficient. All the inlet and outlet temperatures are relatively constant for the period, resulting in the log mean temperature difference being consistent for the period. Hence, the variations in the thermal performance come from variations in gas mass fraction and the flow rate presented in figure 8.19. The convex trend shown in figure 8.17 is a result of the flow rate decreasing and gas fraction increasing. The amount of gas condensing to liquid should increase when the flow rate lowers during a consistent performance. However, the simulations indicate an opposite correlation. It is challenging to draw any conclusion about the thermal performance without any reliable data on the flow rate for the cooling medium.

9.6.2 Hydraulic performance monitoring

There is uncertainty associated with the pressure drop transmitter used to calculate the hydraulic performance shown in figure 8.18. The pressure drop transmitter measures the pressure drop on the gas separated in the overhead receiver. Despite this, the pressure drop shows a relatively good correlation with the flow rate, as shown in figure 8.19. The pressure drop to mass flow squared ratio is relatively constant, with the exception of October and December. The pressure drop does not seem to cohere with the gas fraction in any notable sense. Overall the hydraulic performance does not have an increasing trend indicating fouling. However, due to the uncertainties of the pressure drop to conclude on the performance.

10 Conclusion

In this work, the heat exchangers in an Equinor glycol regeneration process have been monitored. The condition monitoring methods are selected based on a study of the fundamental theory of heat transfer and heat exchangers and a review of previously established methods for condition monitoring. The heat exchangers on the Equinor facility are shell-and-plate type heat exchangers. Due to the limited amount of available information on the heat exchanger geometry and design, a general approach to monitoring the thermal and hydraulic performance has been established and evaluated. The selected methods have been used to monitor four shell-and-plate type heat exchangers over a period of 8 months using field data provided by Equinor and simulation data from Neqsim. In addition, the methods have been evaluated through results from case simulations of a shell-and-tube type heat exchanger using the software HTRI Xchanger Suite.

The thermal performance method is an approach using the calculated actual UA value and comparing it to the design value. This method provides an indication of the thermal efficiency of the heat exchanger compared to design conditions and requires only temperature and flow rate measurements as input parameters. With the assumption of a simple counter-current flow arrangement, the method provides a reasonably good result when the instrumentation level is satisfactory. A downside of the thermal performance model is that it struggles with two-phase flow and composition variation. Of the heat exchangers this method was tested on, HX01 has shown good performance the monitored period. HX02 has shown a general high performance, but a decline in the last months indicates that fouling is occurring. HX03 shows a low performance throughout the period with uncertainty associated with the flow rate of the cooling medium, and HX04 shows varying results with uncertainty associated with two-phase condensation and inadequate instrumentation

The hydraulic performance model is an approach using the ratio between the pressure drop and mass flow for each fluid to determine condition changes in the heat exchanger. This method monitors the time developed pressure drop to mass flow ratio and requires pressure drop and flow rate transmitters as instrumentation. This method has been used on all heat exchangers, except on the cooling medium stream for HX03 and HX04, where the instrumentation level is insufficient. The results for this method have not shown any indication of fouling. However, this method has not given any results that can be considered sufficient. In general, pressure measurements are characterised by too much noise and variation, indicating that they have too high a range and low accuracy. In addition, an identified problem with this

method is that the pressure drop is greatly affected by variations in the two-phase fraction, which could conceal changes in pressure due to fouling.

An observation through this work is that a high level of instrumentation is required when considering the implementation of condition monitoring. The Equinor facility studied in this work is too poorly instrumented to be able to rely on the selected monitoring methods alone. In general, each exchanger should be instrumented with mass flow, temperature and pressure transmitters for the inlet and outlet for both fluids. In addition, the transmitters should have an appropriate range and higher accuracy. However, in circumstances where the transmitters fail or are missing, the results from simulations in Neqsim provide reliable alternatives for both measurable and non-measurable parameters that can be used in condition monitoring.

10.1 Further work

For further work, several points have been identified as recommended areas for improvement and further development. An online implementation of the methods should be developed. This implementation should be visually easy to understand and evaluate the fouling conditions of the different heat exchangers.

The condition monitoring models can be developed further. Currently, there are challenges with the two-phase flow and possible composition changes. The models can be improved to accommodate simulated two-phase flow and composition change. In addition, noise from measurements can be filtered out to increase readability.

This work has only considered thermodynamic and physical relation approaches. It is recommended to additionally research approaches using machine learning principles to help the operator understand the different trending conditions in a heat exchanger. For example, considering all the variable parameters in a heat exchanger process, a simulator can be customised for the individual heat exchanger and indicate trending conditions.

Bibliography

- Astorga-Zaragoza, Carlos-Manuel et al. (2008). ‘Observer-based monitoring of heat exchangers’. In: *ISA transactions* 47.1, pp. 15–24. URL: <https://www.sciencedirect.com/science/article/pii/S0019057807000936>.
- Bandeira, V.F., W.M. Pachekoski and A. Mikowski (2020). ‘Case Studies from Different Types of Heat Exchangers to Plate and Shell Heat Exchanger: A Review’. In: *Revista de Engenharia Térmica* 19.1, pp. 119–125. URL: <https://revistas.ufpr.br/reterm/article/view/76444>.
- Bott, T.R. (1995). *Fouling of Heat Exchangers*. Elsevier Science Technology Books.
- Campbell, John M. (1992). *Gas Conditioning and Processing. Volume 2: The Equipment Modules*. Campbell Petroleum Series.
- Coker, A. Kayode (2010). *Ludwig’s Applied Process Design for Chemical and Petrochemical Plants*. 4th ed. Vol. 2: Distillation, packed towers, petroleum fractionation, gas processing and dehydration. Gulf Professional Publishing, pp. 483–678.
- Diaz-Bejarano, E, F Coletti and S Macchietto (2020). ‘A model-based method for visualization, monitoring, and diagnosis of fouling in heat exchangers’. In: *Industrial & Engineering Chemistry Research* 59.10, pp. 4602–4619.
- Freire, Luciano Ondir and Delvonei Alves de Andrade (2014). ‘On applicability of plate and shell heat exchangers for steam generation in naval PWR’. In: *Nuclear Engineering and Design* 280, pp. 619–627. URL: <https://www.sciencedirect.com/science/article/pii/S0029549314005524>.
- GPSA (2012). *Engineering Data Book*. 13th ed. Vol. 1 and 2. Gas Processors Supplier Association.
- Guo, Boyun and Ali Ghalambor (2005). *Natural Gas Engineering Handbook*. 2nd ed. Gulf Publishing Company.
- Incropera et al. (2011). *Fundamentals of Heat and Mass Transfer*. 7th ed. John Wiley Sons, Inc.
- Jerónimo, MAS et al. (1997). ‘Monitoring the thermal efficiency of fouled heat exchangers: a simplified method’. In: *Experimental Thermal and Fluid Science*

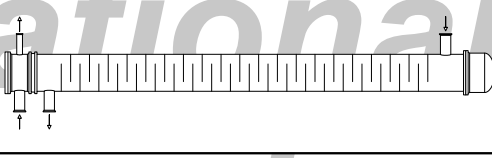
- 14.4, pp. 455–463. URL: <https://www.sciencedirect.com/science/article/pii/S089417779600146X>.
- Kakaç, Sadık, Hongtan Liu and Anchasa Pramuanjaroenkij (2020). *Heat Exchangers: Selection, Rating, and Thermal Design*. 4th ed. Taylor Francis Group.
- Kulacki, Francis A. et al. (2018). *Handbook of Thermal Science and Engineering*. Springer International Publishing, pp. 1634–1639.
- Lyons, William C., Gary J. Plisga and Michael D. Lorenz (2016). *Standard Handbook of Petroleum and Natural Gas Engineering*. 3rd ed. Gulf Professional Publishing.
- Mohanty, Dillip Kumar and Pravin M Singru (2011). ‘Use of C-factor for monitoring of fouling in a shell and tube heat exchanger’. In: *Energy* 36.5, pp. 2899–2904. URL: <https://www.sciencedirect.com/science/article/pii/S0360544211001101>.
- Müller-Steinhagen, H, M. R. Malayeri and A. P. Watkinson (Feb. 2011). ‘Heat Exchanger Fouling: Mitigation and Cleaning Strategies’. In: *Heat Transfer Engineering* 32, pp. 189–196. ISSN: 3-4. URL: https://www.tandfonline.com/doi/full/10.1080/01457632.2010.503108?casa_token=eqpT7T7IC0wAAAAA:y2l4Ed6Wnl5bsAgP-iWRjClmRTmjGDduam1oCuWZqjTHKyKI5-x0P_b-pSI1aTeXelsDI-Z2YhxadA.
- Næss, Erling (n.d.). *Compendium in TEP07 Industrial Heat Engineering*. NTNU, Department of Process Engineering.
- Neqsim (2021). URL: <https://equinor.github.io/neqsimhome/> (visited on Nov. 2021).
- Serth, Robert W. and Thomas G. Lestina (2014). *Process Heat Transfer: Principles, Applications and Rules of Thumb*. 2nd ed. Elsevier Inc.
- Shah, Ramesh k. and Dušan P. Sekulić (2003). *Fundamentals of Heat Exchanger Design*. John Wiley Sons, Inc.
- Stewart, Maurice I. (2014). *Surface Production Operations. Volume 2: Design of Gas-Handling Systems and Facilities*. 3rd ed. Gulf Publishing Company, pp. 279–373.
- Taler, Dawid and Jan Taler (2017). ‘Simple heat transfer correlations for turbulent tube flow’. In: *E3S Web of conferences*. Vol. 13. EDP Sciences, p. 02008. URL: https://www.e3s-conferences.org/articles/e3sconf/abs/2017/01/e3sconf_wtiue2017_02008/e3sconf_wtiue2017_02008.html.

- Tan, Jaime HuiChoo et al. (2020). ‘Transforming Offshore Oil and Gas Production Platforms into Smart Unmanned Installations’. In: *Offshore Technology Conference Asia*. OnePetro. URL: <https://onepetro.org/OTCASIA/proceedings/200TCA/3-200TCA/450839>.
- Theodore, Louis (2008). *Air Pollution Control Equipment*. John Wiley Sons, Inc, pp. 185–190.
- Vahterus (2021). URL: <https://vahterus.com> (visited on 16th Dec. 2021).
- Wang, Ke et al. (2020). ‘Flow patterns and pressure drop in the shell-and-plate heat exchangers’. In: *International Journal of Multiphase Flow* 129, p. 103323. URL: <https://www.sciencedirect.com/science/article/pii/S0301932219310055>.
- Zohuri, Bahman (2017). *Compact Heat Exchangers: Selection, Application, Design and Evaluation*. 1st ed. Springer International Publishing.

Appendix

A HTRI heat exchanger design performance

This appendix contains the complete results for the shell-and-tube heat exchanger designed in HTRI Xhcanger Suite presented in chapter 8. The included report show an overview of the process data, performance and geometry specifications.

HTRI		Final Results		Page 1	
		Released to the following organization:			
Xist E 9 (32 bit) 08.06.2022 18:16 SN: 01022-620519897					SI Units
Shell 1					
Rating - Horizontal Multipass Flow TEMA AES Shell With Single-Segmental Baffles					
Process Data		Hot Shellside		Cold Tubeside	
Fluid name			TEG		VANN/MEG
Fluid condition			Sens. Liquid		Sens. Liquid
Total flow rate	(kg/s)		1,4740		1,6500
Weight fraction vapor, In/Out	(--)	0,0000	0,0000	0,0000	0,0000
Temperature, In/Out	(Deg C)	77,50	47,50	15,00	30,96
Skin temperature, Min/Max	(Deg C)	19,55	42,87	19,09	41,06
Wall temperature, Min/Max	(Deg C)	19,55	42,87	19,09	41,06
Pressure, In/Average	(kPa)	240,00	234,85	650,00	639,45
Pressure drop, Total/Allowed	(kPa)	10,294	50,000	21,098	50,000
Velocity, Mid/Max allow	(m/s)	0,20		1,04	
Mole fraction inert	(--)				
Average film coef.	(W/m2-K)		748,54		2887,7
Heat transfer safety factor	(--)		1,0000		1,0000
Fouling resistance	(m2-K/W)		0,000000		0,000000
Overall Performance Data					
Overall coef., Req/Clean/Actual	(W/m2-K)	555,79	/	561,03	/
Heat duty, Calculated/Specified	(MegaWatts)	0,1027	/		
Effective overall temperature difference	(Deg C)	36,5			
EMTD = (MTD) * (DELTA) * (F/G/H)	(Deg C)	36,9	*	0,9871	* 1,0000
See Runtime Messages Report for warnings.					
Exchanger Fluid Volumes					
Approximate shellside (L)		65,8			
Approximate tubeside (L)		27,1			
Shell Construction Information					
TEMA shell type	AES	Shell ID	(mm)	205,00	
Shells Series	1 Parallel	Total area	(m2)	5,148	
Passes Shell	1 Tube	4	Eff. area	(m2/shell)	5,067
Shell orientation angle (deg)	0,00				
Impingement present	No				
Pairs seal strips	1	Passlane seal rods (mm)	16,000	No. 1	
Shell expansion joint	No	Rear head support plate	No		
Weight estimation Wet/Dry/Bundle		293,07 /	200,15 /	62,76 (kg/shell)	
Baffle Information					
Type	Perpend. Single-Seg.	Baffle cut (% dia)	26,1		
Crosspasses/shellpass		No. (Pct Area)	(mm) to C.L		
Central spacing	(mm)	41	1	23,83	48,991
Inlet spacing	(mm)	52,044	2	0,00	0,000
Outlet spacing	(mm)	222,35			
Baffle thickness	(mm)	148,23			
Use deresonating baffles	(mm)	3,175			
		No			
Tube Information					
Tube type	Plain	Tubecount per shell		42	
Overall length	(m)	2,438	Pct tubes removed (both)	4,55	
Effective length	(m)	2,400	Outside diameter	(mm)	16,000
Total tubesheet	(mm)	38,100	Wall thickness	(mm)	1,000
Area ratio	(out/in)	1,1429	Pitch (mm)	20,000	Ratio 1,2500
Tube metal	Titanium-grade 2 2		Tube pattern (deg)		30

HTRI		Final Results			Page 2	
		Released to the following organization:				
Xist E 9 (32 bit) 08.06.2022 18:16 SN: 01022-620519897					SI Units	
Shell 1						
Rating - Horizontal Multipass Flow TEMA AES Shell With Single-Segmental Baffles						
Shellside Performance						
Nom vel, X-flow/window		0,39 / 0,23				
Flow fractions for heat transfer		0,430				
A=0,0417		B=0,1641		C=0,3177		E=0,2797 F=0,1968
Shellside Heat Transfer Corrections						
Total		Beta	Gamma	End	Fin	
0,922		0,922	1,000	0,943	1,000	
Pressure Drops (Percent of Total)						
Cross		Window	Ends	Nozzle	Shell	Tube
76,04		16,73	1,49	Inlet	2,83	1,46
MOMENTUM			0,00	Outlet	2,91	14,17
Two-Phase Parameters						
Method		Inlet	Center	Outlet	Mix F	
H. T. Parameters						
			Shell		Tube	
Overall wall correction			0,833		1,005	
Midpoint		Prandtl no.	115,39		15,28	
Midpoint		Reynolds no.	553		7995	
Bundle inlet		Reynolds no.	364		6389	
Bundle outlet		Reynolds no.	217		8878	
Fouling layer		(mm)				
Thermal Resistance; %						
Shell		Tube	Fouling	Metal	Over Des	
74,95		22,20	0,00	2,85	0,94	
Total fouling resistance			(m2-K/W)		0,0000	
Differential resistance			(m2-K/W)		1,68e-5	
Shell Nozzles						
Inlet at channel end		No				
				Inlet	Outlet	Liquid Outlet
Number at each position				1	1	0
Diameter		(mm)	52,553	52,553		
Velocity		(m/s)	0,63	0,62		
Pressure drop		(kPa)	0,291	0,300		
Height under nozzle		(mm)	28,190	28,190		
Nozzle R-V-SQ		(kg/m-s2)	428,48	419,07		
Shell ent.		(kg/m-s2)	87,31	85,39		
Tube Nozzle						
				Inlet	Outlet	Liquid Outlet
Diameter		(mm)	52,553	RADIAL	RADIAL	
Velocity		(m/s)	0,74	2,89		
Pressure drop		(kPa)	0,308	2,990		
Nozzle R-V-SQ		(kg/m-s2)	560,66	8542,4		
Annular Distributor						
				Inlet	Outlet	
Length		(mm)				
Height		(mm)				
Slot area		(mm2)				
Diametral Clearances (mm)						
Baffle-to-shell		Bundle-to-shell		Tube-to-baffle		
3,1750		37,559		0,7937		

**Supplementary Results**

Released to the following organization:

Xist E 9 (32 bit) 08.06.2022 18:16 SN: 01022-620519897

SI Units

Shell 1

Rating - Horizontal Multipass Flow TEMA AES Shell With Single-Segmental Baffles

Externally Enhanced Tube Geometry

Type Plain
 Fin density (fin/meter)
 Fin height (mm)
 Fin thickness (mm)
 Root diameter (mm)
 Area/length (m2/m)

Internally Enhanced Tube Geometry

Type None
 Thickness (mm)
 Pitch (L/D)

Mean Metal Temperatures

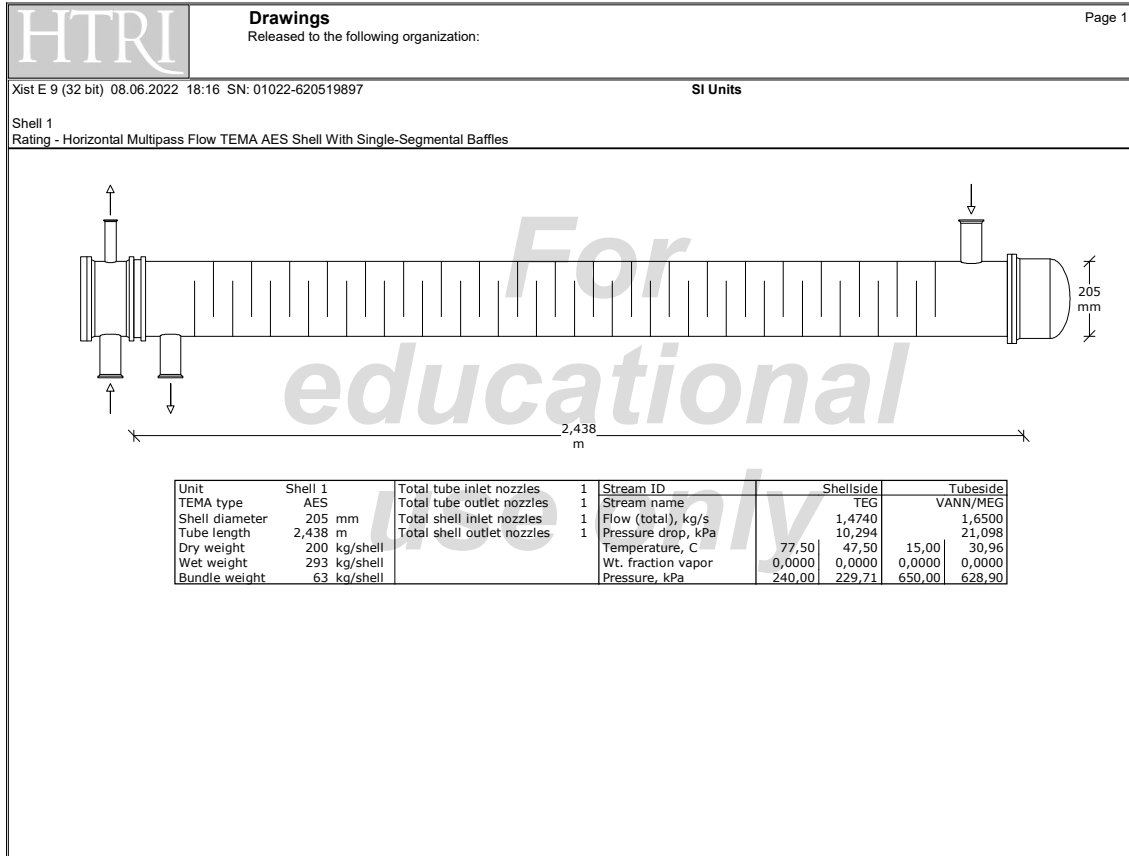
Mean shell temperature 60,63 (C)
 Tubesheet temperature 110,00 (C)

Mean tube metal temperature in each tubepass, (C)

<u>Tube Pass</u>	<u>Inside</u>	<u>Outside</u>	<u>Radial</u>
1	27,21	28,42	27,84
2	30,12	31,23	30,70
3	33,05	34,06	33,58
4	36,03	36,92	36,50

B HTRI heat exchanger design drawings

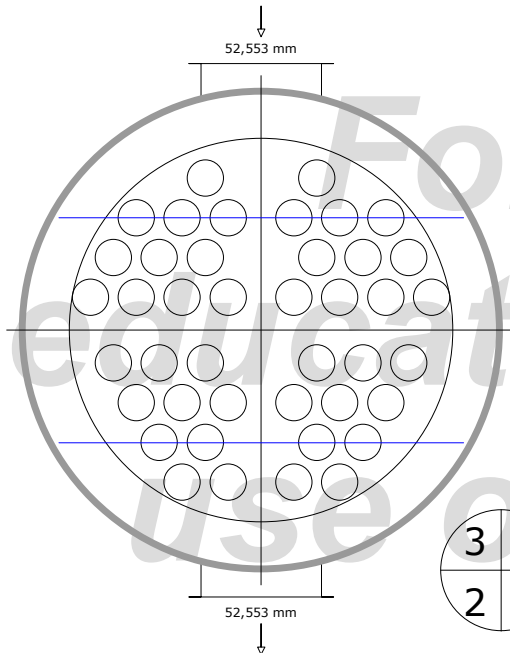
This appendix contains drawings of the shell-and-tube heat exchanger designed in HTRI Xchanger Suite presented in chapter 8. The included drawings show the heat exchanger's internal and external geometry specifications.



Xist E 9 (32 bit) 08.06.2022 18:16 SN: 01022-620519897

SI Units

Shell 1
Rating - Horizontal Multipass Flow TEMA AES Shell With Single-Segmental Baffles



Unit	Shell 1
TEMA type	AES
Shell ID	205,00 mm
Actual OTL	167,44 mm
Height under inlet nozzle	28,190 mm
Height under outlet nozzle	28,190 mm
Tube type	Plain
Tube OD	16,000 mm
Tube pitch	20,000 mm
Tube layout angle	30 deg
Tubes	42
Tube positions available	42
Tie rods	4
Seal strip pairs	1
Passlane seal rods	1
Tube Passes	4
Parallel passlane width	12,700 mm
Perpendicular passlane width	12,700 mm
Baffle cut % diameter	26,1

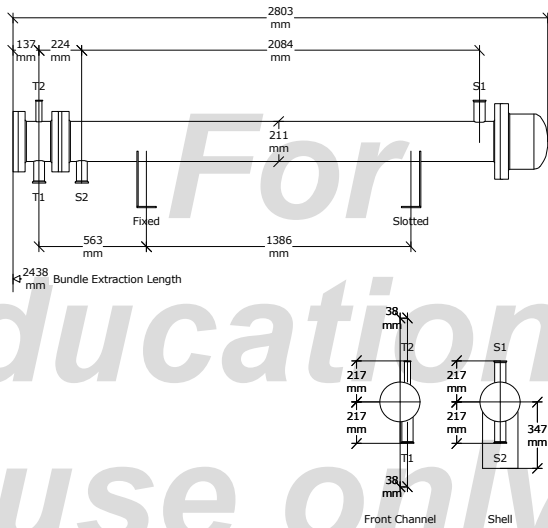
TUBEPASS DETAILS	Pass	Rows	Tubes
	1	4	10
	2	4	10
	3	4	11
	4	4	11

- SYMBOL LEGEND
- Tube
 - Dummy Short Tube
 - ▲ Dummy Long Tube
 - Plugged Tube
 - ⊙ Tie Rod
 - Seal Rod
 - Impingement Rod

Xist E 9 (32 bit) 08.06.2022 18:16 SN: 01022-620519897

SI Units

Shell 1
Rating - Horizontal Multipass Flow TEMA AES Shell With Single-Segmental Baffles



educational use only

Nozzles	OD mm	Rating	Design	Shell	Tube	Weight	kg	Unit	Shell 1
S1 Inlet	57,315		Pres (kPaG)	517,11	620,53	Bundle	63	Company	Ref
T1 Inlet	57,315		Temp (C)	110	43,33	Dry	200	Customer	
S2 Outlet	57,315		Passes	1	4	Wet	293	Item No.	
T2 Outlet	31,407		Thick (mm)	3,175	1			Service	Setting Plan
								TEMA	
								Date	08.06.2022
								Diagram	By
									Rev

C Definition of functions

This appendix contains a list of functions used to calculate the results presented in chapter 8. The functions are based on the theory presented in chapter 4. These functions are a selection from the essential calculations. Different utility functions have been left out.

#Calculating heat transfer:

```
def duty_calc(cp_h, cp_c, flow_h, flow_c, Ti_h, To_h, Ti_c, To_c):
    duty=[]
    for i in range(len(cp_h)):
        duty_hot=flow_h[i]*cp_h[i]*(Ti_h[i]-To_h[i])
        duty_cold=flow_c[i]*cp_c[i]*(To_c[i]-Ti_c[i])
        duty.append((duty_hot+duty_cold)/2)
    return duty
```

#Calculating log mean temperature difference:

```
def LMTD_calc(Ti_h, To_h, Ti_c, To_c):
    Tm=[]
    for i in range(len(Ti_h)):
        try:
            dT1=Ti_h[i]-To_c[i]
            dT2=To_h[i]-Ti_c[i]
            Tm.append((dT1-dT2)/(np.log(dT1/dT2)))
        except:
            Tm.append(Tm[i-1])
    return Tm
```

#Calculating UA based on LMTD and heat transfer:

```
def UA_LMTD_calc(LMTD, duty):
    UA=[]
    for i in range(len(LMTD)):
        try:
            UA.append(duty[i]/LMTD[i])
        except:
            UA.append(UA[i-1])
    return UA_LMTD_calc
```

```

#Calculating thermal effectiveness:
def effectiveness_calc(Duty, cp_h, cp_c, flow_h, flow_c, Ti_h, Ti_c):
    eff=[]
    for i in range(len(Duty)):
        Cmin=min(cp_h[i]*flow_h[i],cp_c[i]*flow_c[i])
        Tmax=Ti_h[i]-Ti_c[i]
        try:
            eff.append(Duty[i]/(Cmin*Tmax))
        except:
            eff.append(NaN)
    return eff

```

```

#Calculating number of transfer units NTU for counterflow:
def NTU_calc(effectiveness,cp_h,cp_c,flow_h,flow_c):
    ntu=[]
    for i in range(len(eff)):
        Cmin=min(cp_h[i]*flow_h[i],cp_c[i]*flow_c[i])
        Cmax=max(cp_h[i]*flow_h[i],cp_c[i]*flow_c[i])
        Cr=Cmin/Cmax
        if Cr<1:
            try:
                ntu.append(1/(Cr-1)*np.log(((eff[i]-1)/(eff[i]*Cr-1))))
            except:
                ntu.append(NaN)
        elif Cr==1:
            try:
                ntu.append(eff[i]/(1-eff[i]))
            except:
                ntu.append(NaN)
        else:
            ntu.append(NaN)
    return ntu

```

```

#Calculating UA based on number of transfer units
def UA_ntu(ntu,cp_h,cp_c,flow_h,flow_c):
    UA=[]
    for i in range(len(ntu)):

```

```
Cmin=min(cp_h[i]*flow_h[i],cp_c[i]*flow_c[i])
UA.append(ntu[i]*Cmin)
return UA
```

#Calculating the thermal performance:

```
def thermal_performance_calc(UA_actual,UA_design):
    TP=[]
    for i in range(len(UA_actual)):
        TP.append(UA_actual[i]/UA_design[i])
    return TP
```

#Calculating the hydraulic performance:

```
def hydraulic_performace_calc(dP,flow):
    HP=[]
    for i in range(len(dP_a)):
        HP.append((dP[i]/(flow[i]**2)))
    return HP
```


D Neqsim simulation

This appendix contains the script used to conduct Neqsim simulations. The script reads field data from a CSV file and runs a simulation for the mean value of each 26th time stamp. The results from the simulation get written to a separate CSV file. Due to confidentiality, the transmitter data tags are anonymised as *TAG-XX-XXX*.

```
#Reading field data from csv file to a dictionary:
```

```
data=dict()
i=0
key_list=[]
with open("NSIM12.csv", 'r') as file:
    reader = csv.reader(file, delimiter=";")
    for row in reader:
        n=0
        for p in row:
            if i ==0:
                data.update({p: []})
                key_list.append(p)
            if i > 0:
                try:
                    data.get(key_list[n]).append(float(p))
                except:
                    data.get(key_list[n]).append(float(0))
            n+=1
        i+=1
file.close()
```

```
#Creating a dictionary with mean values for each 26 data point:
```

```
meandata=dict()
meandata.update({"Interval": []})
interval=26
for n in data.keys():
    meandata.update({n: []})
    m=0
    run =1
    while run ==1:
        if len(data.get(n))<interval*(m+1):
```

```

meandata.get(n).append(average(data.get(n)[interval*m:]))
run = 0
else:
meandata.get(n).append(average(data.get(n)[interval*m:interval*(m+1)]))
m+=1

#Specifying new custom keys for simulation results:
New_keys=["HX02_lean_in_flowR", "HX02_lean_in_liq", "HX02_lean_in_Cp",
"HX02_lean_out_liq", "HX02_lean_out_Cp", "HX02_lean_in_enthalpy",
"HX02_lean_out_enthalpy", "HX02_lean_in_specific_enthalpy",
"HX02_lean_out_specific_enthalpy", "HX02_rich_in_flowR", "HX02_rich_in_liq",
"HX02_rich_in_Cp", "HX02_rich_out_liq", "HX02_rich_out_Cp",
"HX02_rich_in_enthalpy", "HX02_rich_out_enthalpy",
"HX02_rich_in_specific_enthalpy", "HX02_rich_out_specific_enthalpy",
"HX01_lean_in_flowR", "HX01_lean_in_liq", "HX01_lean_in_Cp",
"HX01_lean_out_liq", "HX01_lean_out_Cp", "HX01_lean_in_enthalpy",
"HX01_lean_out_enthalpy", "HX01_lean_in_specific_enthalpy",
"HX01_lean_out_specific_enthalpy", "HX01_rich_in_flowR", "HX01_rich_in_liq",
"HX01_rich_in_Cp", "HX01_rich_out_liq", "HX01_rich_out_Cp",
"HX01_rich_in_enthalpy", "HX01_rich_out_enthalpy",
"HX01_rich_in_specific_enthalpy", "HX01_rich_out_specific_enthalpy",
"HX03_in_flowR", "HX03_in_liq", "HX03_in_Cp", "HX03_out_liq",
"HX03_out_Cp", "HX03_in_enthalpy", "HX03_out_enthalpy",
"HX03_in_specific_enthalpy", "HX03_out_specific_enthalpy",
"HX04_in_flowR", "HX04_in_gas", "HX04_in_Cp",
"HX04_out_gas", "HX04_out_Cp", "HX04_in_enthalpy",
"HX04_out_enthalpy", "HX04_in_specific_enthalpy",
"HX04_out_specific_enthalpy"]

#Updating the average dictionary:
for l in New_keys:
meandata.update({l: []})

#Function for initiating a csv file to write results in:
def initFile(fileName):
wFile = open(fileName, "w")
for o in meandata.keys():
wFile.write(o)

```

```

        wFile.write(";")
    wFile.close

#Initiating the csv file:

initFile("SIMVALUE_FINAL.csv")

#Setting the range for simulation loop:
imax= len(meandata.get('TAG-XX-XXXX.'))

#Starting simulation:
for i in range(imax):

#Keeping track of the simulation by writing the iteration number to a
#separate csv file:
    timeFile=open("Iterationtracker.csv","a")
    tsstring= "Iteration nr: [" +str(i) +"] started "
    + str(datetime.now()) +"\n"
    timeFile.write(tsstring)
    timeFile.close()

#Setting parameters based on active branche:
    if(meandata.get('TAG-XX-XXXX.')[i]>meandata.get('TAG-XX-XXXX.')[i]):
        feedGasT = meandata.get('TAG-XX-XXXX.')[i]
        feedGasP = meandata.get('TAG-XX-XXXX.')[i]+1.01325
    else:
        feedGasT = meandata.get('TAG-XX-XXXX.')[i]
        feedGasP = meandata.get('TAG-XX-XXXX.')[i]+1.01325

#Setting filter pressure drop based on active filter:
    fineFilterDP = max(meandata.get('TAG-XX-XXXX.')[i],
meandata.get('TAG-XX-XXXX.')[i])

#Setting input parameters for Neqsim simulation:
    inputData = {
        'feedGasFlowRate':(max(meandata.get('TAG-XX-XXXX.')[i],

```

```

meandata.get('TAG-XX-XXXX.'35-FIT-1010.INUSE2')[i]))*1000*24.0/1.0e6,
'feedGasTemperature': feedGasT,
'feedGasPressure': feedGasP,
'absorberFeedGasTemperature':meandata.get('TAG-XX-XXXX.')[i],
'absorberFeedGasPressure':meandata.get('TAG-XX-XXXX.')[i]+1.01325,
'leanTEGFlowRate':meandata.get('TAG-XX-XXXX.')[i],
'leanTEGTemperature':meandata.get('TAG-XX-XXXX.')[i],
'flashDrumPressure':meandata.get('TAG-XX-XXXX.')[i]+1.01325,
'reboilerPressure':meandata.get('TAG-XX-XXXX.')[i]/1000.0+1.01325,
'condenserTemperature': meandata.get('TAG-XX-XXXX.')[i],
'reboilerTemperature': meandata.get('TAG-XX-XXXX.')[i],
"regenerationGasCoolerTemperature": 30.0,
"condenserPressure":meandata.get('TAG-XX-XXXX.')[i]/1000.0+1.01325,
"strippingGasRate": meandata.get('TAG-XX-XXXX.')[i]/0.7,
"strippingGasFeedTemperature": 80.0,
"bufferTankTemperatureTEG": meandata.get('TAG-XX-XXXX.')[i],
'hotTEGpumpPressure': meandata.get('TAG-XX-XXXX.')[i]+1.01325,
'finefilterdeltaP': fineFilterDP,numberOfStagesTEGabsorber": 4,
"stageEfficiencyTEGabsorber": 0.7,
"numberOfStagesStripper": 2,
"stageEfficiencyStripper": 1,
"UAvalueLeanRichTEGHeatExchanger": 8316.0,
"UAvalueLeanRichTEGHeatExchanger2": 2224.0,
}

```

#Importing functions from Neqsim:

```

from neqsim.thermo import fluid, printFrame
from neqsim.process import getProcess, clearProcess, mixer, heater,
stream, pump, separator, runProcess, stream, saturator, valve,
filters, heatExchanger, simpleTEGabsorber,distillationColumn,
waterStripperColumn, recycle2, setpoint, calculator

```

#Setting up a a glycol process:

```

clearProcess()
try:

feedGas = fluid("cpa") # create a fluid using the SRK-Eo
feedGas.addComponent("nitrogen", 0.245);

```

```

feedGas.addComponent("CO2", 3.4);
feedGas.addComponent("methane", 85.7);
feedGas.addComponent("ethane", 5.981);
feedGas.addComponent("propane", 2.743);
feedGas.addComponent("i-butane", 0.37);
feedGas.addComponent("n-butane", 0.77);
feedGas.addComponent("i-pentane", 0.142);
feedGas.addComponent("n-pentane", 0.166);
feedGas.addComponent("n-hexane", 0.06);
feedGas.addComponent("benzene", 0.01);
feedGas.addComponent("water", 0.0);
feedGas.addComponent("TEG", 0);
feedGas.setMixingRule(10)
feedGas.setMultiPhaseCheck(False)
feedGas.init(0)

dryFeedGas = stream(feedGas)
dryFeedGas.setName('dry feed gas')
dryFeedGas.setFlowRate(inputData['feedGasFlowRate'], 'MSm3/day')
dryFeedGas.setTemperature(inputData['feedGasTemperature'], 'C')
dryFeedGas.setPressure(inputData['feedGasPressure'], 'bara')

saturatedFeedGas = saturator(dryFeedGas)
saturatedFeedGas.setName("water saturator")

waterSaturatedFeedGas = stream(saturatedFeedGas.getOutStream())
waterSaturatedFeedGas.setName("water saturated feed gas")

feedTEG = feedGas.clone()
feedTEG.setMolarComposition([0.0,0.0, 0.0, 0.0, 0.0, 0.0, 0.0, 0.0,
0.0, 0.0, 0.0,0.015, 0.985])

feedTPsetterToAbsorber = heater(waterSaturatedFeedGas)
feedTPsetterToAbsorber.setName('TP of gas to absorber')
feedTPsetterToAbsorber.setOutPressure(inputData[
'absorberFeedGasPressure'], "bara")
feedTPsetterToAbsorber.setOutTemperature(inputData[
'absorberFeedGasTemperature'], "C")

```

```

feedToAbsorber = stream(feedTPsetterToAbsorber.getOutputStream())
feedToAbsorber.setName("feed to TEG absorber")

TEGFeed = stream(feedTEG)
TEGFeed.setName('lean TEG to absorber')
TEGFeed.setFlowRate(inputData['leanTEGFlowRate'], 'kg/hr')
TEGFeed.setTemperature(inputData['leanTEGTemperature'], 'C')
TEGFeed.setPressure(inputData['absorberFeedGasPressure'], 'bara')

absorber = simpleTEGAbsorber()
absorber.setName("TEG absorber")
absorber.addGasInStream(feedToAbsorber)
absorber.addSolventInStream(TEGFeed)
absorber.setNumberOfStages(inputData['numberOfStagesTEGAbsorber'])
absorber.setStageEfficiency(inputData['stageEfficiencyTEGAbsorber'])

dehydratedGas = stream(absorber.getGasOutStream())
dehydratedGas.setName('dry gas from absorber')

richTEG = stream(absorber.getSolventOutStream())
richTEG.setName("rich TEG from absorber")

glycol_flash_valve = valve(richTEG)
glycol_flash_valve.setName("Rich TEG HP flash valve")
glycol_flash_valve.setOutletPressure(inputData['flashDrumPressure'])

richGlycolHeaterCondenser = heater(glycol_flash_valve.getOutputStream())
richGlycolHeaterCondenser.setName("rich TEG preheater")

heatEx2 = heatExchanger(richGlycolHeaterCondenser.getOutputStream())
heatEx2.setName("cold lean/rich TEG heat-exchanger")
heatEx2.setGuessOutTemperature(273.15 + 60.0)
heatEx2.setUAvalue(inputData['UAvalueLeanRichTEGHeatExchanger2'])

flashSep = separator(heatEx2.getOutputStream(0))
flashSep.setName("degassing separator")

```

```

flashGas = stream(flashSep.getGasOutStream())
flashGas.setName("gas from degasing separator")

flashLiquid = stream(flashSep.getLiquidOutStream())
flashLiquid.setName("liquid from degasing separator")

fineFilter = filters(flashLiquid)
fineFilter.setName("TEG fine filter")
fineFilter.setDeltaP(inputData['finefilterdeltaP'], "bara")

heatEx = heatExchanger(fineFilter.getOutStream())
heatEx.setName("lean/rich TEG heat-exchanger")
heatEx.setGuessOutTemperature(273.15 + 130.0)
heatEx.setUAvalue(inputData['UAvalueLeanRichTEGHeatExchanger'])

glycol_flash_valve2 = valve(heatEx.getOutStream(0))
glycol_flash_valve2.setName("Rich TEG LP flash valve")
glycol_flash_valve2.setOutletPressure(inputData['reboilerPressure'])

stripGas = feedGas.clone()

strippingGas = stream(stripGas)
strippingGas.setName('stripGas')
strippingGas.setFlowRate(inputData['strippingGasRate'], "Sm3/hr")
strippingGas.setTemperature(inputData['strippingGasFeedTemperature'],
"C")
strippingGas.setPressure(inputData['reboilerPressure'], "bara")

gasToReboiler = strippingGas.clone()
gasToReboiler.setName("gas to reboiler")

column = distillationColumn(1, True, True)
column.setName("TEG regeneration column")
column.addFeedStream(glycol_flash_valve2.getOutStream(), 1)
column.getReboiler().setOutTemperature(273.15 +
inputData['reboilerTemperature'])
column.getCondenser().setOutTemperature(273.15 +
inputData['condenserTemperature'])

```

```

column.getTray(1).addStream(gasToReboiler)
column.setTopPressure(inputData['condenserPressure'])
column.setBottomPressure(inputData['reboilerPressure'])

CoolerRegenGas = heater(column.getGasOutStream())
CoolerRegenGas.setName("regen gas cooler")
CoolerRegenGas.setOutTemperature(273.15 +
inputData['regenerationGasCoolerTemperature'])

sepregenGas = separator(coolerRegenGas.getOutStream())
sepregenGas.setName("regen gas separator");

gasToFlare = stream(sepregenGas.getGasOutStream())
gasToFlare.setName("gas to flare");

liquidToTrreatment = stream(sepregenGas.getLiquidOutStream())
liquidToTrreatment.setName("water to treatment")

stripper = waterStripperColumn("TEG stripper")
stripper.addSolventInStream(column.getLiquidOutStream())
stripper.addGasInStream(strippingGas)
stripper.setNumberOfStages(inputData['numberOfStagesStripper'])
stripper.setStageEfficiency(inputData['stageEfficiencyStripper'])

recycleGasFromStripper = recycle2("stripping gas recirc")
recycleGasFromStripper.addStream(stripper.getGasOutStream())
recycleGasFromStripper.setOutletStream(gasToReboiler)

heatEx.setFeedStream(1, stripper.getSolventOutStream())

bufferTank = heater(heatEx.getOutStream(1))
bufferTank.setName("TEG buffer tank")
bufferTank.setOutTemperature(273.15 +
inputData['bufferTankTemperatureTEG'])

hotLeanTEGPump = pump(bufferTank.getOutStream(),inputData
['hotTEGpumpPressure'], "lean TEG LP pump")

```



```

heatEx2.setFeedStream(1, hotLeanTEGPump.getOutStream())

coolerh0Tteg3 = heater(heatEx2.getOutStream(1))
coolerh0Tteg3.setName("lean TEG cooler")
coolerh0Tteg3.setOutTemperature(273.15 + inputData[
'leanTEGTemperature'])

hotLeanTEGPump2 = pump(coolerh0Tteg3.getOutStream(),
inputData['absorberFeedGasPressure'], "lean TEG HP pump")
hotLeanTEGPump2.setName("lean TEG HP pump")
hotLeanTEGPump2.setOutletPressure(inputData[
'absorberFeedGasPressure'])

pumpHPPresSet = setpoint("HP pump set", hotLeanTEGPump2, "pressure",
feedToAbsorber)

leanTEGtoabs = stream(hotLeanTEGPump2.getOutStream())
leanTEGtoabs.setName("lean TEG to absorber")

pureTEG = feedGas.clone()
pureTEG.setMolarComposition([0.0,0.0, 0.0, 0.0, 0.0, 0.0, 0.0, 0.0,
0.0, 0.0, 0.0, 0.0, 1.0])

makeupTEG = stream(pureTEG)
makeupTEG.setName("makeup TEG")
makeupTEG.setFlowRate(1e-6, "kg/hr")
makeupTEG.setTemperature(inputData['leanTEGTemperature'], "C")
makeupTEG.setPressure(inputData['absorberFeedGasPressure'], "bara")

makeupCalculator = calculator("TEG makeup calculator")
makeupCalculator.addInputVariable(dehydratedGas)
makeupCalculator.addInputVariable(flashGas)
makeupCalculator.addInputVariable(gasToFlare)
makeupCalculator.addInputVariable(liquidToTreatment)
makeupCalculator.setOutputVariable(makeupTEG)

makeupMixer = mixer("makeup mixer")
makeupMixer.addStream(leanTEGtoabs)

```

```

makeupMixer.addStream(makeupTEG)

resycleLeanTEG = recycle2("lean TEG recycle")
resycleLeanTEG.addStream(makeupMixer.getOutputStream())
resycleLeanTEG.setOutletStream(TEGFeed)
resycleLeanTEG.setPriority(200)
resycleLeanTEG.setDownstreamProperty("flow rate")

richGlycolHeaterCondenser.setEnergyStream(
column.getCondenser().getEnergyStream())

```

#Running glycol process in Neqsim:

```

TEGprocess = getProcess()

thread = TEGprocess.run()

```

#Updating mean data dictionary with simulation results:

```

HX02_lean_in = TEGprocess.getUnit("lean/rich TEG heat-exchanger"
).getInStream(1).getFluid()
HX02_lean_in.setTemperature(HX02_lean_in.getTemperature('C')+1.0, 'C')
TPflash(HX02_lean_in)
meandata.get("HX02_lean_in_flowR").append(HX02_lean_in.getFlowRate
("kg/hr"))
meandata.get("HX02_lean_in_liq").append(HX02_lean_in.getPhaseOfType(
"aqueous").getPhaseFraction())
meandata.get("HX02_lean_in_Cp").append(HX02_lean_in.getCp('J/kgK'))
meandata.get("HX02_lean_in_enthalpy").append(HX02_lean_in.getEnthalpy(
"W"))
meandata.get("HX02_lean_in_specific_enthalpy").append(
HX02_lean_in.getEnthalpy("J/kg"))

HX02_lean_out = TEGprocess.getUnit("lean/rich TEG heat-exchanger"
).getOutputStream(1).getFluid()
HX02_lean_out.setTemperature(HX02_lean_in.getTemperature('C')+1.0,
'C')
TPflash(HX02_lean_out)

meandata.get("HX02_lean_out_liq").append(HX02_lean_out.getPhase(

```

```

"aqueous").getPhaseFraction()
meandata.get("HX02_lean_out_Cp").append(HX02_lean_out.getCp('J/kgK'))
meandata.get("HX02_lean_out_enthalpy").append(
HX02_lean_out.getEnthalpy("W"))
meandata.get("HX02_lean_out_specific_enthalpy").append(
HX02_lean_out.getEnthalpy("J/kg"))

HX02_rich_in = TEGprocess.getUnit(
"lean/rich TEG heat-exchanger").getInStream(0).getFluid()
HX02_rich_in.setTemperature(HX02_rich_in.getTemperature(
'C')+1.0, 'C')
TPflash(HX02_rich_in)
meandata.get("HX02_rich_in_flowR").append(
HX02_rich_in.getFlowRate("kg/hr"))
meandata.get("HX02_rich_in_liq").append(HX02_rich_in.getPhase(
"aqueous").getPhaseFraction())
meandata.get("HX02_rich_in_Cp").append(HX02_rich_in.getCp('J/kgK'))
meandata.get("HX02_rich_in_enthalpy").append(HX02_rich_in.getEnthalpy(
"W"))
meandata.get("HX02_rich_in_specific_enthalpy").append(
HX02_rich_in.getEnthalpy("J/kg"))

HX02_rich_out = TEGprocess.getUnit(
"lean/rich TEG heat-exchanger").getOutStream(0).getFluid()
HX02_rich_out.setTemperature(
HX02_rich_in.getTemperature('C')+1.0, 'C')
TPflash(HX02_rich_out)

meandata.get("HX02_rich_out_liq").append(
HX02_rich_out.getPhase("aqueous").getPhaseFraction())
meandata.get("HX02_rich_out_Cp").append(HX02_rich_out.getCp('J/kgK'))
meandata.get("HX02_rich_out_enthalpy").append(
HX02_rich_out.getEnthalpy("W"))
meandata.get("HX02_rich_out_specific_enthalpy").append(
HX02_rich_out.getEnthalpy("J/kg"))

HX01_lean_in = TEGprocess.getUnit(
"cold lean/rich TEG heat-exchanger").getInStream(1).getFluid()

```

```

HX01_lean_in.setTemperature(HX01_lean_in.getTemperature('C')+1.0, 'C')
TPflash(HX01_lean_in)
meandata.get("HX01_lean_in_flowR").append(HX01_lean_in.getFlowRate(
"kg/hr"))
meandata.get("HX01_lean_in_liq").append(HX01_lean_in.getPhase(
"aqueous").getPhaseFraction())
meandata.get("HX01_lean_in_Cp").append(HX01_lean_in.getCp('J/kgK'))
meandata.get("HX01_lean_in_enthalpy").append(HX01_lean_in.getEnthalpy(
"W"))
meandata.get("HX01_lean_in_specific_enthalpy").append(
HX01_lean_in.getEnthalpy("J/kg"))

HX01_lean_out = TEGprocess.getUnit(
"cold lean/rich TEG heat-exchanger").getOutputStream(1).getFluid()
HX01_lean_out.setTemperature(HX01_lean_in.getTemperature('C')+1.0,
'C')
TPflash(HX01_lean_out)

meandata.get("HX01_lean_out_liq").append(HX01_lean_out.getPhase(
"aqueous").getPhaseFraction())
meandata.get("HX01_lean_out_Cp").append(HX01_lean_out.getCp('J/kgK'))
meandata.get("HX01_lean_out_enthalpy").append(
HX01_lean_out.getEnthalpy("W"))
meandata.get("HX01_lean_out_specific_enthalpy").append(
HX01_lean_out.getEnthalpy("J/kg"))

HX01_rich_in = TEGprocess.getUnit(
"cold lean/rich TEG heat-exchanger").getInStream(0).getFluid()
HX01_rich_in.setTemperature(HX01_rich_in.getTemperature('C')+1.0, 'C')
TPflash(HX01_rich_in)
meandata.get("HX01_rich_in_flowR").append(HX01_rich_in.getFlowRate(
"kg/hr"))
meandata.get("HX01_rich_in_liq").append(HX01_rich_in.getPhase(
"aqueous").getPhaseFraction())
meandata.get("HX01_rich_in_Cp").append(HX01_rich_in.getCp('J/kgK'))
meandata.get("HX01_rich_in_enthalpy").append(HX01_rich_in.getEnthalpy(
"W"))
meandata.get("HX01_rich_in_specific_enthalpy").append(

```

```

HX01_rich_in.getEnthalpy("J/kg"))

HX01_rich_out = TEGprocess.getUnit(
"cold lean/rich TEG heat-exchanger").getOutputStream(0).getFluid()
HX01_rich_out.setTemperature(HX01_rich_in.getTemperature('C')+1.0,
'C')
TPflash(HX01_rich_out)

meandata.get("HX01_rich_out_liq").append(HX01_rich_out.getPhase(
"aqueous").getPhaseFraction())
meandata.get("HX01_rich_out_Cp").append(HX01_rich_out.getCp('J/kgK'))
meandata.get("HX01_rich_out_enthalpy").append(
HX01_rich_out.getEnthalpy("W"))
meandata.get("HX01_rich_out_specific_enthalpy").append(
HX01_rich_out.getEnthalpy("J/kg"))

HX03_in = TEGprocess.getUnit(
"lean TEG cooler").getInStream().getFluid()
HX03_in.setTemperature(HX03_in.getTemperature('C')+1.0, 'C')
TPflash(HX03_in)

meandata.get("HX03_in_flowR").append(HX03_in.getFlowRate("kg/hr"))
meandata.get("HX03_in_liq").append(HX03_in.getPhaseOfType(
"aqueous").getPhaseFraction())
meandata.get("HX03_in_Cp").append(HX03_in.getCp('J/kgK'))
meandata.get("HX03_in_enthalpy").append(HX03_in.getEnthalpy("W"))
meandata.get("HX03_in_specific_enthalpy").append(HX03_in.getEnthalpy(
"J/kg"))

HX03_out = TEGprocess.getUnit(
"lean TEG cooler").getOutputStream().getFluid()
HX03_out.setTemperature(HX03_in.getTemperature('C')+1.0, 'C')
TPflash(HX03_out)

meandata.get("HX03_out_liq").append(HX03_out.getPhase(
"aqueous").getPhaseFraction())
meandata.get("HX03_out_Cp").append(HX03_out.getCp('J/kgK'))
meandata.get("HX03_out_enthalpy").append(HX03_out.getEnthalpy("W"))

```

```

meandata.get("HX03_out_specific_enthalpy").append(
HX03_out.getEnthalpy("J/kg"))

HX04_in = TEGprocess.getUnit(
"regen gascooler").getInStream().getFluid()
HX04_in.setTemperature(HX04_in.getTemperature('C')+1.0, 'C')
TPflash(HX04_in)

meandata.get("HX04_in_flowR").append(HX04_in.getFlowRate("kg/hr"))
meandata.get("HX04_in_gas").append(HX04_in.getPhase(
"gas").getPhaseFraction())
meandata.get("HX04_in_Cp").append(HX04_in.getCp('J/kgK'))
meandata.get("HX04_in_enthalpy").append(HX04_in.getEnthalpy("W"))
meandata.get("HX04_in_specific_enthalpy").append(
HX04_in.getEnthalpy("J/kg"))

HX04_out = TEGprocess.getUnit(
"regen gas cooler").getOutStream().getFluid()
HX04_out.setTemperature(HX04_out.getTemperature('C'), 'C')
TPflash(HX04_out)

meandata.get("HX04_out_gas").append(
HX04_out.getPhase("gas").getPhaseFraction())
meandata.get("HX04_out_Cp").append(HX04_out.getCp('J/kgK'))
meandata.get("HX04_out_enthalpy").append(HX04_out.getEnthalpy("W"))
meandata.get("HX04_out_specific_enthalpy").append(
HX04_out.getEnthalpy("J/kg"))

meandata.get("Interval").append(str(i))

#Writing simulation results to csv file:
wFile = open("SIMVALUE_FINAL.csv","a")
wFile.write("\n")
for q in meandata.keys():
    wFile.write(str(meandata.get(q)[i]))
    wFile.write(";")
wFile.close

```

#Writing iteration status to tracker filer:

```
timeFile=open("Iterationtracker.csv","a")
tfstring= "Iteration nr: [" +str(i) +"] finished "
+ str(datetime.now()) +"\n"
timeFile.write(tfstring)
timeFile.close()
```

#If simulation fails copying last iteration to current point:

```
except:
    for q in meandata.keys():
        if len(meandata.get(q)) == i:
            meandata.get(q).append(meandata.get(q)[i-1])
timeFile=open("Iterationtracker.csv","a")
tfstring= "Iteration nr: [" +str(i) +"] FAILED " + str(datetime.now()) +"\n"
timeFile.write(tfstring)
timeFile.close()
```

E Plotted figures scripts

This appendix shows the scripts for the plotted figures presented in chapter 8. HX02 and the Neqsim comparison are shown as examples. Below are the scrips for the plots of the thermal and hydraulic performances and comparisons on both the lean and rich glycol sides and the flow rate comparison for Neqsim. Similarly to appendix D, the data tag names are anonymised as 'TAG-XX-XXX' due to confidentiality.

```
#Neqsim flow rate comparison:
```

```
fig, nsim_fig=plt.subplots(figsize=(15, 6))
nsim_fig.plot(time, set_flowrate(remove_outliers(
data.get('TAG-XX-XXX'))), color='coral', label='Measured lean glycol')
nsim_fig.plot(time, set_flowrate(remove_outliers(
data.get('TAG-XX-XXX'))), color='cornflowerblue',
label='Measured rich glycol')
nsim_fig.plot(time, flow_lean, color='darkred', label='Simulated lean glycol')
nsim_fig.plot(time, flow_rich, color='darkblue', label='Simulated rich glycol')
nsim_fig.set_xlabel('Time')
nsim_fig.set_ylabel('Flow rate [kg/s]')
nsim_fig.set_title('Simulated and measured flow rate comparison - HX02')
nsim_fig.set_ylim(1.2, 1.6)
nsim_fig.legend()
nsim_fig.grid(which='major', axis='both')
```

```
#Hydraulic Performance plot Lean TEG:
```

```
fig, HP_lean_fig=plt.subplots(figsize=(15, 6))
HP_lean_fig.set_title('Hydraulic performance - HX02 lean glycol')
HP_lean_fig.axhline(get_first_avg(HP_lean), color='black', linewidth=0.5)
HP_lean_fig.plot(time, HP_lean, '-b', label='Lean glycol')
HP_lean_fig.set_xlabel('Time')
HP_lean_fig.set_ylabel(r'$\frac{\Delta p}{\dot{m}^2}$',
rotation=0, va='center', ha='right', fontsize=16)
HP_lean_fig.legend()
HP_lean_fig.grid(which='major', axis='both')
```

```
#Hydraulic Performance plot Rich TEG:
```



```

fig, HP_rich_fig=plt.subplots(figsize=(15, 6))
HP_rich_fig.set_title('Hydraulic performance - HX02 rich glycol')
HP_rich_fig.axhline(get_first_avg(HP_rich), color='black', linewidth=0.5)
HP_rich_fig.plot(time, HP_rich, '-b', label='Rich glycol')
HP_rich_fig.set_ylim(0.040, 0.090)
HP_rich_fig.set_xlabel('Time')
HP_rich_fig.set_ylabel(r'$\frac{\Delta p}{\dot{m}^2}$',
rotation=0, va='center', ha='right', fontsize=16)
HP_rich_fig.grid(which='major', axis='both')
HP_rich_fig.legend()

```

#Thermal performance plot:

```

fig, TP_fig=plt.subplots(figsize=(15, 6))
TP_fig.axhline(get_first_avg(TP), color='black', linewidth=0.5)
TP_fig.plot(time, TP, '-b')
TP_fig.grid(which='major', axis='both')
TP_fig.set_ylabel(r'$\frac{UA}{(UA)_d}$', va='center',
ha='right', fontsize=16, rotation=0)
TP_fig.set_xlabel('Time', fontsize='14')
TP_fig.set_title('Thermal performance - HX02')

```

#Flow rate and pressure drop comparisons - Lean TEG:

```

fig, lean_fig=plt.subplots(2, figsize=(12, 6))
lean_fig[0].set_title(
'Flow rate and pressure drop comparison - HX02 lean glycol')
lean_fig[0].plot(time, dP_lean, color='red', label='Pressure drop')
lean_fig[1].plot(time, flow_lean, color='blue', label='Flow rate')
lean_fig[0].set_ylim(0.04, 0.05)
lean_fig[1].set_xlabel('Time')
lean_fig[0].set_ylabel('Pressure drop [bar]')
lean_fig[1].set_ylabel('Flow rate [kg/s]')
lean_fig[0].grid(which='major', axis='both')
lean_fig[1].grid(which='major', axis='both')
lean_fig[0].legend()
lean_fig[1].legend()

```

```

#Gas fraction, flow rate and pressure drop comparisons - Rich TEG:
fig, rich_fig=plt.subplots(3, figsize=(12, 9))
rich_fig[0].set_title(
'Flow rate, gas fraction and pressure drop comparison - HX02 rich glycol')
rich_fig[0].plot(time, dP_rich, color='red', label='Pressure drop')
rich_fig[1].plot(time, gas_rich, color='blue', label='Gas phase fraction')
rich_fig[2].plot(time, flow_rich, label='Flow rate')
rich_fig[0].set_ylabel('Pressure drop [bar]')
rich_fig[1].set_ylabel('Gas mass fraction [wt\%]')
rich_fig[2].set_ylabel('Flow rate [kg/s]')
rich_fig[2].set_xlabel('Time')
rich_fig[0].grid(which='major', axis='both')
rich_fig[1].grid(which='major', axis='both')
rich_fig[2].grid(which='major', axis='both')
rich_fig[0].legend()
rich_fig[1].legend()
rich_fig[2].legend()

```

